

**ANALYSIS OF OZONE AND FINE PARTICULATE
MATTER IN THE NORTHEASTERN
UNITED STATES**

FINAL REPORT 03-04

NOVEMBER 2003

**NEW YORK STATE
ENERGY RESEARCH AND
DEVELOPMENT AUTHORITY**





The New York State Energy Research and Development Authority (NYSERDA) is a public benefit corporation created in 1975 by the New York State Legislature. NYSERDA's responsibilities include:

- Conducting a multifaceted energy and environmental research and development program to meet New York State's diverse economic needs.
- Administering the **New York Energy \$martSM** program, a Statewide public benefit R&D, energy efficiency, and environmental protection program.
- Making energy more affordable for residential and low-income households.
- Helping industries, schools, hospitals, municipalities, not-for-profits, and the residential sector, including low-income residents, implement energy-efficiency measures.
- Providing objective, credible, and useful energy analysis and planning to guide decisions made by major energy stakeholders in the private and public sectors.
- Managing the Western New York Nuclear Service Center at West Valley, including: (1) overseeing the State's interests and share of costs at the West Valley Demonstration Project, a federal/State radioactive waste clean-up effort, and (2) managing wastes and maintaining facilities at the shut-down State-Licensed Disposal Area.
- Coordinating the State's activities on energy emergencies and nuclear regulatory matters, and monitoring low-level radioactive waste generation and management in the State.
- Financing energy-related projects, reducing costs for ratepayers.

NYSERDA administers the **New York Energy \$martSM** program, which is designed to support certain public benefit programs during the transition to a more competitive electricity market. More than 2,700 projects in more than 30 programs are funded by a charge on the electricity transmitted and distributed by the State's investor-owned utilities. The **New York Energy \$martSM** program provides energy efficiency services, including those directed at the low-income sector, research and development, and environmental protection activities.

NYSERDA derives its basic research revenues from an assessment on the intrastate sales of New York State's investor-owned electric and gas utilities, and voluntary annual contributions by the New York Power Authority and the Long Island Power Authority. Additional research dollars come from limited corporate funds. Some 400 NYSERDA research projects help the State's businesses and municipalities with their energy and environmental problems. Since 1990, NYSERDA has successfully developed and brought into use more than 141 innovative, energy-efficient, and environmentally beneficial products, processes, and services. These contributions to the State's economic growth and environmental protection are made at a cost of about \$.70 per New York resident per year.

Federally funded, the Energy Efficiency Services program is working with more than 540 businesses, schools, and municipalities to identify existing technologies and equipment to reduce their energy costs.

For more information, contact the Communications unit, NYSERDA, 17 Columbia Circle, Albany, New York 12203-6399; toll-free 1-866-NYSERDA, locally (518) 862-1090, ext. 3250; or on the web at www.nyserda.org

STATE OF NEW YORK
George E. Pataki
Governor

ENERGY RESEARCH AND DEVELOPMENT AUTHORITY
Vincent A. DeIorio, Esq., Chairman
Peter R. Smith, President

**ANALYSIS OF OZONE AND FINE PARTICULATE MATTER
IN THE NORTHEASTERN UNITED STATES**

FINAL REPORT

Prepared for the
**NEW YORK STATE
ENERGY RESEARCH AND
DEVELOPMENT AUTHORITY**
Albany, NY
www.nyserda.org

Mark Watson
Project Manager

Prepared by
THE UNIVERSITY AT ALBANY
Albany, NY

S. Trivikrama Rao
Principal Investigator

NOTICE

This report was prepared by C. Hogrefe and S. T. Rao of the University at Albany in the course of performing work contracted for and sponsored by the New York State Energy Research and Development Authority (hereafter "NYSERDA"). The opinions expressed in this report do not necessarily reflect those of NYSERDA or the State of New York, and reference to any specific product, service, process, or method does not constitute an implied or expressed recommendation or endorsement of it. Further, NYSERDA, the State of New York, and the contractor make no warranties or representations, expressed or implied, as to the fitness for particular purpose or merchantability of any product, apparatus, or service, or the usefulness, completeness, or accuracy of any processes, methods, or other information contained, described, disclosed, or referred to in this report. NYSERDA, the State of New York, and the contractor make no representation that the use of any product, apparatus, process, method, or other information will not infringe privately owned rights and will assume no liability for any loss, injury, or damage resulting from, or occurring in connection with, the use of information contained, described, disclosed, or referred to in this report.

PREFACE

NYSERDA is pleased to publish “Analysis of Ozone and Fine Particulate Matter in the Northeastern United States.” This report was prepared by the University at Albany. The Principal Investigator, Dr. S.T. Rao, is now the Director of the Atmospheric Modeling Division of the U.S. Environmental Protection Agency and has continued his research in air quality modeling and policy analysis.

This project was funded as part of the **New York Energy SmartSM** Environmental Monitoring, Evaluation, and Protection (EMEP) Program and represents one of several air quality modeling studies underway in New York. A summary of findings and policy implications from this study and related work, including a previously published EMEP report entitled “Assessing the Effects of Transboundary Pollution on New York’s Air Quality,” is available from NYSERDA.

ACKNOWLEDGMENTS

The contributions of Drs. Gopal Sistla, Robert F. Henry, Jia-Yeong Ku, Kevin L. Civerolo, Elvira Brankov, Christian Hogrefe and Mr. Winston Hao of the Division of Air Resources, New York State Department of Environmental Conservation, Albany, NY are gratefully acknowledged. Also, Professors Stephen Berman of SUNY-Oneonta, Steven Porter of the University of Idaho, George Kallos of the University of Athens, Dragutin Mihailovic of the University of Novi Sad, Yugoslavia, Somaraju Vempaty of the Engineering College, Bhimavaram, India and Igor Zurbenko of the School of Public Health - SUNY Albany have contributed substantially to accomplish the various research tasks in this project. In addition, Drs. Jhumoor Biswas, Huiting Mao, Jian Zhang, Kesu Zhang, Kiran Alapaty, Edith Gego, and Mr. Georgios Athanassiadis were instrumental to the successful completion of this research. Finally, Professor S. T. Rao, principal investigator of this project, thanks Ms. Janet Joseph and Mr. Mark Watson of NYSERDA for supporting this investigation.

NYSERDA appreciates the input of project reviewers, especially Dr. Praveen Amar, Director, Science and Policy, NESCAUM, and Dr. Daniel Jacob, Professor of Atmospheric Chemistry & Environmental Engineering, Division of Engineering and Applied Science, Harvard University.

ABSTRACT AND KEYWORDS

The objective of this research project was to help improve our understanding of the behavior of ozone and fine particles in the northeastern United States. To this end, a variety of observational data sets, modeling tools and analysis methods were employed to elucidate the processes governing the fluctuations of these pollutants, to establish the spatial scales relevant to the problem, and to develop methods that can be used by air quality managers and decision makers to address these issues in an integrated fashion. An analysis of trace metal observations in New York State pointed to possible source regions for these pollutants. Results of this research project bolster the notion that O₃ and PM_{2.5} pollution is a regional and multi-state, not simply an urban or local problem. Such scales imply that over distances of less than about 100 km, it is difficult to unequivocally attribute sources or distinguish pollution levels observed at upwind, city center, and downwind locations, and that no State in the Northeast by itself will be able to deal with such pollutant problems until the regional air quality management partnerships are in place and region-wide emission control strategies are implemented for O₃ and PM_{2.5}. Additionally, it was shown that the proper treatment of boundary-layer processes and land-surface interactions in atmospheric models is critical if these models are to reproduce the features present in the observations. This finding was highlighted by a comparison of different techniques currently used to estimate the boundary layer evolution and mixing height which revealed significant differences, contributing to the uncertainty in air quality modeling. Additionally, analysis of ozone concentrations and meteorological observations showed a relationship between elevated ozone concentrations and reduced ventilation in the boundary layer. An evaluation of ozone precursor predictions from photochemical model simulations indicated that the current models do not properly reproduce the observed ozone-precursor relationships. Finally, a methodology for integrating observations and model predictions into a probabilistic framework was developed to assist decision makers in assessing the probability of success of a given emission control strategy in meeting and maintaining the relevant National Ambient Air Quality Standards.

Keywords: Ozone, PM_{2.5}, regional-scale transport, trend analysis, atmospheric boundary-layer evolution, land-surface modeling, air quality models, model evaluation, space-time analysis, regulatory policy-making

TABLE OF CONTENTS

Section	Page
EXECUTIVE SUMMARY	S-1
1 Analysis of spatio-temporal features embedded in the time series of ozone and fine particulate matter	
Impact of data reporting practices on trend analysis	1-1
Review of trend analysis and attribution techniques	1-4
Comparison of different spectral decomposition techniques.....	1-4
Spatio-temporal analysis of trace metal observations	1-5
2 Analysis of ozone exceedance days in the Northeast with a special emphasis on the land-atmosphere interactions and boundary-layer processes	
Analysis of boundary layer characteristics and their impact on ground level ozone concentrations....	2-1
Impact of boundary-layer parameterizations on model predictions	2-6
Meteorological effects of changing land-use patterns	2-8
Parameterization of land-surface interactions in atmospheric models	2-12
3 Application of statistical methods, trajectory models and photochemical models to identify potential cause and effect relationships.....	3-1
4 Modeling and analysis of ozone concentrations in the Northeast and the use of photochemical modeling systems for regulatory policy-making as part of the state implementation plan	
Model evaluation.....	4-1
Use of the photochemical modeling systems in the regulatory framework.....	4-7
5 References	5-1
6 Completed publications related to this research project	6-1
7 Research staff supported by this research project.....	7-1
APPENDIX A: Report by K. Alapaty	A-1
APPENDIX B: Report by D. Mihailovic	B-1

EXECUTIVE SUMMARY

To help improve our understanding of the spatial and temporal behavior of ozone and fine particulate matter in the Northeast, research was performed in four major topic areas. The research focus areas were (1) analyses of the spatio-temporal features embedded in time series of ozone and fine particulate matter, (2) analyses of ozone exceedance days in the Northeast with a special emphasis on land-atmosphere interactions and boundary-layer processes, (3) applications of statistical methods, trajectory models and photochemical models to identify potential cause and effect relationships, and (4) modeling of ozone concentrations in the Northeast and using models for regulatory policy-making. The key results of each of these research areas are highlighted below in bullet form and discussed in greater detail in the first four sections of the main part of this report.

1. Analysis of the spatio-temporal features embedded in time series of ozone and fine particulate matter

- Trace element pollution is a regional-scale problem in the Northeast.
- Spatio-temporal features in pollutants are sensitive to differences in the sampling procedures between different networks.
- Changes in data reporting practices in time can cause erroneous trend estimates from observational data bases.

2. Analysis of ozone exceedance days in the Northeast with special emphasis on land-atmosphere interactions and boundary-layer processes

- The predictions of meteorological models are sensitive to changes in land-use patterns.
- Future model development efforts should focus on improving the parameterizations of land-atmosphere interactions and vertical mixing of pollutants.
- Vertical mixing processes play a crucial role in the temporal evolution of the ground-level ozone concentrations.

3. Application of statistical methods, trajectory models and photochemical models to identify potential cause and effect relationships

- O_3 and $PM_{2.5}$ pollution is a regional, multi-state, issue in the Northeast.
- Given the high spatial coherence in O_3 and $PM_{2.5}$ concentrations within 100 km, the regional versus local signal in pollutant concentrations is difficult to discern with data collected at a few monitoring sites within an urban area.

- Long term high-resolution monitoring (i.e., hourly or daily sampling as opposed to the twice a week or weekly sampling) of PM_{2.5} and its species is necessary to evaluate the pollutant transport patterns and potential source regions for pollutants measured in the Northeast.

4. Modeling and analysis of ozone concentrations in the Northeast and the use of photochemical modeling results in regulatory policy-making

- Current photochemical modeling systems are unable to capture the observed ozone-precursor relationships. The models, in general, tend to underestimate the ozone production efficiencies (i.e. the amount of ozone formed per molecule of NO_x emitted over the lifetime of the NO_x molecule) in the Northeast. Also, predicted ozone concentrations and efficacies of VOC and NO_x emission control strategies are very sensitive to the treatment of the boundary-layer evolution and land-use/land-cover processes within photochemical models.
- Air quality models capture the average pollutant concentration and its spatial pattern better than the peak concentration. Predictions of the daily maximum ozone concentrations with different current-generation photochemical modeling systems during an individual ozone episode can vary as much as 30%. This uncertainty can be reduced when the predicted daily maximum ozone concentrations are averaged over all episode days simulated. This finding provided the rationale for the recent U.S. Environmental Protection Agency's modeling guidance on how modeling results must be used in the regulatory setting, namely, the need for using the predicted daily maximum ozone concentrations averaged over all episode days simulated for regulatory purposes as opposed to the peak predicted ozone concentration during one episode.
- Observations and model predictions need to be integrated into a probabilistic framework to enable the decision maker to assess the probability of success of a given emission control strategy in meeting and maintaining the relevant National Ambient Air Quality Standards.

Section 1

ANALYSIS OF SPATIO-TEMPORAL FEATURES EMBEDDED IN TIME SERIES OF OZONE AND FINE PARTICULATE MATTER

Analysis of the spatial and temporal features embedded in observations of atmospheric variables is the key to using these observations for purposes such as trend assessment, identification of pollutant transport patterns, and the examination of possible cause and effect relationships. To this end, observations of carbon monoxide, ozone, fine particles and trace metals from monitoring stations operated by the Empire State Electric Energy Research Corporation (ESEERCO), Northeast States for Coordinated Air Use Management (NESCAUM), National Park Service Interagency Monitoring of Protected Visual Environments (NPS/IMPROVE) and Aerometric Information Retrieval System (AIRS) networks were analyzed in this research project. Since most of the results of these analyses have been published in the peer-reviewed literature, we provide only a brief summary of the key findings in this report, illustrated by selected figures and tables. The reader is encouraged to consult the referred papers in various journals for an in-depth discussion on the techniques employed and results of each study completed during the course of this investigation.

IMPACT OF DATA REPORTING PRACTICES ON TREND ANALYSIS

Air quality managers interested in evaluating the effectiveness of the numerous air pollution control programs implemented during the past three decades must examine the time series of pollutant concentrations for changes, such as trends and breaks, and attribute these changes to the implementation of specific emission control programs. Data inhomogeneities stemming from changes in instrumentation, data acquisition and data reduction procedures, etc. can distort the information present in the time series of pollutant concentration data. Much of the pollutant data of interest has been collected to determine compliance with the relevant air quality standards. A secondary objective may be the determination of long-term trends, hopefully indicating steady progress toward cleaner air, or sudden breaks, revealing the impact of a particular emission control program. Just as the radiosonde data are collected primarily to support the operational weather forecasts, but are now of growing importance for climate studies, databases such as the U.S. Environmental Protection Agency's (EPA) Aerometric Information Retrieval System (AIRS), which are collected primarily for regulatory purposes, will be of growing importance to determine the success or failure of various regulatory programs that have been implemented. Currently, data analysts hoping to determine trends and/or breaks often have no recourse but to use ambient air quality data as reported, and may not be aware that changes in the reporting precision, which are inconsequential from a regulatory perspective but potentially misleading from a trend analysis viewpoint, may have occurred.

During this research project, Henry et al. (2000) analyzed time series of ozone and carbon monoxide observations from the EPA's AIRS network to address the issues mentioned above. Their study demonstrated that inhomogeneities can be introduced into the data when there are changes in the reporting practices. Data analysts may not notice or expect such changes, as they are not flagged in the AIRS data base. The inhomogeneities in the AIRS database do not originate in the database, but rather in the various agencies throughout the states responsible for collecting and reporting their data to AIRS. Many of these data sets (e.g., the database maintained by the California Air Resources Board), are themselves very large, most likely suffer from the same problems as the AIRS database to which they contribute, and will undoubtedly be the subject of increased interest as more researchers attempt to find evidence for the success (or failure) of an emission control program. Henry et al. (2000) illustrated the magnitude of changes in data precision and its impact on data analyses and interpretations. A change in precision appears artificially as an abrupt change which can be erroneously interpreted as a trend. For example, prior to 1994, California reported carbon monoxide (CO) concentrations to the EPA's AIRS database to the nearest ppm. After this time, California CO levels were reported to the nearest tenth of a ppm. Since reported CO concentrations are typically a few ppm, such changes in reporting precision can introduce trends or breaks on the order of tens of percent, perhaps comparable in magnitude with changes anticipated from emission control programs.

To illustrate the above mentioned problem, time series of hourly carbon monoxide concentrations measured in Stockton, California (AIRS 060771002) were extracted from EPA's AIRS database. As indicated before, data were reported to the nearest ppm prior to 1994 while after that time data were reported to the nearest 0.1 ppm as evident from the distributions in Figure 1. The sign and magnitude of the bias produced by this rounding procedure are dependent upon the distribution of the unrounded data. For data distributed like CO at Stockton, CA, rounding to the nearest ppm will shift more of the distributional mass upward than downward. Hence, the mean of the rounded values will be larger than the mean of the raw data. The mean of the unrounded raw values is about 18% smaller than the mean of the homogenized (rounded) data. Changes in ozone data due to differences in reporting practices are smaller than for carbon monoxide but still significant and can affect data analysis. At 225 AIRS ozone monitoring locations change in reporting precision typically caused shifts of several percent in the mean values.

Changes in the reporting procedure will also be manifested in the long-term trend estimates. Analysis of the long-term trend component, derived from three iterations of a 365-d moving average filter, in both raw and homogenized (rounded) Stockton CO data, are shown in Figure 2. These results clearly demonstrate the need to examine the pollutant concentration time-series data for artifacts before the data are used in estimating trends or attributing changes in pollutant levels to an emission control policy.

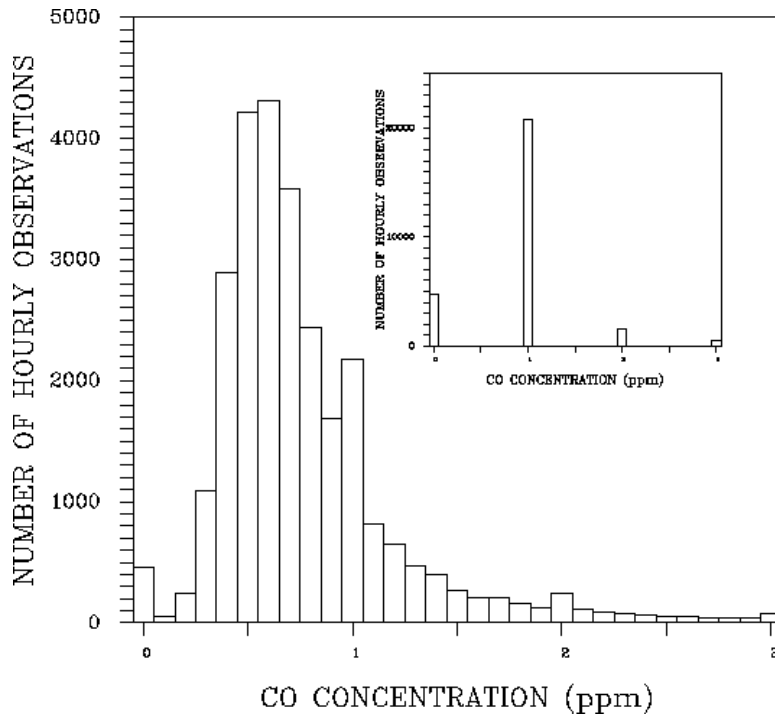


Figure 1 (from Henry et al., 2000): The distribution of raw (unrounded) and rounded CO data (inset) at Stockton, CA (1994 and afterward).

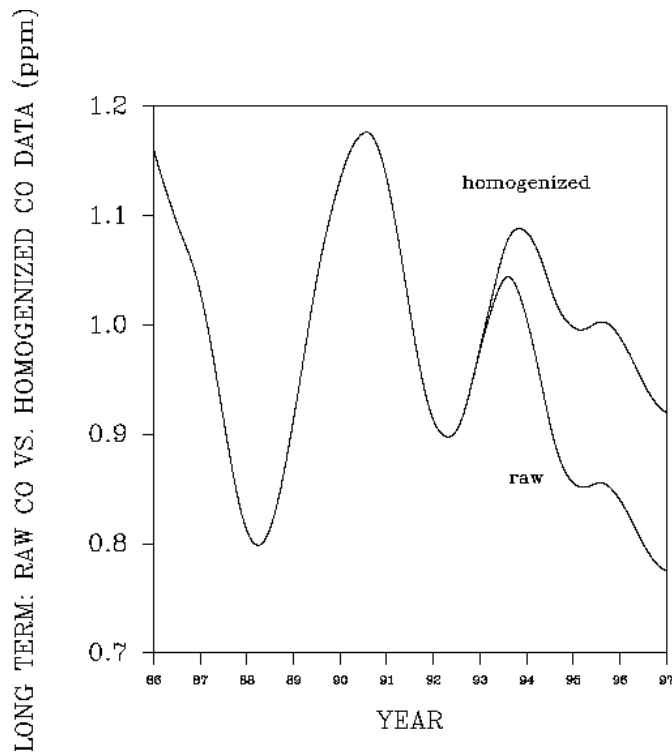


Figure 2 (from Henry et al., 2000): The long-term components in raw and homogenized CO data at Stockton, CA. An artificial decline in the raw data in the post-1994 period is created by changing the way CO data are reported.

Henry et al. (2000) conclude that it is important to properly account for artifacts in the data by homogenizing time-series data so that changes in pollutant concentration levels are not attributed erroneously to the efficacy of an emission reduction policy. The importance of these issues was stressed in the National Academy of Sciences' study on the ozone-forming potential of reformulated gasoline (NRC, 1999).

REVIEW OF TREND ANALYSIS AND ATTRIBUTION TECHNIQUES

Porter et al. (2001) critically reviewed the trend assessment techniques being used in the air pollution field and discussed their strengths and limitations in discerning and attributing changes in ozone to emission control policies. Assessment of regulatory programs aimed at improving ozone air quality is of considerable interest to the scientific community and policy makers. Trend detection, the identification of statistically significant long-term changes, and attribution, linking change to specific climatological (i.e. natural variations) and anthropogenic forcings, are instrumental to this assessment. Detection and attribution are difficult because changes in pollutant concentrations of interest to policy makers may be much smaller than those occurring naturally due to changes in weather and climatic conditions. In addition, there are considerable differences in reported trends seemingly based on similar statistical methods and data bases. Differences arise from the variety of techniques used to reduce non-trend variation in time series, including mitigating the effects of meteorology, and the variety of metrics used to track changes. This work has contributed to the preparation of the NARSTO Ozone Assessment Report (NARSTO, 2000).

COMPARISON OF DIFFERENT SPECTRAL DECOMPOSITION TECHNIQUES

Hogrefe et al. (2003) compared four methods for spectrally decomposing time series of atmospheric variables. Such spectral decomposition is necessary to discern the relative strengths of different dynamical forcings operating on different scales in time series of atmospheric variables. Two of these methods have been previously applied to the analysis of time series of atmospheric variables (Rao and Zurbenko, 1994; Torrence and Compo, 1998), while the others were applied for the first time in this project. The performance of these four filtering methods was illustrated and evaluated using both simulated and observed ozone time series data. The Adaptive Window Fourier Transform (AWFT) filter was shown to extract fluctuations of known frequency as well as the Morlet wavelet and, therefore, is a useful new tool for time-frequency analyses of atmospheric variables. Simulation results indicated that these four filters provide qualitatively similar results when used to extract the energy in five frequency bands of particular interest in time series of atmospheric variables. However, differences can exist when different filters are used to study the temporal variations of the extracted components. In addition, it was shown that all filters are able to capture the year-to-year fluctuations in the magnitudes of individual components. Such analysis can be used to discern the time scales affecting the long-term changes in pollutant concentrations. As no single filter performs best in separating the various time scales,

Hogrefe et al. (2003) caution that great care has to be taken to match the filter characteristics with the objectives of a given analysis.

SPATIO-TEMPORAL ANALYSIS OF TRACE METAL OBSERVATIONS

Analysis of the spatio-temporal features of trace metal observations from the ESEERCO, NESCAUM and NPS networks has been described in Brankov et al. (1999) and Athanassiadis and Rao (2003). To improve our understanding of the problem of long-range transport and source-receptor relationships for trace-level toxic air contaminants, Brankov et al. (1999) examined the use of several multiple comparison procedures (MCP) in the analysis and interpretation of multiply-censored data sets. Censoring is a chronic problem for some of the toxic elements of interest (As, Se, Mn, etc.) because their atmospheric concentrations are often too low to be measured precisely. Such concentrations are commonly reported in a non-quantitative way as “below the limit of detection (LOD),” leaving the data analyst with censored data sets. Since the standard statistical MCPs are not readily applicable to such data sets, Brankov et al. (1999) employed Monte Carlo simulations to evaluate two nonparametric rank-type MCPs for their applicability to the interpretation of censored data. Two different methods for ranking censored data were evaluated: average rank method and substitution with half the detection limit. The results suggest that the Kruskal-Wallis-Dunn MCP (Hochberg and Tamahne, 1987) with the half detection limit replacement for censored data is most appropriate for comparing independent, multiply-censored samples of moderate size (20-100 elements).

To examine the relationship between the synoptic-scale atmospheric transport patterns and observed pollutant concentration levels, Brankov et al. (1999) used the following procedure: The three-dimensional mixed-layer trajectory model HYSPLIT (Draxler, 1992) was employed to calculate three-day back-trajectories from the observational site. One trajectory per sampling day resulted in a large number of trajectories, each associated with a particular synoptic condition. To reduce the many different air flow regimes into a finite number of synoptic patterns, a clustering technique was applied. When trajectories closest to each other and with similar directions are grouped together, the pollutant concentrations are segregated according to trajectory clusters. Comparison of eight concentration clusters is then needed to test for significant differences in the chemical compositions of the clustered data, i.e. to identify potential source regions associated with significantly higher levels of pollution measured at this station. Since our Monte Carlo study has indicated that the KWD procedure with LOD/2 replacement for censored data is superior to the other methods and combinations tested, this method is applied to censored toxic air pollutants, namely, selenium, manganese, vanadium and arsenic measured in the Northeast.

The results for Selenium show that the SW and S clusters are not significantly different from each other, but they are clearly isolated (significantly different) from all other clusters (Table 1). The S and SW

trajectory clusters are adjacent to each other, both containing trajectories coming from the Ohio River Valley region. Significantly higher levels of selenium in these two clusters suggest that the coal burning regions of the Midwest are major sources for Se pollution at the Whiteface Mountain. Similar analysis was also performed for Manganese, Vanadium, and Arsenic data. Highest concentrations of Manganese were associated with the SW cluster which is found to be significantly different from all but the neighboring W cluster. This indicates that industrial regions of the Midwest and Great Lakes are significant sources for Mn pollution at the Whiteface Mountain. Highest concentrations of Vanadium at this site are associated with the NE cluster, which is found to be not significantly different from its southern neighbor, the SE cluster, but it is significantly different from its northern neighbor, the N cluster. Both NE and SE clusters are associated with trajectories coming from the oil-burning region of the Northeast, indicating that this region is a significant source of V. Highest concentrations of Arsenic are associated with the CL and NW clusters, which originate from the Sudbury and Noranda regions of Canada, suggesting that smelters in these regions are significant sources for arsenic pollution at the Whiteface Mountain. Results consistent with those obtained at the Whiteface Mountain are found when applying the trajectory-clustering-MCP methodology to toxic trace elements measured at Ringwood, New Jersey. Significantly higher concentrations of selenium are associated with southwesterly flows (coming from the Midwest), highest concentrations of manganese are associated with westerly flows (from Midwest and Great Lakes regions), and high concentrations of vanadium are associated with air flows from the Northeast. Arsenic clusters at this site are not significantly different from each other.

Table 1 (from Brankov et al., 1999). Results of the trajectory clustering analysis for selenium at Whiteface Mountain. Asterisks in a given column indicate clusters that are not found significantly different from each other.			
Cluster Name	Homogeneous Groups		
South (S)	*		
Southwest (SW)	*		
Close (CL)		*	
West (W)		*	*
Southeast (SE)			*
Northwest (NW)			*
Northeast (NE)		*	*
North (N)			*

As in any test of significance, it is important to remember that equality of groups is not demonstrated when a statistical test fails to reject the null hypothesis. Also, statistical inferences from real-world data should always be assisted by an understanding of the underlying problem. Here, we were concerned with the

comparison of pollutant concentration clusters associated with trajectory clusters and to identify potential pollutant source regions for toxic pollutants. For neighboring trajectory clusters, which are adjacent to each other and perhaps partially overlapping, no significant difference between their concentration levels can be understood and explained, as they can be bringing pollution from the same source region. For non-neighboring clusters, "no significant difference" does not imply equality of pollution levels and it certainly does not imply pollution transport from the same source region. In addition, one has to be aware of the uncertainties involved in the trajectory calculations as well as of the sensitivity of the statistical procedure to various factors like those examined above.

Athanassiadis and Rao (2003) further examined the role of the synoptic-scale systems to the accumulation of trace elements in the northeastern U.S., identified the characteristic spatial scales involved in the pollutant transport, and determined source-receptor relationships. To this end, trace elemental concentrations (Al, As, Br, Cr, Fe, K, Mg, Mn, Na, Se, Ti, V, Zn, and Hg) of atmospheric fine particles measured from the three networks in the Northeast, with sampling periods varying between 1988 and 1998, were analyzed. These three networks (NPS/IMPROVE, NESCAUM, and ESEERCO) covering 18 sites in the Northeast measured daily 24-hr period $PM_{2.5}$ mass concentrations ($\mu g\ m^{-3}$ of air), 2-3 times a week, for different periods during 1988 to 1998. Chemical analysis of the samples was performed by independent university laboratories. X-ray fluorescence was used for NPS and NESCAUM, and instrumental neutron activation for ESEERCO. Thirteen species (Al, As, Br, Cr, Fe, K, Mg, Mn, Na, Se, Ti, V, and Zn) were selected because all 18 sites had available data for them to perform spatial analysis. In addition, particulate Hg was measured by ESEERCO at 5 sites in NY. Athanassiadis et al. (2003) analyzed particulate mercury associated with $PM_{2.5}$ rather than vapor phase mercury because it can be used in source identification and apportionment studies because of its limited atmospheric residence time and low natural background levels compared to vapor phase mercury. The atmospheric concentrations ($ng\ m^{-3}$ of air) of certain elements (Br, Fe, K and Zn) were relatively high and easily detected, but the levels of some others (As, Mg, Mn, Se, and V) were often too low to be measured precisely, and were reported as "below detection limit" (BDL).

One method for determining spatial scales for the pollutants is based on the correlation coefficients between same day measurements of a particular species at station pairs. These scales provide the distances from a given monitor that pollutant concentrations might be predicted with confidence. Athanassiadis and Rao (2003) generated a spatial correlation matrix (18×18 station pairs) for each trace element, using the weather-fluctuation-related short-term component of the data. The sample size for the correlations is on the order of 50 to 500 for censored elements, 500 to 1000 for uncensored. Then, the spatial correlation coefficient is plotted against the distance of site pairs for 13 trace elements. It should be noted that the sites considered were in general along the SW to NE orientation, which is the prevailing wind direction in the Northeast. Plots for all 13 elements show a larger variation (spread) of the correlations for any distance as compared to the results

reported by Civerolo et al. (2003) for O₃ or total PM_{2.5}. A plausible explanation might be that in addition to being chemical components with low concentrations of total PM_{2.5} as measured by 3 different networks, trace elements exhibit unique and spatially inhomogeneous sources of emissions in a region, affecting the site-specific concentrations and therefore, their spatial correlations.

Athanassiadis and Rao (2003) also showed that the scatter plots for some species (Al, Br, Fe, K, Na, Ti, and Zn) showed one lobe well separated from the main cloud. The data for these species are characterized by low or no censoring. The lobe consists of data points with very low correlation coefficients at small distances. The lobe is not present or well defined for species with highly censored data. A subsequent analysis for one of the elements (K), revealed that these data points correspond to pairs of ESEERCO sites and their surrounding NPS or NESCAUM sites. Therefore, differences due to location are ruled out. Since K data are uncensored, a difference in measurement/sample analysis techniques between ESEERCO and the other networks might be the plausible explanation for the lobe. This demonstrates the importance of insuring uniformity in air pollution data acquisition monitoring methods. Thus, this statistical method is useful in discerning inconsistencies between different monitoring networks.

The decay of the correlation coefficient with distance is approximated by an exponential function. The e-folding distance (defined as the distance by which the correlation falls to the value of 1/e) is often termed as the spatial scale for the pollutant. The spatial scales for most elements (Al, Br, Fe, K, Na, Se, Ti, and Zn) were found between 200 and 400 km (Table 2), and an example is provided for Fe (Figure 3).

Table 2 (from Athanassiadis and Rao, 2003): E-folding spatial scales for various trace elements.

Element	Spatial Scale (km)
Al	400
As	150
Br	350
Cr	<100
Fe	350
K	200
Mg	<100
Mn	150
Na	200
Se	350
Ti	250
V	100
Zn	300

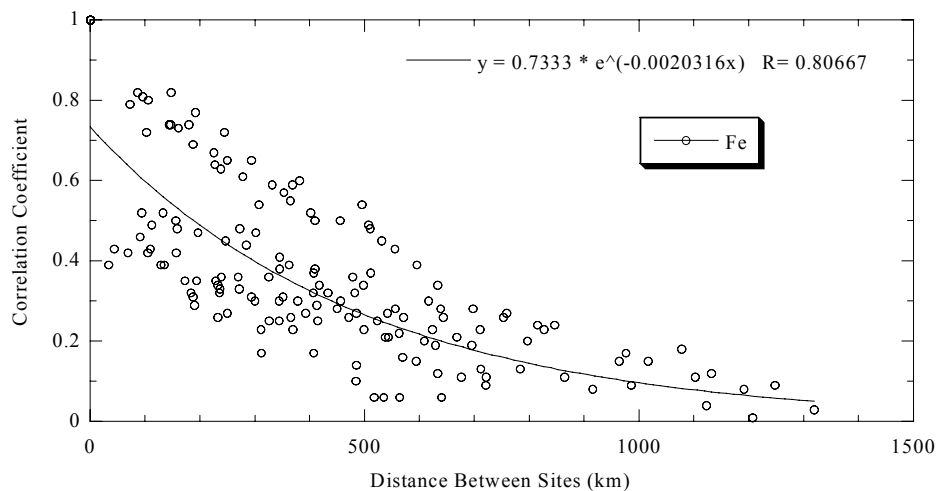


Figure 3 (from Athanassiadis and Rao, 2003): Correlation coefficient between short-term components of Fe as a function of distance.

These scales show that trace elemental concentrations can be predicted up to distances of about 350 km from a given monitor. When the amount of censoring is more than about 50%, the spatial scales are less than 200 km (As, Cr, Mg, Mn, and V) implying that the information on synoptic-scale forcing (spatial scales) can be lost when data are highly censored.

A species correlation matrix (13×13 trace elements here) at a particular site can be useful for determining the commonality of sources in a region affecting the receptor. High correlation between short-term components of two elements suggests they were carried together in the same air mass, indicating commonality of sources for these elements. Thus, Athanassiadis and Rao (2003) investigated the uniformity of the correlation between trace elements at different sites in the northeastern U.S. to further assess the regional nature of these pollutants. For this analysis, the short-term data (weather-related variations) from 5 sites in NY were selected. These data came from the ESEERCO network (1991-1993), with site distances of up to 500 km, and are reported uncensored. Results for Moss Lake are presented in Table 3. By comparing all 5 matrices for NY, it can be seen that there is an excellent uniformity of the species correlation pattern among the sites, suggesting similar pollutant relationships within a 500 km-diameter area. The number of element pairs (out of possible 78) with correlation $R \geq 0.6$ is found between 10 and 16 for 4 of the sites, 21 for Perch River. In particular, Zn correlates well ($R \geq 0.6$) with As, Br, Fe, Mn, and Se at all 5 sites. Four of the above elements As, Br, Se, and Zn are highly correlated with each other at all 5 sites in NY. It is suspected that their sources are either the same or next to each other. Other elements with high correlated pairs include Fe, Mn, and V. Mercury was uncorrelated with the other elements ($0.3 < R < 0.5$ with As, Fe, Mn, and Zn at 4 out of 5 sites).

Table 3 (from Athanassiadis and Rao, 2003): Species short-term correlation matrix for Moss Lake, NY (1991–1993)

	Al	As	Br	Cr	Fe	K	Mg	Mn	Na	Se	Ti	V	Zn	Hg
Al	1	0.42	0.5	0.24	0.59	0.39	0.5	0.63	0.61	0.38	0.45	0.51	0.5	0.29
As	0.42	1	0.63	0.31	0.57	0.48	0.31	0.62	0.34	0.68	0.3	0.41	0.63	0.47
Br	0.5	0.63	1	0.27	0.58	0.5	0.31	0.71	0.47	0.64	0.27	0.51	0.67	0.29
Cr	0.24	0.31	0.27	1	0.32	0.2	0.22	0.3	0.21	0.23	0.18	0.21	0.3	0.24
Fe	0.59	0.57	0.58	0.32	1	0.49	0.46	0.7	0.47	0.61	0.33	0.48	0.64	0.34
K	0.39	0.48	0.5	0.2	0.49	1	0.39	0.58	0.4	0.53	0.27	0.42	0.56	0.28
Mg	0.5	0.31	0.31	0.22	0.46	0.39	1	0.42	0.47	0.25	0.35	0.3	0.34	0.24
Mn	0.63	0.62	0.71	0.3	0.7	0.58	0.42	1	0.51	0.67	0.35	0.6	0.73	0.39
Na	0.61	0.34	0.47	0.21	0.47	0.4	0.47	0.51	1	0.29	0.27	0.48	0.43	0.18
Se	0.38	0.68	0.64	0.23	0.61	0.53	0.25	0.67	0.29	1	0.28	0.48	0.69	0.42
Ti	0.45	0.3	0.27	0.18	0.33	0.27	0.35	0.35	0.27	0.28	1	0.3	0.35	0.18
V	0.51	0.41	0.51	0.21	0.48	0.42	0.3	0.6	0.48	0.48	0.3	1	0.53	0.28
Zn	0.5	0.63	0.67	0.3	0.64	0.56	0.34	0.73	0.43	0.69	0.35	0.53	1	0.36
Hg	0.29	0.47	0.29	0.24	0.34	0.28	0.24	0.39	0.18	0.42	0.18	0.28	0.36	1

Back trajectories have been used successfully for the identification of potential pollution source regions and atmospheric patterns associated with the long-range transport of trace-level air contaminants. Athanassiadis and Rao (2003) selected New York State receptor sites for the following reasons: (1) most of the data were reported as not missing, and collected by one network (ESEERCO) at remote locations throughout NY; (2) back-trajectories were available from Whiteface Mountain, NY from a previous study; (3) factor analysis results for New York receptor sites could be used for source identification; and (4) the species correlation pattern was very similar at all 5 sites, triggering further investigation. The trajectory-clustering methodology applied has been used by Brankov et al. (1999) for source-receptor relationships using NESCAUM trace element data (1988-1993) from Whiteface Mountain, NY as described above. The 3 day back-trajectories from the HYSPLIT model were grouped according to their direction leading to 8 clusters (named: N, NW, CL, W, SW, S, SE and NE), each associated with pollutant transport from a different source region. The letters CL stand for "close" shorter trajectories ending in Canada at the NW direction from New York. Since only 2 years of pollutant data were available (about 300 measurements per site), it was decided for this study to incorporate the 3 sites in the Adirondacks region (Moss Lake, Perch River, and Willsboro) as one

receptor area for the trajectory analysis, to increase the sample size confidence in the statistical results; these sites have similar pollutant concentration distributions. It is important that seasonality and long-term trends are filtered out from the pollutant time series before cluster segregation, since only the short-term component contains weather-induced variations that relate to the synoptic-scale transport. The short-term component of the time series data used by Athanassiadis and Rao (2003) has a mean of zero (as expected), and a median of almost zero. After cluster segregation, a positive median indicates that higher levels of the pollutant are associated with that air flow pattern (positive forcing).

Results of this analysis (Figure 4, Table 4) show that positive forcing for Zn is associated with SW and CL flows, negative with the NE cluster. The results illustrate that relatively high concentrations of most anthropogenic trace elements in the Adirondacks region of New York are associated with southwesterly winds from the midwestern U.S. (SW), and short northwesterly winds from Canada (CL). Two interesting exceptions are Br and V, with additional strong sources from the north (N) and the southeast (SE), respectively. High medians (in log units) were found for Al, As, Br, Mn, Se, V, and Zn. Except Al, these elements were also found to correlate well with each other in New York. Also, the spatial scale of about 350 km for Br, Se, and Zn was among the highest as discussed above.

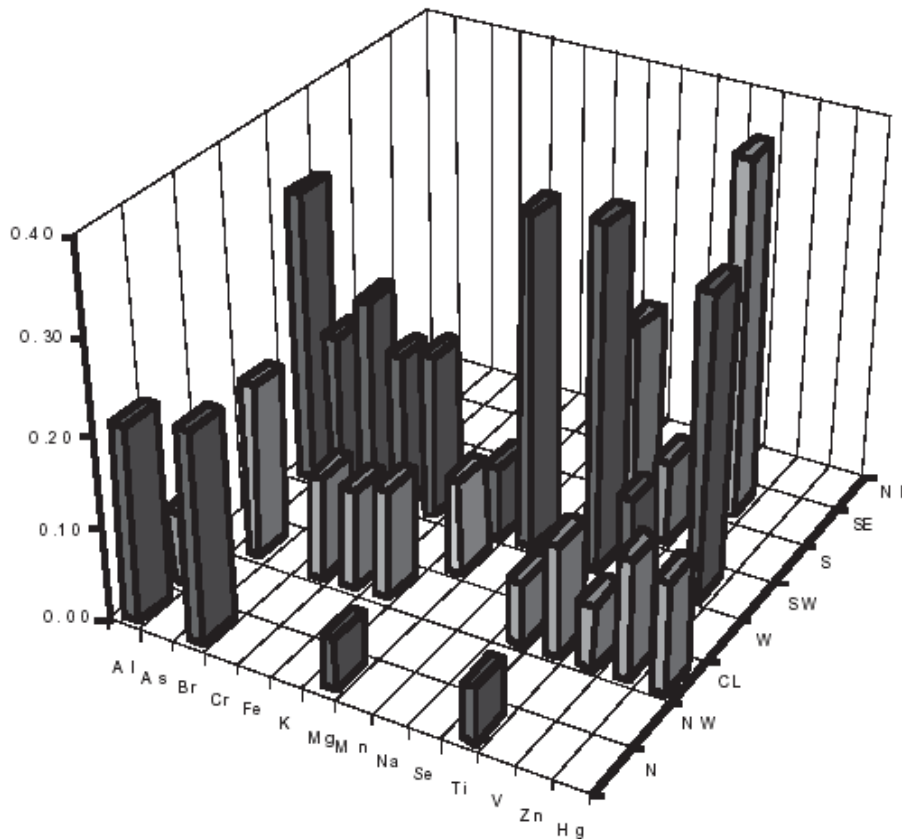


Figure 4 (from Athanassiadis and Rao, 2003): Short-term median (log e scale) for positive forcing of trace elements associated with the trajectory clusters for Adirondacks, NY.

Table 4 (from Athanassiadis and Rao, 2003): Sources of trace elements impacting the Adirondacks region of NY

Element	Cluster	Source Regions and Sources of Pollution
As	CL	Canadian Smelters
	SW	U.S. Regional (Coal Combustion)
Br	N	Canadian Regional
	SW	U.S. Regional (Mixed Sources)
Se	CL	Canadian Industrial Areas
	SW	U.S. Regional (Coal Combustion)
	S	Coal Combustion, Industrial Urban
Zn	CL	Canadian Industrial Areas
	SW	U.S. Regional (Mixed Sources, Iron/Steel Works)
Fe	CL	Canadian Industrial Areas
	SW	U.S. Regional (Mixed Sources, Iron/Steel Works)
Mn	SW	U.S. Regional (Mixed Sources)
V	CL	Canadian Oil-Related Industrial Areas
	SE	N.E. Oil Combustion, Industrial Urban
Hg	CL	Canadian Cu-Smelters
	SW	U.S. Regional (Coal Combustion)

The trajectory-clustering analysis helped identify the source regions and the air flow patterns associated with the relatively high levels of trace elements at the Adirondacks. Results further indicate specific industries in Canada (northwest of New York) and the mid-western U.S. are major sources of elemental pollution in the Adirondacks. Higher levels of As come from Canadian smelters; Se from coal combustion in the Midwest; Br, Zn, Fe, and Mn from mixed industries in the Midwest and some in Canada. Vanadium is oil-related from the Northeast and Canada, while Hg is transported from Canadian Cu-smelters and midwestern coal combustion industries. These findings agree with those by Brankov et al. (1999) who used NESCAUM's 5-year data. Thus, these gross source-receptor relationships can be determined regardless of which network collected the data.

The Hg raw data (1992-1993) for all the sites in New York show a sharp decline of Hg concentrations starting around February 1993, not observed in any other element. To examine whether the lower concentrations were due to reductions in Hg emissions at some major source, Athanassiadis and Rao (2003) applied the trajectory-clustering methodology separately for 1992 and 1993. The results for 1992 indicate significant contribution from the Canadian smelters (CL cluster), and the midwestern U.S. coal-fired power

plants (SW cluster), both major sources of Hg in New York. For 1993 however, the only positive forcing is associated with the S cluster, while the CL forcing is much smaller. This difference could be attributed to year-to-year changes in weather system movements. Since the percentage of Hg data points in each cluster (except W and SE) is about the same from one year to the next, the lowering of Hg levels associated with the CL flow pattern must have been induced by the reduction in Hg emissions at the Canadian Cu-smelting facilities.

Section 2

ANALYSIS OF OZONE EXCEEDANCE DAYS IN THE NORTHEAST WITH A SPECIAL EMPHASIS ON LAND-ATMOSPHERE INTERACTIONS AND BOUNDARY-LAYER PROCESSES

ANALYSIS OF BOUNDARY-LAYER CHARACTERISTICS AND THEIR IMPACT ON GROUND LEVEL OZONE CONCENTRATIONS

It is well known that the evolution of the planetary boundary-layer plays a crucial role in determining the afternoon ozone concentrations. As part of this research project, both observations and model predictions were analyzed in an effort to describe the boundary-layer characteristics and their impact on the ground-level ozone concentrations. A study of the temporal and spatial variations of the mixing layer height over the Ozone Transport Region of the northeastern United States for the summer of 1995 was presented by Berman et al. (1999) using meteorological data obtained from the North American Research Strategy for Tropospheric Ozone-Northeast (NARSTO-NE) 1995 field program. Rawinsonde balloon soundings made every 4 h during 13 ozone episode days during NARSTO-NE provided the principal source of upper-air data, supplemented by virtual temperature profiles from five radio acoustic sounder system sites. Forty-four weather stations provided the surface-level data. The daytime mixing depths were estimated with the profile-intersection technique (Holzworth, 1967). The height of the surface inversion was used as a measure of the depth of the turbulent boundary layer at night. For the 13 ozone episode days, the average maximum mixing depth ranged from less than 500 m offshore to greater than 2000 m inland, with most of the increase occurring within the first 100 km of the coastline. The coefficient of variation of maximum mixing depths averaged over the 13 episode days varied from 0.65 at coastal stations to 0.19 at inland locations. Greater variability along the coastline may be caused by the interplay of sea-breeze circulations with synoptic wind patterns there. The rate of growth of the mixing depth between 0600 and 1000 EST averaged 165 m/hr for all stations, ranging from 20–60 m/hr at coastal sites to more than 350 m/hr at inland stations. Ventilation coefficients were about 50% lower on ozone episode days than on nonepisode days from 0700–0900 EST (Figure 5). For the ozone episode of 13–15 July 1995, a comparison was made of mixing depth estimates from three different methods: rawinsonde virtual potential temperature profiles, C_n^2 (the atmosphere's refractive index structure parameter), and output from running the Fifth-Generation Pennsylvania State University–National Center for Atmospheric Research Mesoscale Model version 1 (MM5v1) (Grell et al., 1994), a widely used nonhydrostatic mesoscale model. Estimates obtained from the three methods varied by as much as 200 m at night and by up to 500 m during the daytime. Mixing depths obtained from running MM5 were in good agreement with estimates from the other methods at Gettysburg, Pennsylvania, an inland station, but were 10%–20% too low at New Brunswick, New

Jersey, a location within 30 km of the Atlantic coast. The discrepancy may be caused by the model's 12-km grid spacing being too coarse to locate the marine–continental airmass boundary with high precision.

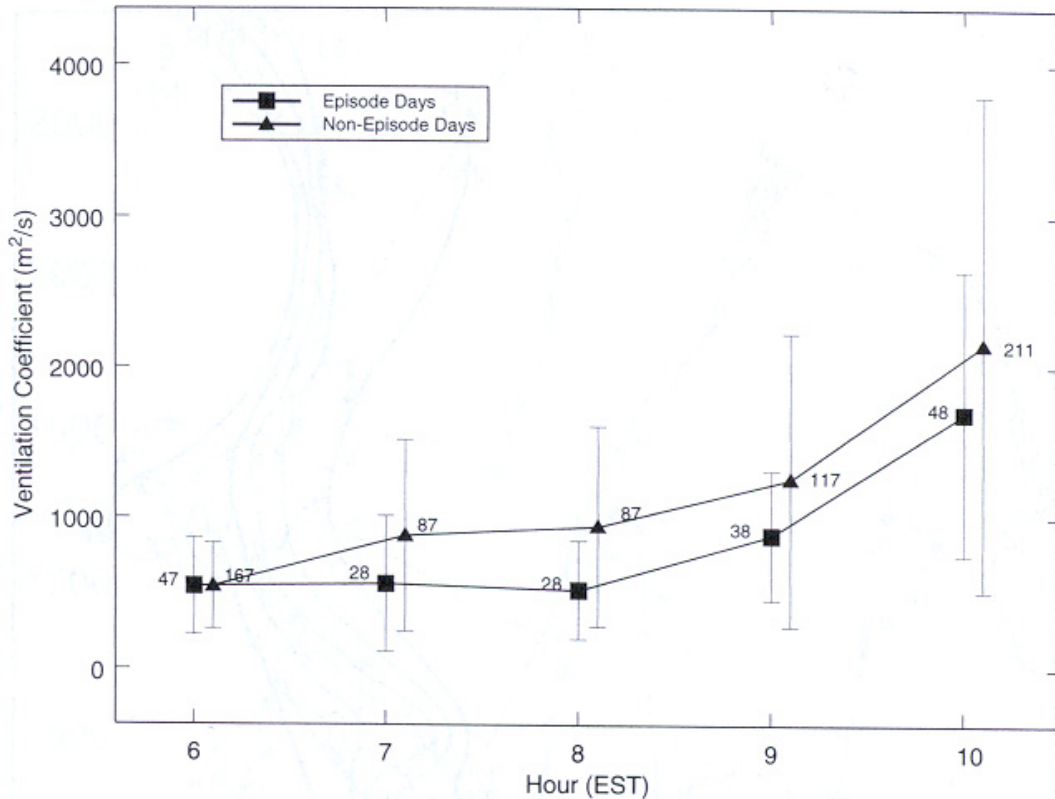


Figure 5 (from Berman et al., 1999): Average hourly ventilation coefficients for episode and non-episode days from 0600 – 1000 EST for June 15 to August 31, 1995, obtained from RASS profiles. The number of values used to calculate each average is given for each point.

Meteorological fields from the MM5v1 mesoscale model were further used to prepare a comprehensive analysis of summertime (June 2 - August 30, 1995) mixing heights and ventilation coefficients for the eastern United States. Ventilation coefficients can be defined as the product of the mixing height and the wind speed vertically averaged over the depth of the mixing height. These results were reported by Rao et al. (2003). It was found that in general, mixing heights were higher on high ozone days than on low ozone days with the largest differences occurring in the afternoon hours. Regionally, differences in the mixing height between high and low ozone days were largest over the Midwestern states with much smaller differences found along the Great Lakes and Atlantic seaboard. Sea- and bay-breeze circulations bringing cooler marine air inland may partly be responsible for the smaller differences seen there. Cloud cover during the morning and afternoon hours averaged 0.15 (i.e. 15% of the sky) over most of the eastern United States on high ozone days, but was

twice as large (0.30) on low ozone days. On high ozone days, analysis of surface wind observations showed a core of minimum speed (1-2 m/s) centered over Kentucky and Tennessee, increasing to 4 m/s located ~750 km out from the center. On low ozone days, wind speeds were 1-2 m/s higher overall, and showed little spatial variation. Ventilation coefficients tended to be about 50% lower in the Midwest on high ozone days than on low ozone days (Figure 6). Other regions showed large variability. The Northeast region displayed a complicated spatial pattern, probably a result of complex topography and vigorous synoptic-scale circulations that frequent the region. Slightly higher ventilation coefficients on high ozone days were also seen along the southeastern coast, perhaps due to higher winds associated with sea-breeze circulations.

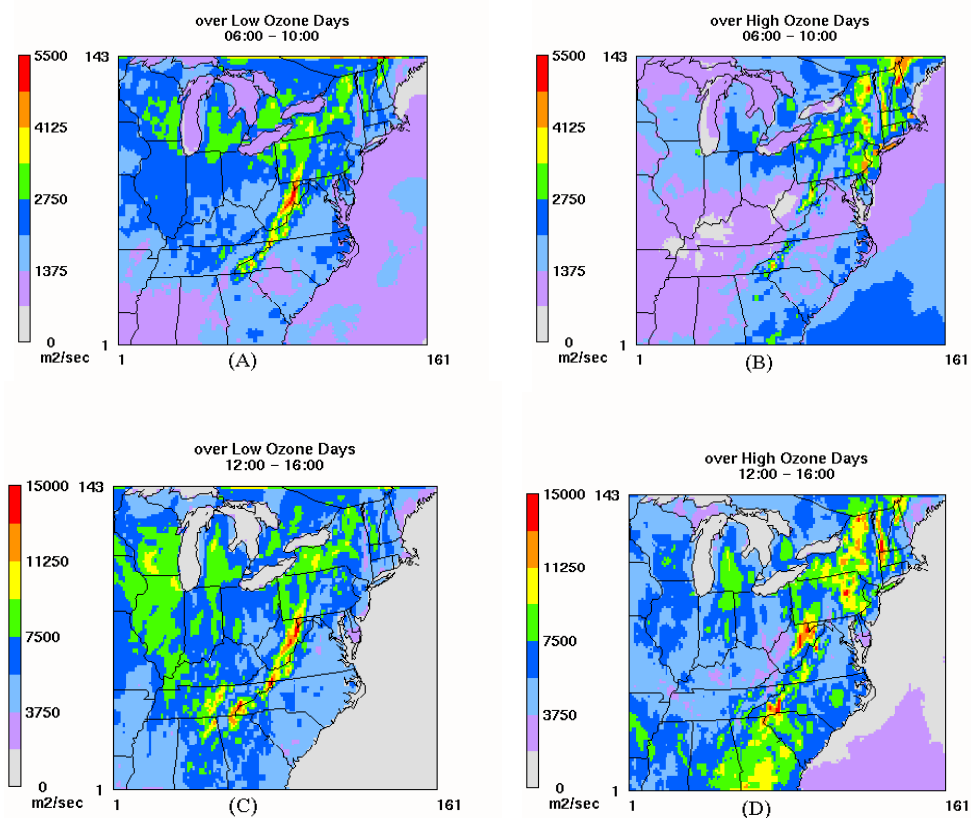


Figure 6 (from Rao et al., 2003): Averaged ventilation coefficient (m^2/s) for morning and afternoon hours on low and high ozone days.

The characteristic low cloud cover (Figure 7), light wind speeds, and large daytime mixing heights seen on high ozone days is consistent with a large surface anticyclone centered over the mid-south near Kentucky and Tennessee (Vukovich, 1995). An examination of surface weather maps for the summer of 1995 shows anticyclonic pressure systems commonly occurring over the eastern United States on high ozone days.

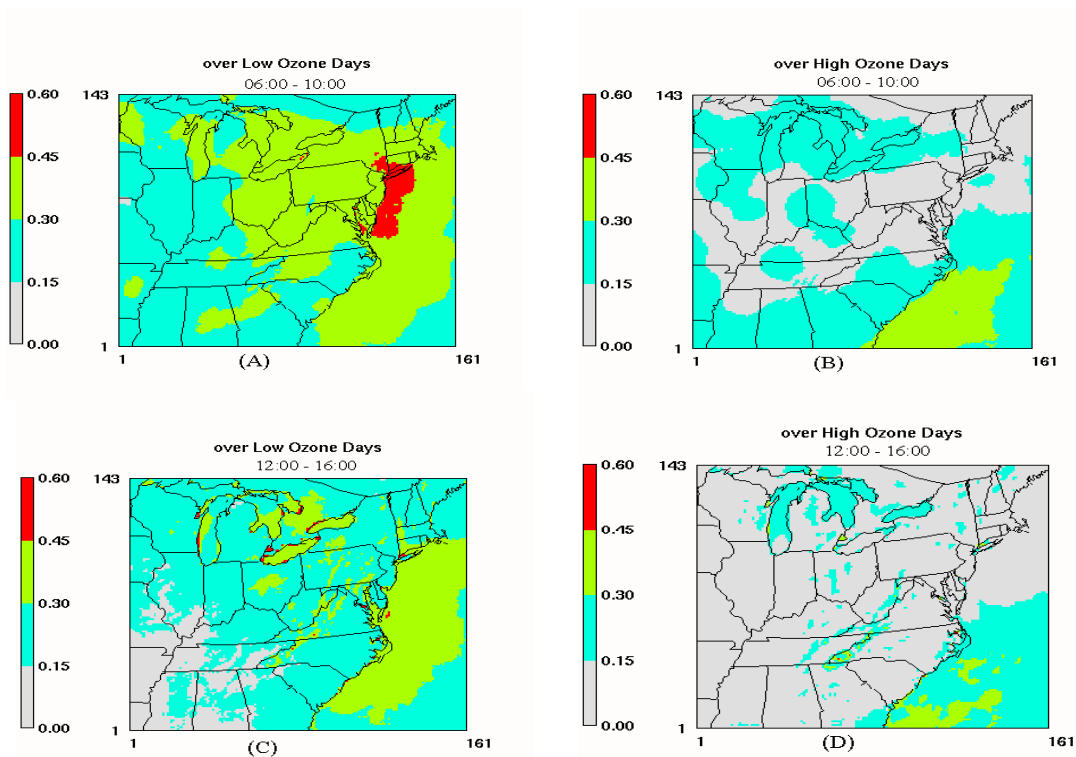


Figure 7 (from Rao et al., 2003): Averaged cloud cover (in tenths) for the morning and afternoon hours on low and high ozone days.

These anticyclones tend to be centered over the south-central states. More disturbed synoptic weather patterns (e.g., low pressure, fronts, greater cloud cover, precipitation areas) occur more frequently on low ozone days.

Zhang and Rao (1999) analyzed aircraft measurements taken during the North American Research Strategy for Tropospheric Ozone-Northeast (NARSTO-NE) field study. Their analysis revealed the presence of ozone concentration levels in excess of 80 ppb on a regional scale in the nocturnal residual layer during ozone episodes. The air mass containing increased concentrations of ozone commonly is found on a horizontal spatial scale of about 600 km over the eastern United States. The diurnal variation in ozone concentrations at different altitudes, ozone flux measurements, and vertical profiles of ozone suggest that ozone and its precursors trapped aloft in the nocturnal residual layer can influence the ground-level ozone concentrations on the following day as the surface-based inversion starts to break up. A simple one-dimensional model, treating both meteorological and chemical processes, has been applied to investigate the relative contributions of vertical mixing and photochemical reactions to the temporal evolution of the ground-level ozone concentration during the daytime. Zhang and Rao (1999) demonstrated that the vertical mixing process contributes significantly to the ozone

buildup at the ground level in the morning as the mixing layer starts to grow rapidly (Figure 8). When the top of the mixing layer reaches the ozone-rich layer aloft, high ozone concentrations are brought down into the mixing layer, rapidly increasing the ground-level ozone concentration because of fumigation. As the mixing layer grows further, it contributes to dilution while the chemical processes continue to contribute to ozone production. Model simulations also were performed for an urban site with different amounts of reduction in the ground-level emissions as well as a 50% reduction in the concentration levels of ozone and its precursors aloft. The results revealed that a greater reduction in the ground-level ozone concentration can be achieved by decreasing the concentrations of ozone and precursors aloft than that can be achieved from a reduction of local emissions. Given the regional extent of the polluted dome aloft during a typical ozone episode in the northeastern United States, these results demonstrated the necessity and importance of implementing emission reduction strategies on the regional scale; such region-wide emission controls would reduce effectively the long-range transport of pollutants in the Northeast. The results reported by Zhang and Rao (1999) have been used in the National Academy of Sciences's report on the ozone forming potential of reformulated gasoline (NRC, 1999).

Athanassiadis et al. (2002a and b) have analyzed the observations and MM5v3 model predictions for July 1999. A comparison of daytime mixing height estimates using hourly MM5v3 output profiles, with the parcel, bulk Richardson number, and MM5v3 methods, was made at Philadelphia, PA. In the parcel or Holzworth method (Holzworth, 1967), the virtual potential temperature θ_v at the surface is extrapolated adiabatically upward until it intersects the θ_v profile obtained from the model output. Thus, the mixing height is taken as the equilibrium level of an air parcel with this temperature. The second method for estimating the mixing height from profile data is based on the bulk Richardson number (Ri_b). The mixing height was chosen as the height where Ri_b reached a critical value Ri_c . The critical values of 0.25 (theoretical) and 0.7 (to account for thicker upper-level model layers) were selected in this study of daytime convective boundary layer evolution. In general, the bulk Richardson number mixing height is ~10% higher than that of the parcel method and at least 25% higher than MM5v3.

The maximum value of the mixing height growth rate of ~450 m/h occurred from 0700 to 0900 EST, when the rate of increase in the ground-level O₃ concentration was also maximum (~8 ppb/hr⁻¹), indicating that entrainment of air from the O₃-rich residual layer trapped aloft is as important in the morning as photochemical production later in the day. The daily maximum mixing heights were almost 50% larger on episode days than on non-episode days. At 0800 EST, however, ventilation coefficients were about 30% lower on episode days than on non-episode days, due to slower surface winds (less mixing) at that time. The results of Athanassiadis et al. (2002a and b) lend further support to the findings reported by Zhang and Rao (1999) and Rao et al. (2003).

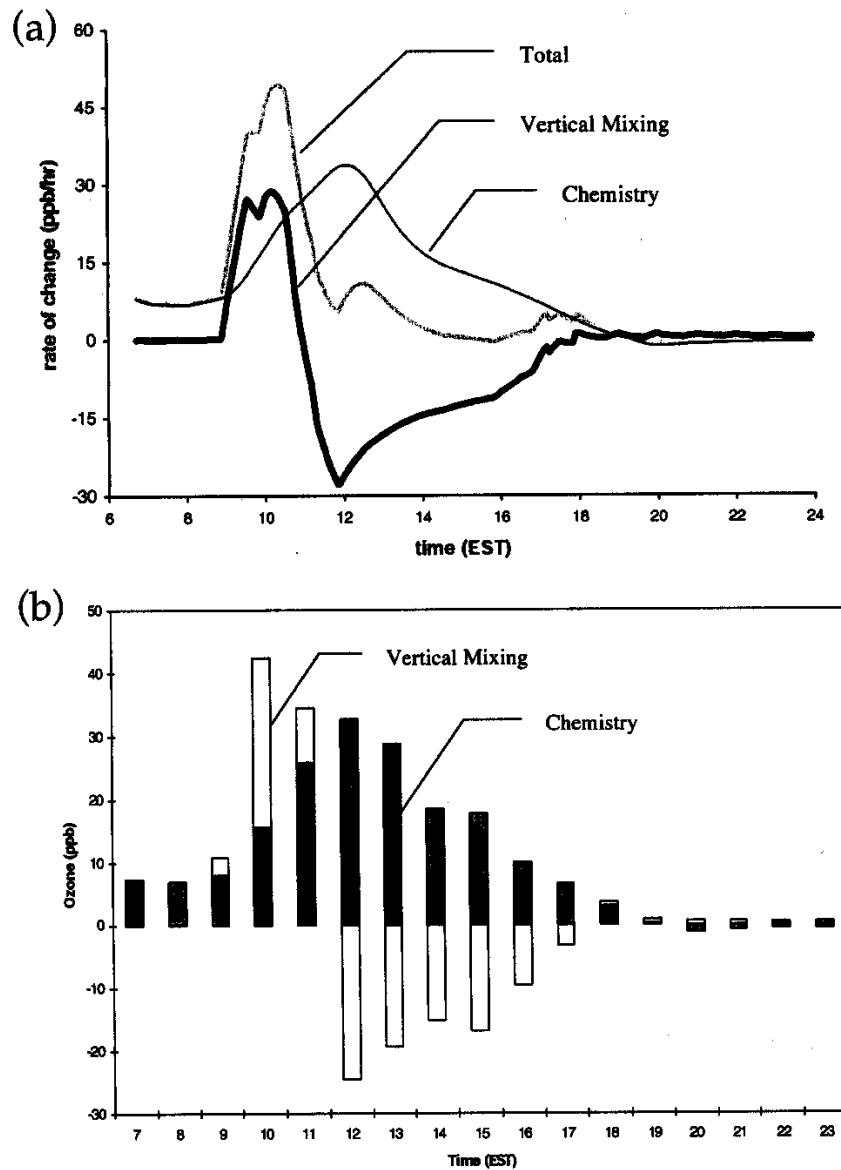


Figure 8 (from Zhang and Rao, 1999): (a) Rate of change in the ground-level ozone concentration for 14 July 1995. The thick dark line indicates the contribution from the vertical mixing process, the thin solid line represents the chemical contribution, and the gray line is for the total rate of change; (b) contributions from vertical mixing and chemical reactions to the ground-level ozone concentration within 1-hr intervals for 14 July 1995.

IMPACT OF BOUNDARY-LAYER PARAMETERIZATIONS ON MODEL PREDICTIONS

Meteorological and photochemical simulations were performed for July 1999 for the purpose of comparing different methods of boundary-layer estimation and mixed layer parameterization, investigating the nocturnal low-level jet (LLJ) phenomenon, and for determining the impact of these phenomena on the

prediction of ground-level pollutant concentrations and the efficacy of emission control strategies. These simulations have been described in detail in Zhang et al. (2001) and Ku et al. (2001). For these simulations, the MM5v3 mesoscale meteorological model and Community Multiscale Air Quality (CMAQ) model (Byun and Ching, 1999) were used. Model predictions were compared to observations measured by aircraft, RASS and wind profiler, lidar, and tethered balloon platforms.

A comparison of the daytime mixing height estimates from different methods using the hourly MM5 output profiles at the Baxter site revealed the uncertainty associated with adequately estimating this parameter. It was found that the mixing height growth rate reaches a maximum between 0700 and 0900 EST, when the rate of increase in ground-level O₃ concentration was also maximum, indicating the importance of entrainment of air from the O₃-rich residual layer trapped aloft. Again, the daily maximum mixing heights were larger on high ozone episode days than on non-episode days. The observations tend to support the non-local mixing parameterization better than the layer-to-layer eddy diffusion in the convective PBL. It was also shown that the choice of data assimilation during model execution affects the model's ability to properly simulate the evolution of the LLJ phenomenon, a region of high wind speed in the nighttime residual layer that may play an important role in regional-scale pollutant transport. The meteorological fields obtained from the two boundary-layer schemes were used to drive the photochemical model to simulate O₃ concentrations in the northeastern United States for an O₃ episodic period. In addition to large differences in the predicted O₃ levels at individual grid cells, the predicted daily maximum hourly O₃ concentration appears at different regions of the modeling domain in these simulations, due to the differences in the vertical exchange formulations used in these two schemes. An examination of the photochemical model's response to changes in the emissions inventory reveals that the choice of equally valid boundary-layer parameterizations can significantly influence the efficacy of emission reduction strategies (Figure 9). Based on the results of this study, the EPA released a new version of the meteorological preprocessor MCIP (available online at <http://www.cmascenter.org>), allowing for the direct passage of the meteorological fields to the photochemical model rather than re-diagnosing the PBL variables to help improve CMAQ's performance in reproducing the observed pollutant concentration fields.

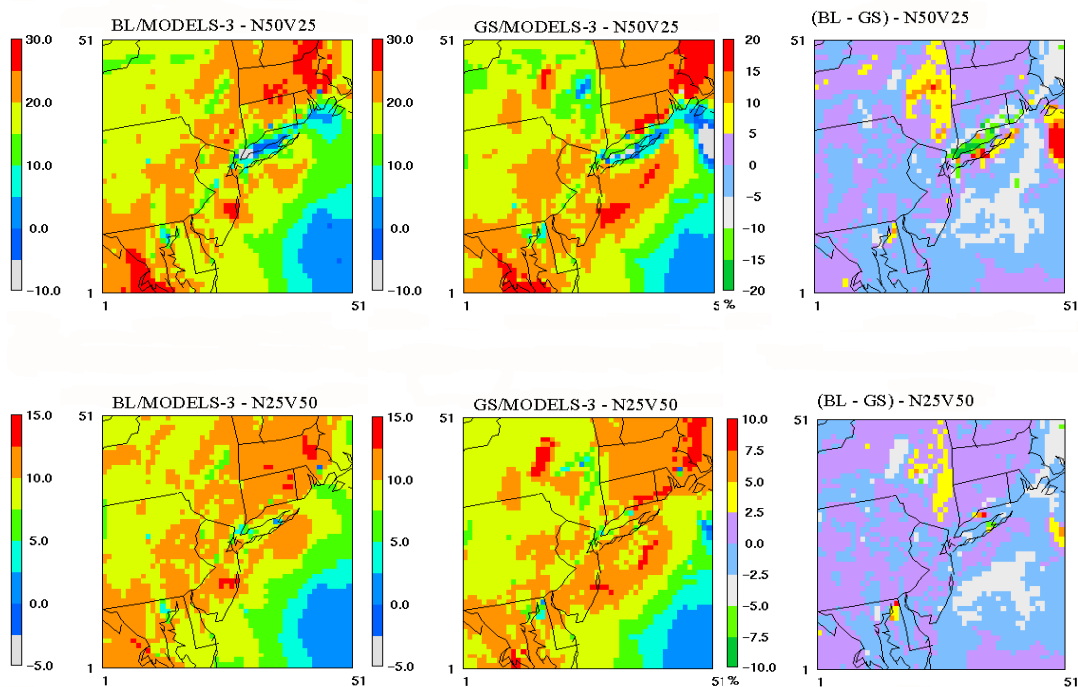


Figure 9 (from Ku et al, 2001): The differences (“BL minus GS”) in the index of improvement of daily maximum 1-hour O₃ concentrations, for the MODELS-3 re-diagnosed simulations. The two emissions control scenarios are NO_x-focused (NO_x reduced by 50% and VOC reduced by 25% denoted as N50V25) or VOC-focused (NO_x reduced by 25% and VOC reduced by 50% denoted as N25V50). The upper panels correspond to the N50V25 case, and the lower panels correspond to the N25V50 case.

METEOROLOGICAL EFFECTS OF CHANGING LAND-USE PATTERNS

A critical component in an assessment of air quality is the need to predict the spatial and temporal evolution of the pollutant plumes over a given modeling domain. Toward this end, meteorological models with associated post-processors have been applied to historical periods to develop the meteorological fields needed for air quality models. In these applications, air quality scenarios for a future year were simulated on the basis of historical meteorological data, without any adjustments to the land-use/land-cover patterns even though changes in projected emissions were included. However, analysis of the US Census Bureau and Federal Highway Administration demographic data compiled over the past several decades identifies more than 30 metropolitan areas and surrounding hinterlands threatened by sprawl. Over the past three decades, population densities in large cities such as Baltimore, MD and Washington, DC have decreased dramatically. At the same time, the rate of development of open spaces in the outermost suburbs and beyond continues to increase, in some areas by 50–90% in this decade alone. Thus, land-use needs to be viewed as a dynamic variable.

Meteorological and air quality models require, among other inputs, terrain features and surface characteristics that differ by their land-use/land-cover patterns. It is well known that surface parameters such as moisture availability and longwave emissivity are critical to the transfer of heat and water vapor in the boundary layer and to predicting local temperature and wind fields in the meteorological models. Similarly, surface parameterizations are important inputs to the photochemical models that define the grid cells in terms of deposition, diffusivity and dispersion characteristics. As an example, vegetation can have a significant effect on the local environment by transpiring water vapor, changing surface deposition velocities, intercepting solar radiation, altering surface wind patterns, and retaining heat less efficiently than impervious human-made surfaces. Also, trees emit a variety of hydrocarbons including highly reactive isoprene. All of these effects, in turn, have implications for pollutant formation and removal. Therefore, we examined the effects of urban vegetation on biogenic emissions, ozone levels, and meteorological parameters. The results were published in Civerolo et al (2000) who addressed the changes in the meteorological fields due to changes in the land-use patterns. The meteorological model selected for this application was the non-hydrostatic, prognostic Penn State/NCAR mesoscale model, MM5 Version 1. The model domain, with a horizontal grid spacing of 4 km on the Lambert-conformal grid projection, included the major urban areas of Washington, DC; Baltimore, MD; Philadelphia, PA and Camden, NJ; New York City, NY and surrounding metropolitan area; Hartford, CT; and Albany, NY. In the MM5 modeling system, each grid cell is assigned one land-use based upon the dominant category in that grid cell. Of the 13 land-use types in the model, six categories – urban land; agriculture; deciduous forest; mixed forest and wetland; water; and marsh or wetland – fully described the entire domain, with 33.1% classified as water, and less than 3% as urban land. The largest non-water-based category is deciduous forest (29.3%). Each land-use category has six different surface parameterizations – albedo, moisture availability, emissivity, roughness length, thermal inertia, and surface heat capacity per unit volume – based on representative values from the literature.

To simulate the effects of increased vegetation on the meteorological fields, 40% of the urban land grid cells were reclassified as deciduous forest, the dominant vegetation type in the domain. This reclassification changed 189 of the 473 urban land grid cells across the domain. The rationale for the selection of the 189 grid cells was based on: (a) cells could not contain existing airports or anthropogenic sources with stack heights >65 m, and (b) cells along the peripheries of the metropolitan areas were selected more frequently, rather than only changing cells in the central business downtown areas. The base case MM5 simulation was carried out from 12 July (0700 EST) to 16 July (0100 EST), 1995, using the default land-use patterns as representative of the current land-use patterns in the Northeast. Using the same initial and boundary conditions, the modified land-use case was simulated for the same period.

To examine how large the temperature differences between the base case and modified land-use case simulations can typically be, Civerolo et al. (2000) determined the maximum cell-by-cell temperature

differences between the two model simulations in the three urban areas. In each case, the largest differences occurred about midday (± 1 h), although the maximum predicted temperatures occurred around 1400–1500 EST. Decreases in temperature ranged from about 3°C over the Baltimore region to as high as 5°C in the New York City and Philadelphia areas. These temperature decreases were often associated with grid cells having modified land-use, although the largest differences are not confined to only those grid cells at which the land-use pattern was altered.

Spatial images of temperature differences at 1500 EST on 14 July showed that temperature differences in individual grid cells range from about -4 to +3°C throughout the urban northeastern corridor domain, with large (1–4°C) decreases occurring in the urban areas. However, for this hour, the largest predicted temperature differences actually occurred downwind of New York City along the Connecticut coast (Figure 10). The land-use was unchanged in these cells, yet the temperature depression was >4°C in a few of these coastal cells, indicating again that the land-use changes can also affect surrounding grids. Local temperature depressions in grid cells with modified land-use could lead to lower wind speeds and increased stability. Along the downwind direction, this reduced ventilation and increased stability could lead to areas of reduced vertical mixing and increased surface temperatures. On 14 July (1500 EST), urban core areas tend to exhibit lower temperatures and wind speeds due to land-use modification; to the immediate north and east of these urban cells are regions of increased surface temperatures, and farther to the north and east, increases in the wind speed are evident.

The results of research reported by Civerolo et al. (2000) suggest that additional vegetation cover in urban areas could affect pollutant concentrations and dispersal, energy demand (anthropogenic emissions) and biogenic emissions in surrounding areas. Increased temperatures would tend to increase emissions, but increased wind speeds would tend to increase pollutant mixing and dispersion. The interaction of these altered temperatures and wind speeds could increase pollutant levels in some areas and decrease them in others. Because relatively small changes were made to the land-use in the modeling domain (only about 1% of the grid cells were modified), and noting that land-use is simply one of many inputs to the modeling system, changes in temperature are fairly localized but not confined to only those cells where land-use changes were made. At the urban-level, since these land-use changes can lead to fairly substantial changes in the near-surface meteorological fields, they should be incorporated in modeling of future air quality scenarios. Also, although surface temperatures and wind speeds decreased in the modified grid cells (urban land changed to deciduous forest), temperatures could actually increase downwind, potentially offsetting some air quality benefits of a large-scale simulated increased vegetation scenario. However, higher wind speeds in other areas could increase pollutant dispersion and mixing, leading to lower pollutant concentrations elsewhere.

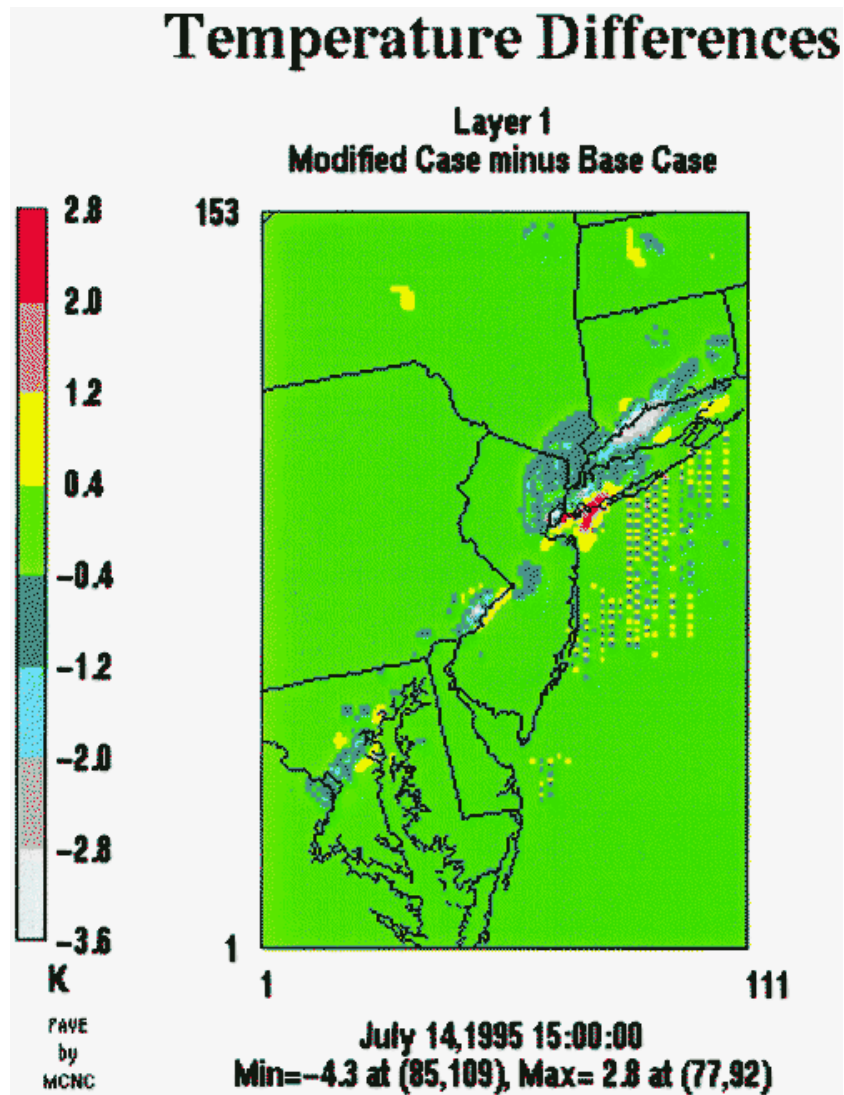


Figure 10 (from Civerolo et al., 2000): Layer 1 temperature differences, modified case minus base case, at 1500 EST, 14 July, 1995 across the entire domain.

While these results reported in Civerolo et al. (2000) suggest that one should take the changing land-use patterns into consideration when using models to evaluate changes in the predicted ozone levels stemming from various emissions reduction scenarios in urban areas, uncertainties remain about the proper characterization of land-surface interactions in atmospheric models. An area of particular interest is the treatment of subgrid-scale variability in surface parameters. As subcontractors to this research project, Drs. Kallos, Mihailovic and Alapaty have addressed these issues in detail.

PARAMETERIZATION OF LAND-SURFACE INTERACTIONS IN ATMOSPHERIC MODELS

A method was developed to generalize the calculation of the exchange of momentum between the atmosphere and a very heterogeneous surface in atmospheric models. The proposed method for estimating the wind profile over heterogeneous grid cells was compared with some earlier approaches and meteorological observations obtained during NE-OPS. This work is described in detail in Mihailovic et al. (2002a,b) and Lazic et al. (2002). Further, a scheme was developed to improve upon the method currently used in atmospheric models to calculate albedo over heterogeneous grid cells. This scheme takes into account geometrical properties of the different surface elements present in a grid cell and is described in Mihailovic et al. (2003) as well as in Appendices A and B.

The Land-Air Parameterization Scheme (LAPS) was implemented into a 1-D atmospheric boundary-layer model and evaluated utilizing the special observational data collected during summer of 1987 from the First International Satellite Land Surface Climatology Project (ISLSCP) Field Experiment (FIFE) special observations over Manhattan, Kansas. The LAPS simulation results were compared with the results obtained from using another sophisticated but relatively simpler land surface parameterization scheme (referred to as NPJS) that is already available in the 1-D model. Results from two case studies were analyzed during which boundary-layer processes dominated the lower atmospheric processes. Both the LAPS and NPJS use simple but different formulations estimating outgoing and incoming radiation fluxes resulting in minor differences in the estimated net radiation reaching the surface. We found that an underestimation of net radiation and higher stomatal resistance in LAPS may have triggered many of the differences in results between LAPS and NPJS in the first case study. In the NPJS negative sensible heat fluxes that exist after late evening hours occurred an hour before than that in LAPS and the observations. LAPS underestimated latent heat fluxes in the first case more than in the second case when compared to observations and NPJS. Trends in soil heat flux are very similar in LAPS and NPJS. In the second case only minor differences existed between respective net radiation and stomatal resistance fields, leading to similar boundary-layer structures. Diagnostic results indicate that in both cases direct evaporation fluxes are significantly different while transpiration fluxes are somewhat similar. Growth rates of and depths of atmospheric boundary-layer in both schemes are also very similar. Vertical profiles of virtual potential temperatures, water vapor mixing ratio, and horizontal winds are also found to be very similar in LAPS and NPJS. Differences in concentrations of various chemical species are mainly due to differences in depths of boundary-layer resulting from using different land surface models. There were some general features that were associated with each of the schemes in both of the simulations. Simulated direct evaporation fluxes are higher in LAPS while they are significantly lower in NPJS. Further, diurnal variation in direct evaporation fluxes is significant in NPJS while it is absent in the LAPS. Also, transpiration fluxes are lower in both the simulations in LAPS compared to those in the NPJS. In our future studies, we propose to perform sensitivity studies for further evaluation of LAPS in simulating boundary-layer structures. Finally, we

will move to the mesoscale model, Version 5 (MM5) to evaluate LAPS in simulating mesocale circulations influenced by surface processes.

Further details on the research performed by project subcontractors Drs. Kallos, Mihailovic and Alapaty can be found in Appendices A and B.

Section 3

APPLICATION OF STATISTICAL METHODS, TRAJECTORY MODELS AND PHOTOCHEMICAL MODELS TO IDENTIFY POTENTIAL CAUSE AND EFFECT RELATIONSHIPS

Ozone (O₃) and fine particulate matter (PM_{2.5}) are ubiquitous pollutants, and analyses of such air quality data are complicated by the fact that the time series exhibit both anthropogenic and natural forcings operating on different temporal and spatial scales (Rao et al., 1997). The shift from the 1-hour to the new 8-hour ozone NAAQS will greatly expand the spatial extent of the O₃ problem in the eastern US (Chameides et al., 1997). In addition to the 8-hour O₃ standard, the EPA has proposed new daily and annual standards for PM_{2.5}. Hence, as these new pollutant standards are considered, it becomes evident that we need to examine the spatial extent, or the airshed, for such pollutants, in assessing population exposure and in designing effective emission control strategies.

The concept of the spatial extent of an airshed is less well-defined than that for a given watershed. While watersheds have definite physical dimensions, the atmosphere is not bounded in such a way. Whereas transport through a watershed is limited to rivers and other bodies of water, and the surrounding land surfaces, pollutant transport through the atmosphere can occur over much longer distances. The airshed associated with nitrogen deposition into the Chesapeake Bay has been defined as the geographic region that contributes about 70-80% of the nitrate to the Bay watershed (Appleton, 1995; Dennis, 1997); this region is about five times as large as the area of the watershed itself, defining the region of influence of nitrate to be greater than 700 km.

In the case of O₃, the meteorological features associated with high O₃ events in the eastern United States have been examined previously (Vukovich, 1995; Eder et al., 1993; Rao et al., 2003). A common synoptic-scale feature associated with O₃ episodes over the eastern US is the presence of a high pressure system aloft (500 mb), that is usually accompanied by subsidence, clear skies, strong shortwave radiation, high temperatures, and stagnant air masses near the ridge line of the sea-level high pressure region (Zhang and Rao, 1999; Zhang et al., 2001). In addition, westerly and southwesterly low-level jets during these episodic events facilitate the transport of pollutants over long distances. These synoptic conditions augment local photochemical production and contribute to elevated levels of pollutant concentrations which blanket much of the northeastern US for several days (Zhang et al., 1998).

In this report, we briefly discuss the temporal and spatial scales and attempt to define the airshed associated with O₃ and other pollutants using five different methods since these results have been published in

Civerolo et al. (2003). First, we examined the O₃ observations to characterize the persistence of high concentrations aloft. Next, linear regression was performed between the synoptic-scale or weather-induced variations (characteristic time scale of 2 to 21 days) embedded in the time series of PM_{2.5} and O₃ at different locations to determine the distances over which a high degree of correlation is maintained. Also, mixed-layer forward trajectory analysis was done on a climatological basis to define the airshed for 1-day pollutant transport, the potential spatial extent over which pollutant concentrations are affected by a given source region. Civerolo et al. (2003) corroborated these findings by quantifying atmospheric transport using 3-dimensional particle trajectories with a Lagrangian particle dispersion model for three O₃ episodic periods that occurred in the summer of 1995. Finally, they compared a base case photochemical model simulation using the UAM-V model with hypothetical emission reduction scenarios to examine the spatial extent over which ozone benefits can be realized when emissions in a source region are reduced.

Civerolo et al. (2003) first analyzed O₃ measurements aloft rather than those near the ground level since nighttime pollutant concentrations measured at high elevation sites are more typical of free tropospheric values and are less affected by pollutant removal processes at the surface. High ozone concentrations aloft have been shown to contribute substantially to ground-level O₃ through vertical mixing processes, as the surface-based inversion starts to break-up in the morning (Zhang and Rao 1999). At two sites analyzed, high O₃ levels are most likely to persist for 1-3 days, consistent with the results of Berman et al. (1999) who examined observations from the Sears Tower in Chicago, IL (366 m AGL) and a television tower in North Carolina (411 m AGL). Although the mean duration of O₃ persistence was about 2 days at the World Trade Center and Shenandoah National Park sites, high O₃ can persist for 10 or more days at both sites (Figure 11). Aloft wind speeds in the nocturnal layer of 10-20 m s⁻¹ imply that inert pollutants which are slowly removed from the atmosphere could be transported over distances on the order of 1000 km during the course of 1-2 days (Rao et al., 1997). Since O₃ and PM_{2.5} are reactive pollutants, however, their characteristic transport distances may not be as large because of entrainment into the daytime mixed layer and interaction with fresh emissions.

From 1988-1997, the mean and the standard deviation daytime PM_{2.5} mass at Pinkham Notch (1910 m MSL) at Mt. Washington, NH were 15.8 and 12.6 µg m⁻³, respectively. Defining concentrations more than one standard deviation above the mean to be "elevated," there were five multi-day periods from 1988-1997; four were 2 days long, one was 4 days long. However, this number could be higher, since during this time there were an additional 15 single "elevated" days with no data available either on the previous or following day. Pollutant time series data consist of forcings operating on different time and space scales; they include intra-day, diurnal, synoptic, seasonal, and long-term (trend) components. The synoptic-scale component includes the effects of weather systems on pollutant concentrations. This highlights the need for long-term, high-resolution monitoring (i.e., daily sampling as opposed to weekly or twice a week sampling) of PM_{2.5} to evaluate pollutant transport patterns and potential source regions for pollutants measured in New York State.

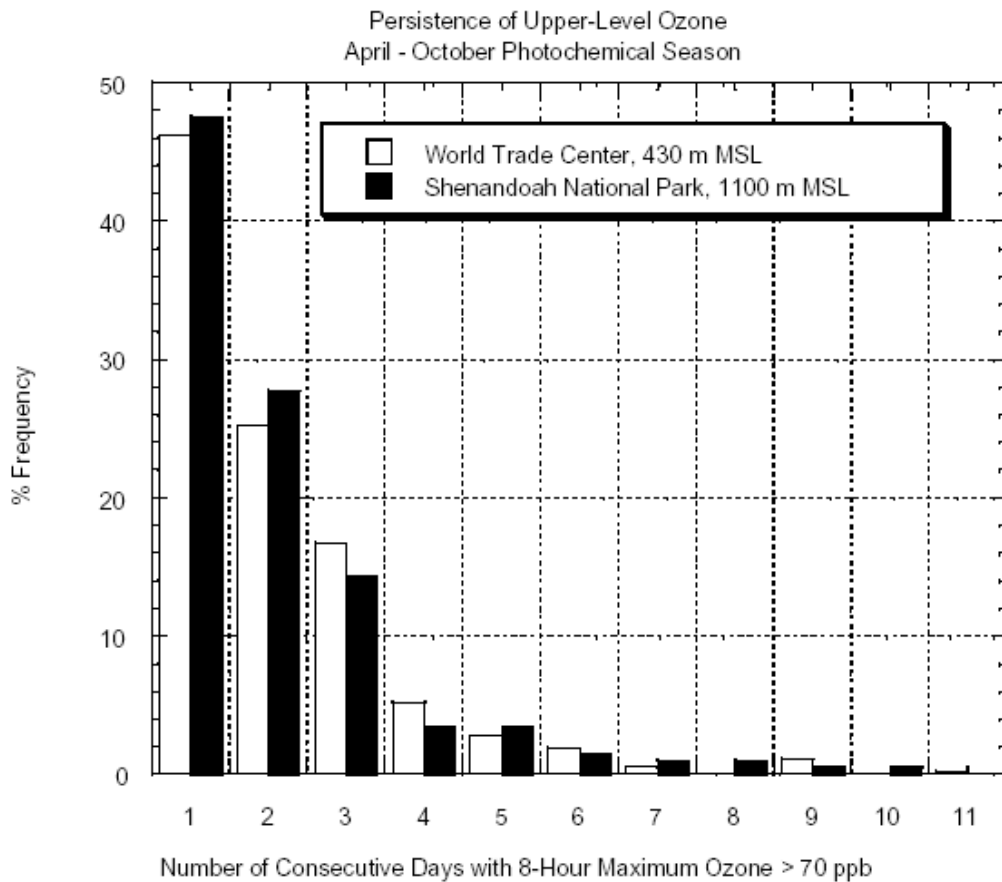


Figure 11 (from Civerolo et al., 2003): Histogram of the persistence of elevated (> 70 ppbv) daily maximum 8-hour O₃ concentrations aloft at the World Trade Center in New York City, NY and Shenandoah National Park, VA during the April to October photochemical season from 1983-1998.

Using the daily maximum 1-hour O₃ concentrations, Rao et al. (1997) previously showed that along the direction of the prevailing wind, the characteristic length scale for O₃ is on the order of 600 km. We performed a similar analysis, using both daily average PM_{2.5} mass and daily maximum 8-hour O₃ concentrations from various locations throughout the eastern United States. This methodology provides a measure of the coherence in pollutant levels among different monitors embedded within the same synoptic weather pattern. Once the five-year long O₃ time series data were spectrally decomposed, we performed a linear regression between the synoptic forcing in the O₃ data from two locations — Pittsburgh and Philadelphia, PA — and every other site included in this analysis. The correlation coefficients generally fall off along an axis that is oriented from southwest to northeast along the urban corridor, the predominant summertime flow in the mid-Atlantic region. There is substantial overlap between the two ozone spatial footprints which cover parts of

southern Canada and 14 eastern states. This implies that source attribution for receptor areas such as central New York State can be a complicated problem.

In order to assess the characteristic 1-2 day transport distances associated with the synoptic-scale O₃ component, we performed a time-lagged correlation analysis using the data from Pittsburgh and every other monitor. We lagged each time series with respect to that at Pittsburgh by 0 and ± 1 days, then determined the number of lags needed to maximize the correlation. While statistical analyses cannot establish causal relationships, results from this analysis suggest that O₃ levels in a region from Virginia to Maine can potentially be affected by emissions in the Pittsburgh area within 1 day; similarly, air masses from as far away as Michigan or the Carolinas have the potential to affect pollutant levels at Pittsburgh (Figure 12). In other words, the airshed for 1-2 day transport can encompass the entire eastern US. (Civerolo et al., 2003).

One limitation associated with the analysis of daily PM_{2.5} mass data is that, until more monitoring locations go on-line and more data become available, PM_{2.5} data are currently both temporally and spatially sparse. On average, these data sets consist roughly of twice-per-week measurements. Much of the information

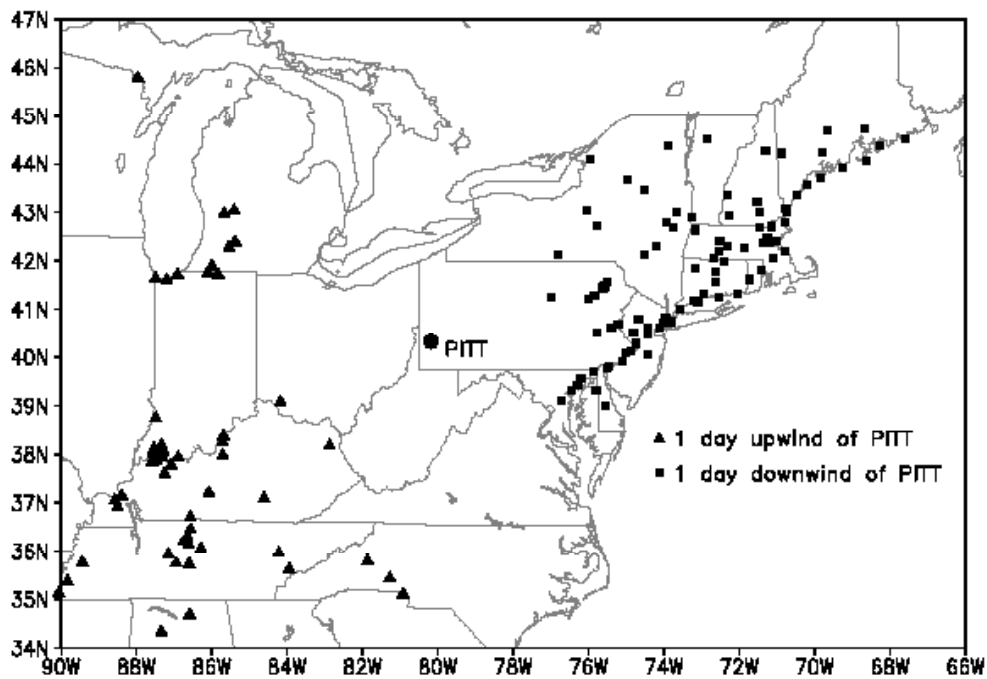


Figure 12 (from Civerolo et al., 2003): Number of days needed to maximize the summertime synoptic-scale O₃ correlations between Pittsburgh (large dot) and various locations throughout the eastern US. Only the sites which Pittsburgh lags by 1 day (triangles) or leads by 1 day (squares) are shown, and only the statistically significant (95%) correlation coefficients were considered.

on the synoptic time scales of about 2-5 days (i.e. weaker systems) is missing in the PM_{2.5} database. Therefore, we refer to the weather-induced variations in the PM_{2.5} data time series as intra-seasonal, rather than synoptic-scale variations in the time series of PM_{2.5}. Since we only included fifteen sets of PM_{2.5} time series in this analysis, we performed a pairwise correlation between all locations, rather than a spatial correlation from one central point. The results of this analysis show that the spatial extent (e-folding distance for the correlation coefficient) for the synoptic forcing in O₃ and PM_{2.5} data is on the order of 500-600 km. With a limited sampling schedule and so few monitoring locations, the synoptic information in the PM_{2.5} data on time scales of about 2-3 days has been lost. Hence, the spatial scale for PM_{2.5} should be viewed as a lower estimate.

The type of analysis discussed above is statistically-based (i.e., correlations), and as such does not explicitly take the physical and chemical processes (i.e. cause-and-effect) that affect pollutant concentration levels into account. Although we can associate correlation with pollutant transport, this is purely a statistical analysis, and, therefore, does not provide a mechanism for the pollutant transport. Therefore, Civerolo et al. (2003) also adopted a mixed-layer modeling approach which represents a simple physical basis for the pollutant transport. For each summertime day during the 1992 to 1996 period, forward trajectories from Philadelphia and Pittsburgh were computed with the HYbrid Single Particle Lagrangian Integrated Trajectory (HY-SPLIT, Version 3.0) model, using the National Weather Service's Nested Grid Model (NGM) data, archived every two hours with a horizontal grid dimension of approximately 180 km. All 1-day mixed-layer trajectories were started at 1200 EST at a height of 500 m above the surface. After all trajectories were generated, a 2.5° longitude × 2.0° latitude grid was superimposed upon the eastern US region, and the number of times that a trajectory passed through each grid cell was counted. The distribution of trajectories at each grid location was then normalized to the grid cell surrounding Pittsburgh and Philadelphia (the respective cells containing the maximum number of trajectory "hits").

Since the above trajectories were calculated with coarsely-gridded and temporally-sparse meteorological data, the absolute error associated with these trajectories increases roughly linearly with time and/or distance from the source. The errors associated with individual trajectories can typically be on the order of 100-200 km, or on the order of 30% of the trajectory path length, even for 1-2 day trajectories (Stohl, 1998). However, since five years of summertime trajectories are considered, the approximate summertime airshed region identified here for 1-day transport in the mixed layer is robust. In other words, we defined the approximate region that can be influenced by 1-day transport from the two locations by focusing on the entire set of trajectories on a climatological basis, rather than examining them on an individual trajectory basis because of the inherent uncertainty associated with individual trajectories.

We analyzed the spatial extent over which the trajectories originating from Pittsburgh and Philadelphia were at least 10% as likely to fall; such a region will encompass most of the trajectories without showing the

outliers. For example, the region about Philadelphia includes parts of 12 states extending from northern Virginia to southern Maine (Figure 13).

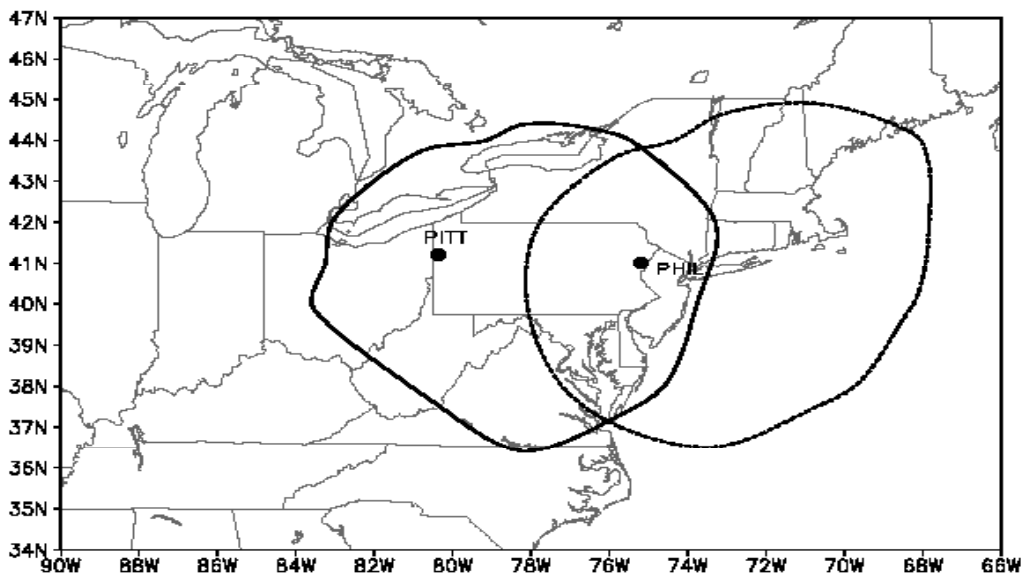


Figure 13 (from Civerolo et al., 2003): Regions within which 1-day HY-SPLIT forward trajectories during the summer seasons (June 1 through August 31) of 1992-96, originating from Philadelphia (broken line) and Pittsburgh (solid line), are at least 10% as likely to fall with respect to their maxima.

As with the correlation analysis in the previous section, there is substantial overlap between the two airsheds, and a general southwest to northeast orientation of the trajectory distributions, reflecting the prevailing flow during the summer. Because of the substantial overlap of the airsheds of pollutant transport, source attribution would be a difficult task for the mid-Atlantic region through southeastern New York State. The distance from Philadelphia to the edge of the contour along the major axis is approximately 600 km. This finding suggests that emission sources from a city such as Philadelphia have the potential to affect pollution levels across a much larger area within 1-day of transport and that the pollutant transport problem is a regional, national, and international issue. From a regulatory point of view, a minimum of 11 surrounding states should have a vested interest in any emissions control program envisioned for the Philadelphia area. Similarly, emissions from Pittsburgh can affect pollution levels in southern Canada and at least seven surrounding US states, making it especially difficult to attribute pollutant levels in receptor areas of central Pennsylvania, New

York, and Ontario to specific emission sources. Therefore, it is important to consider these factors in designing monitoring networks and interpretation of data from other nearby monitoring stations.

The Mesoscale Dispersion Modeling System (MDMS) is a Lagrangian model which utilizes 3-dimensional meteorological fields from the Regional Atmospheric Modeling System (RAMS) (Walko et al., 1995). The MDMS allows us to release tracer particles at a fixed rate and tracks them in 3-dimensional space over time. For this analysis, Civerolo et al. (2003) relied on the results of season-long RAMS modeling for the eastern US with 12 km horizontal grid dimensions to drive the dispersion model, focusing on three O₃ episodic periods in 1995 - June 18-20, July 13-15, and July 31-August 2. They attempted to define the potential region that a city such as Philadelphia can affect within 1-2 days of transport through forward trajectory modeling, as well as define the region which can potentially impact air quality in Philadelphia through backward trajectory modeling. Each forward trajectory was initialized at 1200 EST on June 18, July 13, and July 31 for the three episodes, and allowed the model to proceed for 48 hours. The particle release rate was set to 2 s⁻¹. The results revealed that in the lower layer, the distribution of particles does not change much throughout the day, and follow the prevailing flow direction. Within 12-24 hours, tracer particles from Philadelphia have already reached Massachusetts, and are observed about 600 km downwind, off the coast of southern Maine.

The situation is different for the particle distributions in the upper part of the boundary layer. During the nighttime and early morning hours, this residual layer becomes detached from the surface layer, and particles in the vicinity of the source region are confined to the surface layer. There are effectively no particles in the residual layer over the immediate Philadelphia area; any particles in the residual layer have been transported far downwind of Philadelphia. During the afternoon hours, the two layers become well-mixed and coupled, so that surface emissions can reach the upper parts of the atmospheric boundary layer.

Previous studies demonstrated that surface concentrations of pollutants such as O₃ are highly dependent on pollutant levels aloft. Zhang and Rao (1999) used various observational and modeling techniques, including a similar dispersion modeling approach to investigate the effect of vertical mixing on surface O₃ concentrations, and found that during the morning evolution of the boundary-layer, O₃-rich air trapped in the residual layer mixes downward. Rao et al. (2003) found that on days with high surface O₃ concentrations, the O₃ levels aloft were about 40% higher than corresponding days with low surface O₃, and that O₃ aloft has an approximate atmospheric residence time of 2-3 days. It appears that the dispersion model used here is able to simulate the boundary-layer processes that affect surface layer pollutant concentrations described by these authors.

The predicted tracer particle concentration fields depend upon the locations of the emission sources, local meteorological fields, and terrain/surface features. To examine how these concentration fields can vary in

space, we released particles from seven additional locations — Pittsburgh, PA; Richmond, VA; Washington, DC; Columbus and Cincinnati, OH; Detroit, MI; Toronto, Ont., Canada. The release rate at each location was kept at 2 s^{-1} . As expected, within 24 hours, the Detroit/Toronto, the Ohio/Pittsburgh, and the Richmond/Washington/Philadelphia plumes tend to merge together. This illustrates the difficulty in attributing the particle concentrations in New England to any of the eight point sources individually by the second day. Each tracer particle plume extends over distances of $>500 \text{ km}$ by the second day of transport, and thus, has the potential to contribute to observed pollutant levels over such distances. Note that there is a substantial overlap between the individual particle airsheds. These results again illustrate the problems in identifying source-receptor relationships using data from a few monitoring stations within a given urban area.

The above analysis is source-oriented, but the MDMS can also be used for receptor-oriented analysis. As further evidence that urban areas such as Philadelphia or New York City are not isolated, we performed corresponding backward trajectories from Philadelphia, keeping the initial time and particle release rate the same as with the forward trajectories. By calculating particle dispersion backward in time, one can estimate the influence function, which depicts the areal extent of the emission sources which have the potential to impact a city such as Philadelphia. Such analysis shows that within two days of transport, sources 600 km south of Philadelphia have the potential to contribute to pollution levels observed over Philadelphia. This region includes the urban centers of Richmond, Washington, Baltimore, MD, and Wilmington, DE. Hence, while local emissions will certainly contribute to O_3 and $\text{PM}_{2.5}$ levels observed in a city such as Philadelphia, one cannot simply attribute pollutant levels downwind of Philadelphia to emissions from Philadelphia alone. Again, emissions management policies implemented some 600 km upwind will have the potential to affect air quality in Philadelphia itself.

The analysis presented above is most pertinent to passive, non-reactive pollutants. For reactive pollutants, such as O_3 and $\text{PM}_{2.5}$, the problem is considerably more complex because of the photochemistry. To quantitatively describe the potential airshed for a variety of pollutants, one needs to perform 3-dimensional modeling reflecting atmospheric physical and chemical processes. In addition to linking the seasonal RAMS simulation to the MDMS, Civerolo et al. (2003) also used the RAMS meteorological fields to drive seasonal photochemical simulations with the Urban Airshed Model (UAM-V) (SAI 1995), a 3-dimensional photochemical model that uses the Carbon Bond IV chemical reaction mechanism. Details of the UAM-V simulation and model performance can be found in Sistla et al. (2001). Employing the same 1995 anthropogenic and biogenic emissions inventory as in Sistla et al. (2001), a base case photochemical simulation was carried out, covering much of the eastern US for the entire summer of 1995. To assess the effects of hypothetical reductions in anthropogenic emissions, we then removed all anthropogenic emissions from two $26 \text{ grid cell} \times 22 \text{ grid cell}$ regions that covered the greater Philadelphia and Pittsburgh areas. Emissions were removed individually from these two regions. The purpose of these sensitivity simulations was to determine the

spatial extent to which these “across-the-board” or uniform anthropogenic emission reductions in the greater Philadelphia and Pittsburgh areas could potentially affect O₃ concentrations throughout the region, while keeping the meteorology constant.

Over the entire 89-day modeling period and at each grid cell, we computed the mean and standard deviation of the difference between the base case daily maximum 8-hour O₃ and each sensitivity case daily maximum 8-hour O₃ ($\Delta O_3 = O_3(\text{base}) - O_3(\text{sensitivity})$), and the upper 95% confidence interval for ΔO_3 was computed. We then normalized by the largest differences — 24 ppb in the Pittsburgh region, 27 ppb in the Philadelphia region. As expected, the largest O₃ reductions are evident in the near-field where anthropogenic emissions were eliminated, and the O₃ reductions fall off along a general southwest-to-northeast orientation (Figure 14). Even though these anthropogenic emissions reductions are small across the entire domain (roughly 10% reductions in NO_x and VOC emissions), their effects can be felt as far away as the central and Cape Cod regions of Massachusetts. Throughout much of southeastern New York and southern New England, average O₃

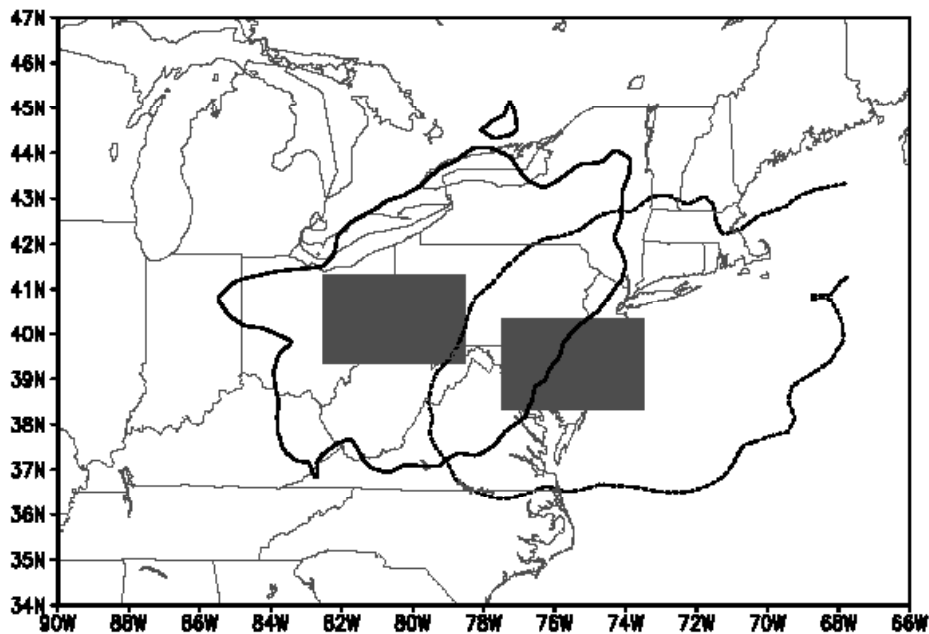


Figure 14 (from Civerolo et al., 2003): The 95% probability region within which the O₃ improvement (base case minus sensitivity case) is at least 10% of the maximum improvement, over the 1995 summer season. The maximum O₃ improvement was 24 ppb in the Pittsburgh region (solid line), and 27 ppb in the Philadelphia region (broken line). The shaded boxes indicate where anthropogenic emissions were removed from the Pittsburgh and Philadelphia areas.

improvements are in the range of 10-20% of the maximum changes in the near-field. This implies that the airshed for O₃ precursor emissions released from cities such as Philadelphia and Pittsburgh is on the order of 600 km.

The northeastern urban corridor, from Richmond to Boston, MA (with Philadelphia as the approximate center) contains many pollution sources which cannot be isolated from each other, as evident from the previous analysis involving three-dimensional dispersion modeling. The emissions reduction scenario presented in this photochemical modeling analysis is obviously hypothetical. However, these photochemical simulations demonstrate that the effects of emissions from one location can be seen hundreds of kilometers downwind.

In summary, using various approaches (spatio-temporal analysis of observations, trajectory modeling, and mesoscale dispersion modeling) it was demonstrated that the spatial scales associated with ozone and other pollutants are on the order of several hundreds of kilometers in the northeastern US, as evident from the overlapping airsheds. While each methodology has its own limitations, the different analyses — a combination of observational and modeling approaches — consistently show that O₃ and PM_{2.5} pollution is a regional, multi-state, and even international issue, not simply an urban or local problem. That is, the areal extent of the airshed is about 600 km in this region. Such scales imply that over distances of less than 100 km, it is difficult to unequivocally attribute sources or distinguish pollution levels observed at upwind, city center, and downwind locations. This finding should be of particular interest to those trying to investigate the effects of out-of-state versus in-state contributions to reactive pollutants such as O₃, PM_{2.5}, and Hg based on data from a few monitoring sites within an urban area in New York. For example, emissions from Baltimore, MD and Washington, DC have the potential to affect Philadelphia, PA which, in turn, can impact pollution levels downwind throughout New York state and New England. Further, these results also imply that no State in the Northeast alone can deal with such pollutant problems until region-wide control strategies are implemented for O₃ and PM_{2.5}. These results have been communicated to the EPA, since they have been concerned with the definitions for O₃/PM_{2.5} non-attainment areas and designations.

Section 4

MODELING AND ANALYSIS OF OZONE CONCENTRATIONS IN THE NORTHEAST AND THE USE OF PHOTOCHEMICAL MODELING SYSTEMS FOR REGULATORY POLICY-MAKING AS PART OF THE STATE IMPLEMENTATION PLAN

MODEL EVALUATION

Photochemical models such as UAM-V, the Comprehensive Air Quality Model with Extensions (CAMx) (Environ, 2000), the SARMAP Air Quality Model (SAQM) (Chang et al., 1997) or CMAQ have been used to design emission control strategies aimed at meeting and maintaining the NAAQS. Meteorological fields for these models are provided by simulations with mesoscale meteorological models such as MM5 or RAMS. Therefore, it is critical that a meaningful and thorough model evaluation of these meteorological and air quality modeling systems be performed. However, traditional statistical techniques such as bias or standard error of model predictions give only a partial picture of the models' ability to capture the spatio-temporal features embedded in observations. During the course of this project, we developed innovative techniques to evaluate the performance of regional-scale photochemical models than will be used for preparing the State Implementation Plans (SIPs).

Liu et al. (2003) introduced two new statistical methods for model evaluation, namely, spatial correlation coefficients and temporal correlation dimensions. These tools examine the model's ability to reproduce spatial and non-linear temporal features embedded in the observations. The utility of these methods was illustrated by evaluating the temperature simulations from two mesoscale meteorological models widely used in air quality simulations. The results indicate that the absence of clouds in simulations with RAMS led to an overestimation of the spatial coherency in the temperature fields and an underestimation of the degree of non-linearity of the temporal temperature fluctuations. On the other hand, the MM5 simulations, which included a treatment for cloud processes, captured the strength and spatial pattern of the observed degree of non-linearity. These results indicate that the model evaluation tools proposed by Liu et al. (2003) can provide insights into the model's ability to reproduce the key spatio-temporal features embedded in the observations.

Photochemical model evaluation studies conducted over the last decade in the northeastern United States have often placed emphasis on the assessment of spatial and temporal features of peak ozone levels. Even though other chemical constituents such as oxides of nitrogen (NO_x), non-methane organic compounds (NMOCs) and carbon monoxide (CO) also partake in oxidant chemistry, they have not received the same level of emphasis as ozone. Even though there is no NAAQS in the case of NO_y , which represents the total oxidized nitrogen in the system, it is considered an important parameter in ozone chemistry and as such is useful in the

diagnostic assessment of the nitrogen budget of the model. Although the state-of-the-art measurements for reactive nitrogen species and hydrocarbons have been mainly in the research and development arena, these techniques have been incorporated into the routine monitoring networks under the regulatory framework only in recent years. However, prior studies on the assessment of some of the ozone precursor species have been limited to high ozone events. As part of this research project, Sistla et al. (2002) examined the performance of the regional-scale photochemical model, UAM-V in reproducing the measured CO, NO₂ and NO_y levels for the summer of 1995 over the eastern United States. The monitoring data were obtained from the research sites operating under the auspices of the North American Research Strategy for Tropospheric Ozone Northeast 95 (NARSTONE 95), Southern Oxidant Study (SOS), and from the routine monitoring under the State and Local Air Monitoring System and National Aerometric Monitoring System (SLAMS/NAMS) and the Photochemical Assessment Monitoring System (PAMS) programs. The research sites are generally located in rural areas, while the routine monitoring stations are usually located in urban/suburban areas. In the case of CO, there were 264 routine and 15 research monitors, while for NO₂ there were a total of 200 routine and 6 research monitors over the modeling domain. The routine NO_y measurements were limited to 15 monitors in North Carolina and one in Maine, while the research networks operated a total of 18 sites distributed over New England, the Mid-Atlantic and the Tennessee Valley region.

Sistla et al. (2002) examined the predictive ability of the RAMS/UAM-V modeling system in reproducing the observed concentrations of CO and reactive nitrogen species (NO₂ and NO_y) on a qualitative and quantitative basis over an extended period rather than for an episode. Scatter plots of measured and predicted CO averages show that measured and predicted concentrations at the research sites are in the 150 to 300 ppb range while at the routine locations the measured concentrations varied from about 150 to 3000 ppb compared to 150 to 700 ppb based on predicted data (Figure 15). Thus, it is evident that there is a significant amount of underprediction by the modeling system, with a majority of predictions at routine locations being lower by a factor of two. On the other hand, predictions at the research monitors are found to fall within the 1-to-2 and 2-to-1 envelope, with a tendency towards underprediction. Unlike CO, the measured and predicted average NO₂ concentrations fall within a common range that extends from a few ppb to about 50 ppb, with concentrations at the research stations reporting generally below the 5 ppb range. The model exhibits a tendency to underpredict at the routine stations, but unlike CO, the model predictions on average are generally within the 1-to-2 and 2-to-1 envelope. A scatter plot for NO_y shows that concentrations at the routine sites are underpredicted while they are overpredicted at the research sites, with a majority of them falling within the 1-to-2 and 2-to-1 envelope.

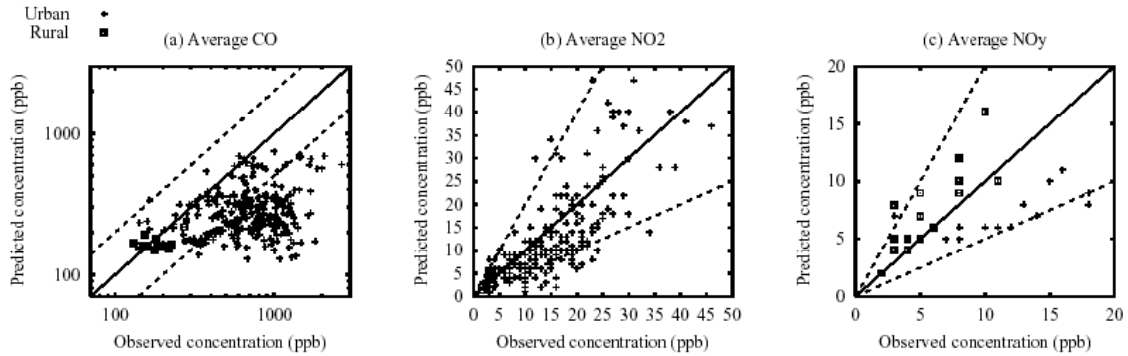


Figure 15 (from Sistla et al., 2002): Scatter plots of observed and predicted average concentrations of (a) CO, (b) NO₂, and (c) NO_y. Also shown are the 1-to-1 line (solid line) and 1-to-2 and 2-to-1 envelope (dashed lines).

Sistla et al. (2002) further examined the predictive ability of the model by comparing the coefficient of variation (CV), defined as the ratio of the standard deviation to the mean, for both measured and predicted concentrations. This metric provides for a normalized comparison of the dispersion or variability in the measured and predicted concentrations over the entire summer. Results show that the model does not appear to be able to simulate the day-to-day variation in the measured CO data well. For NO₂, both measurements and predictions yield the same range of the CVs, indicating that on an overall basis the predictive ability of the modeling system is quite good for this pollutant. For NO_y, with the exception of one or two research sites, the observed and predicted CVs are evenly distributed about the 1-to-1 line, while at the routine sites the model exhibits less dispersion compared to the measured data.

Sistla et al. (2002) also evaluated the modeling system's ability to predict average diurnal concentrations. For CO, although the modeling system is able to predict the 0600 to 0800 measured peak for the routine monitors and the 0700 to 0900 maximum for the research monitors, on average the model underpredicts the absolute levels for both monitor groups. Results presented by Sistla et al. (2002) suggest that the modeling system is able to better predict the CO profile during the morning hours, and on an overall basis it tends to severely underpredict both at the routine and research sites through the diurnal cycle (Figure 16). This level of underprediction by the model suggests possible deficiencies in the CO emissions inventory. For NO₂, the measured diurnal patterns are simulated quite well by the modeling system for both the routine and research monitors. In terms of the amplitude, at routine monitoring locations the model tends to underpredict the afternoon minimum and overpredict the morning peak. At the research-grade monitoring sites, the model tends to capture the afternoon minimum but overpredicts throughout the rest of the day. Unlike CO, there appears to be little systematic bias at either the research or the routine locations. The measured diurnal patterns of NO_y

have been simulated quite well by the modeling system for both the routine and rural monitors, but not in terms of absolute magnitude. Unlike NO_2 the model underpredicts throughout the diurnal cycle at the routine monitors and overpredicts at the research sites.

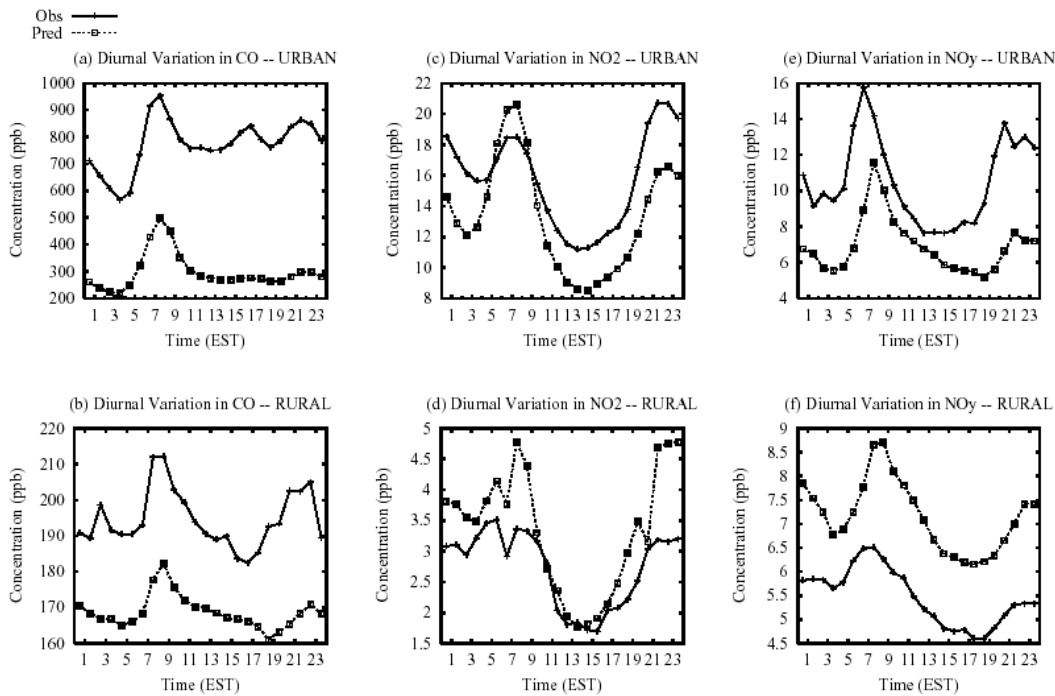


Figure 16 (from Sistla et al., 2002): Average diurnal concentration profiles for observed and predicted concentrations of CO , NO_2 , and NO_y .

Since the rate of ozone formation, namely, the ozone production efficiency (OPE), is dependent upon reactive nitrogen compounds, Sistla et al. (2002) compared the measured and predicted OPEs by considering NO_x and NO_z by generating scatter plots of NO_z vs. O_3 for the measured and predicted concentrations for the routine and research sites. OPE can be thought of as the amount of ozone formed per molecule of NO_x emitted over the lifetime of the NO_x molecule. NO_z is calculated by subtracting NO_x from NO_y . It was assumed that aged plumes were characterized by a ratio of < 0.3 for NO_x to NO_y , with the data being restricted to only non-precipitation periods and to the 1200 to 1800 time period. The slope, which is an indicator of the efficiency of the production of O_3 , was found to be 8.8 and 6.5 for the measured data at the routine and research sites, respectively. However, the estimated slopes were found to be 5.7 and 3.7 for the model predictions at the routine and research sites (Figure 17).

Thus, the key findings of this work as published by Sistla et al. (2002) were that (1) the summer seasonal average concentrations of CO at the routine monitors are substantially underpredicted, (2) the measured and predicted diurnal patterns of the three pollutants are in fair agreement at both the routine and research sites but both CO and NO_y levels are significantly underpredicted at the routine sites, (3) the ozone production efficiencies derived from models are lower than those obtained from the measured data.

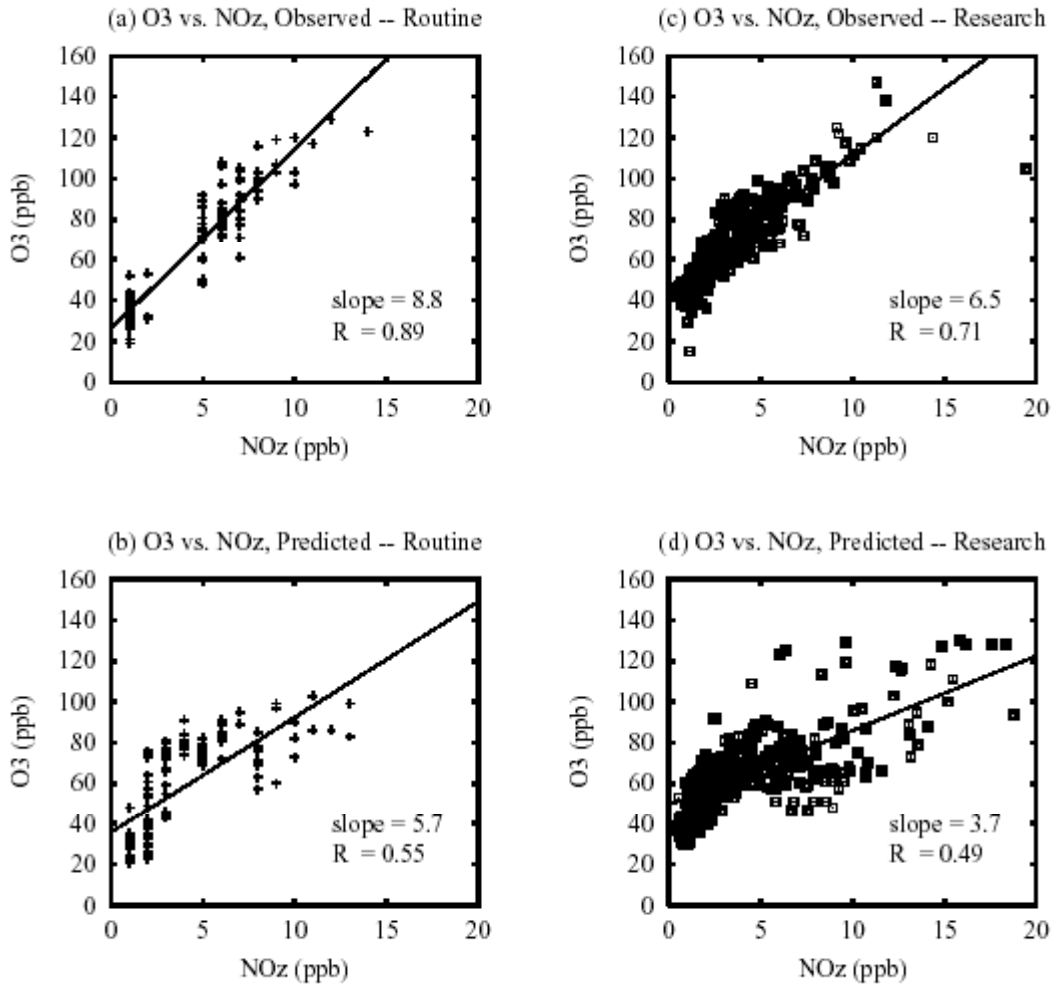


Figure 17 (from Sistla et al., 2002): Scatter plots between hourly O₃ and NO_z concentrations for the 1200–1800-hr period; (a) and (b) show routine sites for observed and predicted data, respectively; (c) and (d) show research sites for observed and predicted data, respectively. The regression line is shown as solid.

It has been proposed that ozone production efficiency (O_3/NO_x) can be used as an indicator to assess the relative impact of NO_x and hydrocarbons on ozone formation. Further analysis of the model-predicted efficiency of ozone formation from anthropogenic nitrogen oxide emissions was performed by Biswas et al. (2002). Currently, regional-scale photochemical modeling systems such as UAM-V, MAQSIP (Odman and

Ingram, 1996) and CMAQ are being used as tools to guide emission management decisions to deal with the ozone non-attainment problem. Thus, an evaluation of the predicted ozone-precursor relationships is crucial. Biswas et al. (2002) compared the predicted ozone-precursor relationships from 3-month simulations with the RAMS/UAM-V and the MM5/MAQSIP modeling systems for the summer of 1995 with the observations from a rural site (Harvard Forest, Massachusetts). Although MM5/MAQSIP predicts a higher OPE than RAMS/UAM-V, both modeling systems underpredict the ozone production efficiencies and show spatial differences in the ozone production efficiencies, especially in the northeastern United States, with MM5/MAQSIP generally exhibiting higher ozone production efficiencies than RAMS/UAM-V. Further, the relationship between the ratio O_3/NO_x and the model-predicted sensitivity towards NO_x/VOC controls for the 3 month's simulation with the RAMS/UAM-V modeling system was examined. It was shown that this ratio is not a consistent indicator of NO_x/VOC sensitivity for this extended simulation period, contrary to previous findings based on episodic modeling (Silman et al., 1997).

Until recently, grid-based photochemical modeling systems have been used predominantly to simulate historic high-ozone events (in hindcasting mode). Recent developments in computing technology have now made it possible to apply these modeling systems for providing real-time air quality forecasts. Numerical models can provide higher spatial and temporal resolution than traditional statistical methods, but it is necessary to evaluate the quality of these predictions and estimate the modeling systems' uncertainty before photochemical models can be more widely used for real-time air quality predictions. As part of this project, Hogrefe et al. (2002) studied ozone predictions from a hindcast simulation for the summer of 1995 generated by the RAMS/UAM-V modeling system (Sistla et al., 2001) to establish a "best case" scenario for model performance (in hindcast simulations, meteorological observations are routinely assimilated using 4DDA techniques). The forecasting performance of a photochemical hindcast simulation was evaluated using a set of threshold-based statistical metrics. Traditional air quality forecasts using regression techniques, weather prediction, and expert judgment seem to outperform the predictions from numerical models. Hogrefe et al. (2002) proposed a method to estimate a lower bound of uncertainty for model forecasts at each grid cell derived from spectrally decomposed observed ozone time series. The application of this method was illustrated using both a 1995 hindcast simulation and ozone predictions from a real-time numerical air quality forecasting system. As expected, the uncertainty in the real-time forecast simulation was larger than that of the hindcast simulation. Using the proposed methodology, model predictions were transformed into a probabilistic framework. Hogrefe et al. (2002) conclude that predicting a range of possible ozone concentrations rather than a single number takes into account the well-documented inability of photochemical modeling systems to correctly predict the observation at a single point in space and time while still providing useful information about the temporal and spatial patterns of ozone concentrations.

While fluctuations in meteorological and air quality variables occur on a continuum of spatial scales, the horizontal grid spacing of coupled meteorological and photochemical models sets a lower limit on the spatial scales that they can resolve. However, both computational costs and data requirements increase significantly with increasing grid resolution. Therefore, it is important to examine for any given application whether the expected benefit of increased grid resolution justifies the extra costs. Gego et al. (2003a) examined temperature and ozone observations and model predictions for three high ozone episodes that occurred over the northeastern United States during the summer of 1995. In the first set of simulations, the meteorological model RAMS4a was run with three two-way nested grids of 108/36/12 km grid spacing covering the United States and the photochemical model UAM-V was run with two grids of 36/12 km grid spacing covering the eastern United States. In the second set of simulations, RAMS4a was run with four two-way nested grids of 108/36/12/4 km grid spacing and UAM-V was run with three grids of 36/12/4 km grid spacing with the finest resolution covering the northeastern United States. The analysis focused on the comparison of model predictions for the finest grid domain of the simulations, namely, the region overlapping the 12 km and 4 km domains. A comparison of 12 km versus 4 km fields showed that the increased grid resolution leads to finer texture in the model predictions; however, comparisons of model predictions with observations do not reveal the expected improvement in the predictions. While high-resolution modeling has scientific merit and potential uses, Gego et al. (2003a) concluded that the currently available monitoring networks do not allow confirmation of the superiority of the high-resolution model predictions.

USE OF PHOTOCHEMICAL MODELING SYSTEMS IN THE REGULATORY FRAMEWORK

A special focus of the research in this topic area was the use of models from a regulatory perspective. Sistla et al. (2001) examined the performance of two commonly-used regional-scale Eulerian photochemical modeling systems, namely, RAMS/UAM-V and MM5/SAQM. The model's performance in reproducing the observed ozone air quality over the eastern United States was evaluated for three typical high ozone episodic events that occurred during June 16-20, July 12-16, and July 30-August 2 of 1995. The results suggest that the performance of the RAMS/UAM-V and MM5/SAQM systems in reproducing the observed ozone concentrations is comparable when model outputs are averaged over all simulated days. For different emissions reduction (i.e. VOC and NO_x controls) options, the response of both modeling systems in terms of changes in ozone levels were directionally similar, but the magnitude of ozone improvement differed for individual episode days at individual grid cells. The results of ozone predictions for the three episodes reveals that the two modeling systems exhibit differences in their temporal and spatial ozone patterns for individual episode days at individual grid cells even though they utilized the same emissions database. However, the modeling systems were found to yield similar levels of operational performance when model outputs are averaged over all episode days. In a related study, Rao et al. (2001) examined the modeling simulations performed for three high-ozone

events over the eastern United States with several state-of-science photochemical modeling systems (RAMS/UAM-V, MM5/UAM-V, MM5/SAQM, and MM5/MAQSIP). The results revealed that predictions of the daily maximum ozone concentrations with current-generation photochemical modeling systems during an individual ozone episode can vary as much as 30%, and that the choice of the modeling system itself introduces a large amount of uncertainty. Therefore, the use of these modeling systems in traditional ozone attainment demonstrations can lead to highly uncertain results. It was further shown that this uncertainty can be reduced when the predicted daily maximum ozone concentrations are averaged over all episode days simulated. These results provided the basis for the recent EPA Guidance on the need for using the daily maximum concentrations averaged over all episode days simulated rather than the peak concentration during an episode for regulatory purposes (U.S. EPA, 2001).

How one should use the modeling results in a regulatory setting is a topic of considerable debate. It is now well recognized one needs to integrate the observations and modeling results to increase our confidence in the models being used in the regulatory setting. Findings from this research project showed that it is erroneous to use model results in an absolute sense in the process of attainment demonstration (Rao et al., 2002; Rao and Hogrefe, 2002). We developed a method for integrating the observations and model predictions into a probabilistic regulatory framework using geostatistical techniques (Gego et al., 2003b). In this framework, spatial maps of the probability of exceeding the air quality standard were estimated through kriging and geostatistical simulations utilizing observed ozone concentrations at routine monitors. Kriging is perhaps the most widely used technique for estimation of values at unsampled locations and creation of contour maps of the resulting information. Kriging utilizes the fact that observations made at nearby locations are more correlated than those made far apart. Assessing the uncertainty of estimates is progressively becoming an inherent part of geostatistical data analysis because it allows decision-makers to evaluate the risk taken when classifying areas as complying or not complying with a given standard. Since kriging allows computation of an estimate and its variance, a simple option for uncertainty assessment is to assume a normal process. However, since the variances of kriged estimates only depend on the spatial configuration of the observations and not on their local variability, stochastic simulations have been increasingly used for assessing estimation uncertainty. A stochastic simulation consists of generating multiple equally likely maps (realizations) that honor the observations as well as their global features (histogram, variance and spatial correlation features), to the detriment of local accuracy. When examined together, the simulated realizations allow estimation of spatial interpolation uncertainty and the production of maps indicating the probability of a given affirmation being true, in this case, maps representing the likelihood of ozone design values being higher than the air quality standard. Gego et al. (2003b) used both techniques to generate maps of the probability of exceeding the 8-hr ozone NAAQS based on ozone observations from 1998 - 2000. An illustration is provided in Figure 18.

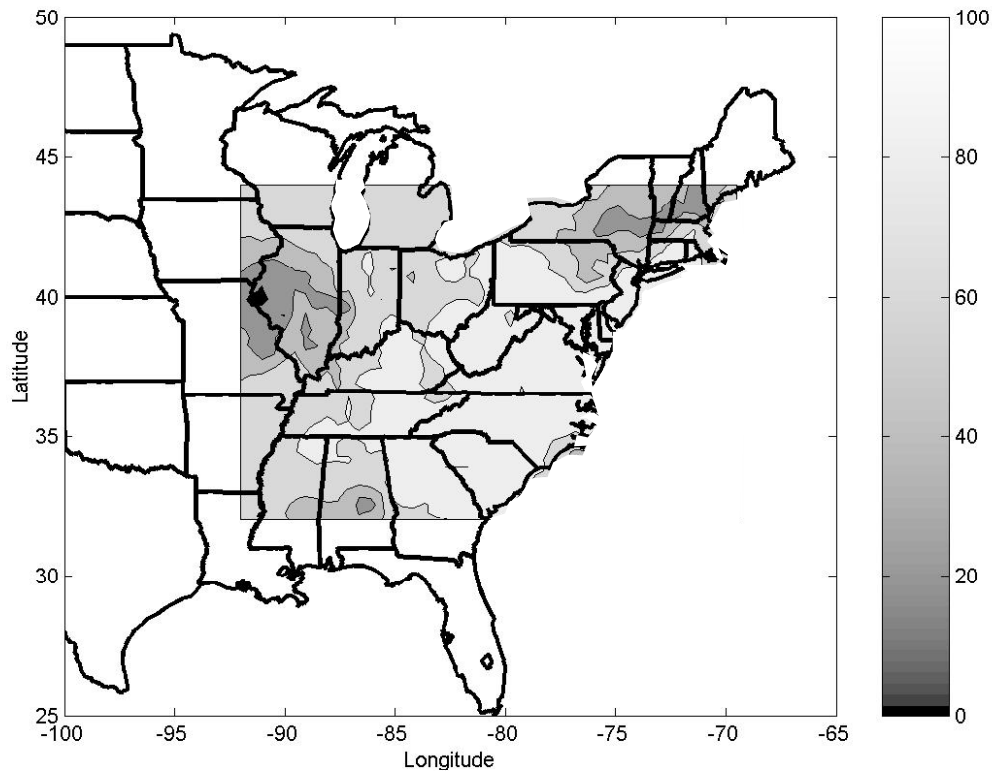


Figure 18 (from Gego et al., 2003): Probability of exceeding the 8-hr ozone NAAQS of 85ppb. This map is based on a kriging analysis of ozone observations from 1998-2000.

To assess future attainment of the NAAQS resulting from mandated emission reductions, U.S. EPA mandates the use of photochemical models. Model predictions of mean daily ozone maxima are derived from two air quality model runs; one with the present-day emissions (base case simulation) and one with emissions that reflect a future emission control policy (control case simulation). The relative reduction factor (RRF) at a given location is defined as the ratio of the mean daily maximum ozone concentrations for the emission control case and the base case. These RRF are then used to scale observed design values to determine future attainment of the NAAQS. Gego et al. (2003b) generated 500 equally likely maps of “scaled” design values through the sequential Gaussian geostatistical simulation. In their analysis, RRF from NO_x SIP Call emission reductions simulated by the RAMS/UAM-V modeling system were used. From the 500 equally likely maps, the probability of exceeding the 8-hr ozone NAAQS in the future with this particular emissions control strategy

was estimated (Figure 19). These techniques would be of particular interest to the states in the preparation of their State Implementation Plans for meeting and maintaining the ozone and fine particulate matter standards.

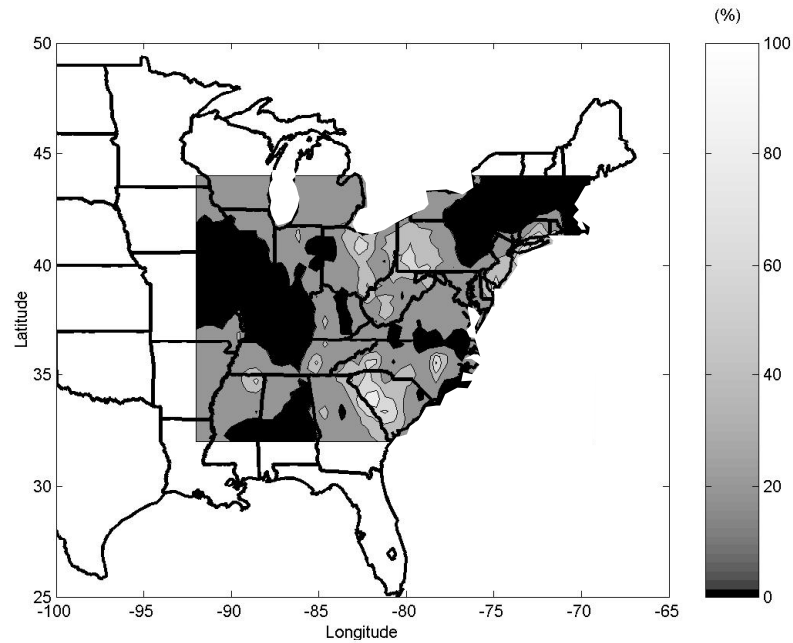


Figure 19 (from Gego et al., 2003b): Probability of exceeding the 8-hr ozone NAAQS of 85ppb after scaling observed design values by RRF from RAMS/UAM-V NO_x SIP-call simulations. This map is based on 500 replications of the sequential Gaussian geostatistical simulation technique.

Section 5

REFERENCES

- Appleton, E. L., A cross-media approach to saving the Chesapeake Bay. *Environ. Sci. & Technol.*, **29**, 550A-555A, 1995.
- Athanassiadis, G. A., and S. T. Rao, Spatial and temporal variations in the trace elemental data over the northeastern United States, *Env. Poll*, **123**, 439-449, 2003.
- Athanassiadis, G. A., S. T. Rao, J.-Y. Ku, and R. Clark, Boundary-layer evolution and its effects on ground-level ozone concentrations, 4th Conference on Atmospheric Chemistry, Orlando, FL, *Amer. Meteor. Soc.*, 97-102, 2002a.
- Athanassiadis, G.A., S.T. Rao, J.-Y. Ku, and R.D. Clark, Boundary-layer evolution and its influence on ground-level ozone concentrations, *Env. Fluid Mech.*, **2**, 339-357, 2002b.
- Berman, S., J.-Y. Ku, and S.T. Rao, Spatial and temporal variation in the mixing depth over the northeastern United States during the summer of 1995, *J. Appl. Meteor.*, **38**, 1661-1673, 1999.
- Biswas, J., C. Hogrefe, and S. T. Rao, Temporal and spatial variability of ozone production efficiencies over the eastern United States, Proceedings of the 95nd Annual Meeting of the Air & Waste Management Association, June 23 - 27, Baltimore, MD, 2002.
- Brankov, E., Rao, S.T., and P.S. Porter, A trajectory-clustering-correlation methodology for examining the long-range transport of air pollutants, *Atmos. Environ.*, **32**, 1525-1534, 1998.
- Brankov, E., S.T. Rao, and P.S. Porter, Identifying pollution source regions using multiply-censored data, *Env. Sc. Tech.*, **33**, 2273-2277, 1999.
- Byun, D.W. and Ching, J.K.S. (eds.), Science algorithms of the EPA Models-3 Community Multiscale Air Quality Model (CMAQ) modeling system. *EPA/600/R-99/030*, U. S. Environmental Protection Agency, Office of Research and Development, Washington, DC 20460, 1999.
- Chameides, W. L., R. D. Saylor, and E. B. Cowling, Ozone pollution in the rural U.S. and the new NAAQS, *Science*, **276**, 916, 1997.
- Chang, J. S., S. Jin, Y. Li, M. Beauharnois, C. H. Lu, H. C. Huang, S. Tanrikulu, and J. DaMassa, The SARMAP Air Quality Model, final report. *Air Resource Board*, California Environmental Protection Agency, Sacramento, CA, 1997.
- Civerolo, K.L., G. Sistla, S.T. Rao, and D.J. Nowak, The effects of land-use in meteorological modeling: implications for assessment of future air quality scenarios, *Atmos. Env.*, **34**, 1615-1621, 2000.
- Civerolo, K., H. Mao, and S. T. Rao: The airshed for ozone and fine particulate pollution in the eastern United States, *Pure Appl. Geoph.*, **160**, 81-105, 2003.
- Dennis, R. L., Using the regional acid deposition model to determine the nitrogen deposition airshed of the Chesapeake Bay Watershed. In *Atmospheric Deposition of Contaminants to the Great Lakes and*

- Coastal Waters*, J. E. Baker (Ed.). Proceedings from the Society of Environmental Toxicology and Chemistry (SETAC) 15th Annual Meeting, November, 1994, Denver, CO, pp. 293-304, 1997
- Draxler, R. R. *Hybrid Single-Particle Lagrangian Integrated Trajectories (HY-SPLIT): Version 3.0 - User's guide and model description*; NOAA Technical Memorandum ERL-ARL-195; Air Resources Laboratory: Silver Spring, MD, 1992.
- Eder, B.K., J.M. Davis, P. Bloomfield, A characterization of the spatiotemporal variability of non-urban ozone concentrations over the eastern United States, *Atmos. Environ.*, **27A**, 2645-2668, 1993.
- ENVIRON, User's guide to the Comprehensive Air Quality Model with Extensions (CAMx) Version 3.00. Available from ENVIRON International Corporation, 101 Rowland Way, Novato, CA 94945, 2000.
- Gego, E., C. Hogrefe, G. Kallos, A. Voudouri, J.S Irwin, and S.T. Rao, Examination of model predictions at different horizontal grid resolutions, submitted to *Env. Fluid Mech.*, 2003a.
- Gego, E., C. Hogrefe, S. T. Rao, and P. S. Porter, Probabilistic assessment of regional scale ozone pollution in the eastern United States, To appear in *NATO Science Series*, Kluwer Academic Publishers, 2003b.
- Grell, G. A., J. Dudhia, and D. Stauffer, A description of the fifth-generation Penn State/NCAR Mesoscale Model (MM5). *NCAR Technical Note*, NCAR/TN-398 + STR, 1994.
- Henry, R.F., S.T.Rao, I.G.Zurbenko, P.S.Porter, Effects of changes in data reporting practices on trend assessments, *Atmos. Env.*, **34**, 2659- 2662, 2000.
- Hochberg, Y., and A.C. Tamahne, *Multiple Comparison Procedures*. John Wiley & Sons, New York, 450 pp, 1987.
- Hogrefe, C., S. T. Rao, and K. L. Demerjian, Using the current-generation meteorological/photochemical modeling systems for real-time ozone forecasting. Proceedings of the 16th Conference on Probability and Statistics in the Atmospheric Sciences, January 13 – 17, *Amer. Meteor. Soc.*, Orlando, FL, 2002.
- Hogrefe, C., S. Vempaty, S. T. Rao, and P. S. Porter, A comparison of four techniques for separating different time scales in atmospheric variables, *Atmos. Env.*, **37**, 313-325, 2003.
- Holzworth, G.C., Mixing depths, wind speeds and air pollution potential for selected locations in the United States, *J. Appl. Meteor.*, **3**, 1039-1044, 1967.
- Ku, J.-Y., H. Mao, K. Zhang, K. Civerolo, S. T. Rao, C. R. Philbrick, B. Doddridge, and R. Clark, Numerical investigation of the effects of boundary-layer evolution on the prediction of ozone and the efficacy of emission control options in the northeastern United States, *Env. Fluid Mech.*, **1**, 209–233, 2001.
- Lazic, J., D.T. Mihailovic, S.T. Rao, and C. Hogrefe, Land air surface scheme (LAPS) for use in urban modeling, *International Environmental Modelling and Software Society (iEMSs) 2002 Conference*, June 24 – 27, Lugano, Switzerland, 448-453, 2002.
- Liu, G., C. Hogrefe, and S. T. Rao, Evaluating the performance of regional-scale meteorological models: effect of clouds simulation on temperature prediction, to appear in *Atmos. Env.*, 2003.

- Mihailovic, D. T., S.T. Rao, C. Hogrefe and R. Clark, An approach for the aggregation of aerodynamic surface parameters in calculating the turbulent fluxes over heterogeneous surfaces in atmospheric models. *Env. Fluid Mech.*, **2**, 315-337, 2002a.
- Mihailovic, D.T, Environmental modeling of physical, biophysical and chemical processes in the atmosphere-plant-soil-interaction: how nonlinearity affects the solutions?, *International Environmental Modelling and Software Society (iEMSs) 2002 Conference*, June 24 – 27, Lugano, Switzerland, 383-388, 2002b.
- Mihailovic, D.T., D. Kapor, C. Hogrefe , J. Lazic and T. Tasic, Parameterization of albedo for heterogeneous surfaces in land surface schemes for environmental modeling I: Theoretical background and simple model, to appear in *Env. Fluid Mech.*, 2003
- National Research Council, Ozone-forming potential of reformulated gasoline, National Academy Press, Washington, DC, 252 pp., 1999.
- NARSTO, An assessment of tropospheric ozone pollution: a North American perspective, NARSTO Synthesis Team, available online at <http://www.cgenv.com/Narsto/>, 2000.
- Odman, M. T., and C. L. Ingram, Multiscale Air Quality Simulation Platform (MAQSIP): Source code documentation and validation. Tech. Rep. ENV-96TR002-v1.0, 83 pp., MCNC Environmental Programs, Research Triangle Park, NC 27709, 1996.
- Porter, P. S., S. T. Rao, I. G. Zurbenko, A. Dunker, and G. Wolff: Ozone air quality over North America: part II - an analysis of trend detection and attribution techniques, *J. Air Waste Manag. Assoc.*, **51**, 283-306, 2001.
- Rao, S.T., and I. G. Zurbenko, Detecting and tracking changes in ozone air quality. *J. Air & Waste Manage. Assoc.*, **44**, 1089 – 1092, 1994.
- Rao, S. T., I. G. Zurbenko, R. Neagu, P. S. Porter, J. Y. Ku, and R. F. Henry, Space and time scales in ambient ozone data. *Bull. Amer. Meteor. Soc.*, **78**, 2153 - 2166, 1997.
- Rao, S. T., C. Hogrefe, H. Mao, J. Biswas, I. G. Zurbenko, P. S. Porter, P. Kasibhatla, and D. A. Hansen, How should the photochemical modeling systems be used in guiding emissions management decisions? In: *Air Pollution Modeling and Its Application XIV*; Gryning, S. E. and F. Schiermeier, eds., Kluwer Academic/Plenum, New York, 25 – 34, 2001.
- Rao, S. T., and C. Hogrefe, Using air quality models for emissions management decisions, “Uncertainty Treatment in Integrated Assessment Modelling” workshop of the *UN/ECE Task Force on Integrated Assessment Modelling*, January 24 – 25, 2002, IIASA, Laxenburg, Austria, 2002.
- Rao, S. T., E. Gego, and C. Hogrefe, Using regional-scale photochemical models for guiding emissions management decisions, *BMU/UBA-USEPA-EMEP Workshop*, October 7 - 11, 2002, Bad Breisig, Germany, 2002.
- Rao, S. T., J.-Y. Ku, S. Berman, K. Zhang, and H. Mao: Summertime characteristics of the atmospheric boundary-layer and relationships to ozone levels over the eastern United States, *Pure Appl. Geophys.*, **160**, 21-55, 2003.

- Sillman, S., He, D., Cardelino, C., Imhoff, R.E., The use of photochemical indicators to evaluate ozone-NO_x-hydrocarbon sensitivity: case studies from Atlanta, New York, and Los Angeles. *J. Air Waste Manag. Assoc.*, **47**, 1030 - 1040, 1997.
- Sistla, G., W. Hao, J.-Y. Ku, G. Kallos, K. Zhang, H. Mao, and S. T. Rao: An operational evaluation of two regional-scale ozone air quality modeling systems over the eastern United States, *Bull. Amer. Meteor. Soc.*, **82**, 945-964, 2001.
- Sistla, C., K.L. Civerolo, W. Hao, and S.T. Rao, An evaluation of the UAM-V predicted concentrations of carbon monoxide and reactive nitrogen compounds over the eastern United States during Summer 1995, *J. Air Waste Manag. Assoc.*, **52**, 1324-1332, 2002.
- Stohl, A., Computation, accuracy and applications of trajectories - a review and bibliography, *Atmos. Environ.*, **32**, 947-966, 1998.
- Systems Applications International, Users Guide to the Variable Grid Urban Airshed Model (UAM-V). *Systems Applications International*, San Rafael, CA, 131 pp. [Available from Systems Applications International, 101 Lucas Valley Rd., San Rafael, CA 94903], 1995.
- U.S. Environmental Protection Agency, Draft Guidance for demonstrating attainment of air quality goals for PM_{2.5} and regional haze, Draft 2.1, January 2, 2001, available online at http://www.epa.gov/scram001/guidance/guide/draft_pm.pdf, 273 pp.
- Torrence, C. and G.P. Compo, A practical guide to wavelet analysis. *Bull. Amer. Met. Soc.*, **79**, 61 – 78, 1998.
- Vukovich, F.M., Regional-scale boundary-layer ozone variations in the eastern United States and their association with meteorological variations, *Atmos. Environ.*, **29**, 2259-2273, 1995.
- Walko, R. L., C. J. Tremback, and R. F. A. Hertenstein, RAMS - The Regional Atmospheric Modeling System, Version 3b, User's guide. *ASTER Division, Mission Research Corporation*, Fort Collins, CO, 1995.
- Zhang, J., S. T. Rao, and S. M. Daggupaty, 1998, Meteorological processes and ozone exceedances in the northeastern United States during the 12-16 July 1995 episode. *J. Appl. Meteor.*, **37**, 776-789, 1998.
- Zhang, J., and S.T. Rao, The role of vertical mixing in the temporal evolution of ground-level ozone concentrations, *J. Appl. Meteor.*, **38**, 1674-1691, 1999.
- Zhang, K., H. Mao, K. Civerolo, S. Berman, J.-Y. Ku, S. T. Rao, B. Doddridge, C. R. Philbrick, and R. Clark, Numerical investigation of boundary-layer evolution and nocturnal low-level jets: local versus non-local PBL schemes, *Env. Fluid. Mech.*, **1**, 171 –208, 2001.

Section 6

COMPLETED PUBLICATIONS RELATED TO THIS RESEARCH PROJECT

JOURNAL ARTICLES

- Athanassiadis, G. A., and S. T. Rao, Spatial and temporal variations in the trace elemental data over the northeastern United States, *Env. Poll, Env. Poll*, **123**, 439-449, 2003.
- Athanassiadis, G.A., S.T. Rao, J.-Y. Ku, and R.D. Clark, Boundary-layer evolution and its influence on ground-level ozone concentrations, *Env. Fluid Mech.*, **2**, 339-357, 2002.
- Berman, S., J.-Y. Ku, and S.T. Rao, Spatial and temporal variation in the mixing depth over the northeastern United States during the summer of 1995, *J. Appl. Meteor.*, **38**, 1661-1673, 1999.
- Brankov, E., S.T. Rao, and P.S. Porter, Identifying pollution source regions using multiply-censored data, *Env. Sc. Tech.*, **33**, 2273-2277, 1999.
- Civerolo, K.L., G. Sistla, S.T. Rao, and D.J. Nowak, The effects of land-use in meteorological modeling: implications for assessment of future air quality scenarios, *Atmos. Env.*, **34**, 1615-1621, 2000.
- Civerolo, K., H. Mao, and S. T. Rao: The airshed for ozone and fine particulate pollution in the eastern United States, *Pure Appl. Geoph.*, **160**, 81-105, 2003.
- Gego, E., C. Hogrefe, G. Kallos, A. Voudouri, J.S Irwin, and S.T. Rao, Examination of model predictions at different horizontal grid resolutions, submitted to *Env. Fluid Mech.*, 2003a.
- Gego, E., C. Hogrefe, P.S. Porter, J.S. Irwin, and S.T. Rao, Comparison of the space-time signatures of air quality data from different modeling networks, to be submitted to *Pure Appl. Geoph.*
- Henry, R.F., S.T.Rao, I.G.Zurbenko, P.S.Porter, Effects of changes in data reporting practices on trend assessments, *Atmos. Env.*, **34**, 2659- 2662, 2000.
- Hogrefe, C., S. Vempaty, S. T. Rao, and P. S. Porter, A comparison of four techniques for separating different time scales in atmospheric variables, *Atmos. Env.*, **37**, 313-325, 2003.
- Ku, J.-Y., H. Mao, K. Zhang, K. Civerolo, S. T. Rao, C. R. Philbrick, B. Doddridge, and R. Clark, Numerical investigation of the effects of boundary-layer evolution on the prediction of ozone and the efficacy of emission control options in the northeastern United States, *Env. Fluid Mech.*, **1**, 209-233, 2001.
- Liu, G., C. Hogrefe, and S. T. Rao, Evaluating the performance of regional-scale meteorological models: effect of clouds simulation on temperature prediction, to appear in *Atmos. Env.*, 2003.
- Mihailovic, D. T., S.T. Rao, C. Hogrefe and R. Clark, An approach for the aggregation of aerodynamic surface parameters in calculating the turbulent fluxes over heterogeneous surfaces in atmospheric models. *Env. Fluid Mech.*, **2**, 315-337, 2002.

- Mihailovic, D.T., D. Kapor, C. Hogrefe, J. Lazic and T. Tasic, Parameterization of albedo for heterogeneous surfaces in land surface schemes for environmental modeling I: Theoretical background and simple model, to appear in *Env. Fluid Mech.*, 2003.
- Porter, P. S., S. T. Rao, I. G. Zurbenko, A. Dunker, and G. Wolff: Ozone air quality over North America: part II - an analysis of trend detection and attribution techniques, *J. Air Waste Manag. Assoc.*, **51**, 283-306, 2001.
- Rao, S. T., J.-Y. Ku, S. Berman, K. Zhang, and H. Mao: Summertime characteristics of the atmospheric boundary-layer and relationships to ozone levels over the eastern United States, *Pure Appl. Geophys.*, **160**, 21-55, 2003.
- Sistla, G., W. Hao, J.-Y. Ku, G. Kallos, K. Zhang, H. Mao, and S. T. Rao: An operational evaluation of two regional-scale ozone air quality modeling systems over the eastern United States, *Bull. Amer. Meteor. Soc.*, **82**, 945-964, 2001.
- Sistla, C., K.L. Civerolo, W. Hao, and S.T. Rao, An evaluation of the UAM-V predicted concentrations of carbon monoxide and reactive nitrogen compounds over the eastern United States during Summer 1995, *J. Air Waste Manag. Assoc.*, **52**, 1324-1332, 2002.
- Zhang, J., and S.T. Rao, The role of vertical mixing in the temporal evolution of ground-level ozone concentrations, *J. Appl. Meteor.*, **38**, 1674-1691, 1999.
- Zhang, K., H. Mao, K. Civerolo, S. Berman, J.-Y. Ku, S. T. Rao, B. Doddridge, C. R. Philbrick, and R. Clark, Numerical investigation of boundary-layer evolution and nocturnal low-level jets: local versus non-local PBL schemes, *Env. Fluid. Mech.*, **1**, 171 -208, 2001.

CONFERENCE PAPERS

- Athanassiadis, G. A., S. T. Rao, J.-Y. Ku, and R. Clark, Boundary-layer evolution and its effects on ground-level ozone concentrations, 4th Conference on Atmospheric Chemistry, Orlando, FL, *Amer. Meteor. Soc.*, 97-102, 2002.
- Biswas, J., C. Hogrefe, and S. T. Rao, Temporal and spatial variability of ozone production efficiencies over the eastern United States, Proceedings of the 95nd Annual Meeting of the Air & Waste Management Association, June 23 - 27, Baltimore, MD, 2002.
- Gego, E., C. Hogrefe, S. T. Rao, and P. S. Porter, Probabilistic assessment of regional scale ozone pollution in the eastern United States, To appear in *NATO Science Series*, Kluwer Academic Publishers, 2003.
- Gego, E., C. Hogrefe, P.S. Porter, J.S. Irwin, and S.T. Rao, Comparison of the space-time signatures of air quality data from different modeling networks, To appear in *Air Pollution Modeling and Its Application XVI*, Kluwer Academic Publishers, 2003.

- Hogrefe, C., S. T. Rao, and K. L. Demerjian, Using the current-generation meteorological/photochemical modeling systems for real-time ozone forecasting. Proceedings of the 16th Conference on Probability and Statistics in the Atmospheric Sciences, January 13 – 17, *Amer. Meteor. Soc.*, Orlando, FL, 2002.
- Lazic, J., D.T. Mihailovic, S.T. Rao, and C. Hogrefe, Land air surface scheme (LAPS) for use in urban modeling, *International Environmental Modelling and Software Society (iEMSs) 2002 Conference*, June 24 – 27, Lugano, Switzerland, 448-453, 2002.
- Mihailovic, D.T, Environmental modeling of physical, biophysical and chemical processes in the atmosphere-plant-soil-interaction: how nonlinearity affects the solutions?, *International Environmental Modelling and Software Society (iEMSs) 2002 Conference*, June 24 – 27, Lugano, Switzerland, 383-388, 2002.
- Rao, S. T., C. Hogrefe, H. Mao, J. Biswas, I. G. Zurbenko, P. S. Porter, P. Kasibhatla, and D. A. Hansen, How should the photochemical modeling systems be used in guiding emissions management decisions? In: *Air Pollution Modeling and Its Application XIV*; Gryning, S. E. and F. Schiermeier, eds., Kluwer Academic/Plenum, New York, 25 – 34, 2001.

INVITED TALKS AT INTERNATIONAL CONFERENCES

- Rao, S. T., and C. Hogrefe, Using air quality models for emissions management decisions, “Uncertainty Treatment in Integrated Assessment Modelling” workshop of the *UN/ECE Task Force on Integrated Assessment Modelling*, January 24 – 25, 2002, IIASA, Laxenburg, Austria, 2002.
- Rao, S.T., E. Gego, C. Hogrefe, Spatial analysis of meteorological and air quality data: Observations and model outputs, RAMS Workshop, Santorini, Greece, September 30 - October 4, 2002.
- Rao, S. T., E. Gego, and C. Hogrefe, Using regional-scale photochemical models for guiding emissions management decisions, *BMU/UBA-USEPA-EMEP Workshop*, October 7 - 11, 2002, Bad Breisig, Germany, 2002.

Section 7

RESEARCH STAFF SUPPORTED BY THIS RESEARCH PROJECT

GRADUATE STUDENTS

- Georgios Athanassiadis: M.S. Thesis, 2001, "Spatial and temporal variations in the trace elemental data over the northeastern United States"
- Jhumoor Biswas, Ph.D. Dissertation, 2000, "Uncertainties in photochemical modeling of ozone and its precursors in the eastern United States"
- Elvira Brankov: Ph.D. Dissertation, 1999, "Influence of atmospheric transport on ozone and toxic air contaminants in the Northeastern United States" (Won Distinguished Doctoral Dissertation Award)
- Christian Hogrefe: Ph.D. Dissertation, 2000, "Evaluating the regional-scale photochemical modeling systems and using them for regulatory policy-making" (Won N. Gokhale and P. Lemon awards for outstanding dissertation)
- Jian Zhang: Ph.D. Dissertation, 1998, "Effects of vertical mixing and photochemical processes on the ground-level ozone in the Northeast"

POST-DOCTORAL RESEARCH ASSOCIATES

- Dr. Jhumoor Biswas investigated the relationship between ozone and its precursors in both observations and model predictions.
- Dr. Edith Gego used geostatistical techniques to develop a methodology for integrating observations and model predictions into a probabilistic regulatory framework.
- Dr. Christian Hogrefe applied and compared different statistical techniques for the evaluation of photochemical modeling systems.
- Dr. Huiting Mao performed simulations with a particle dispersion model to study regional-scale pollutant transport and analyzed the effects of different boundary-layer parameterizations on predictions from meteorological and air quality models.

VISITING SCIENTISTS AND THEIR CONTRIBUTIONS TO THIS PROJECT

- Dr. Kiran Alapaty used a 1-D atmospheric boundary-layer model to evaluate an advanced land-surface scheme utilizing the special observational data collected during summer of 1987 from the First

International Satellite Land Surface Climatology Project (ISLSCP) Field Experiment (FIFE) special observations over Manhattan, Kansas.

- Professor George Kallos performed simulations with the RAMS model to study the effect of horizontal grid resolution on model predictions. He further provided guidance on the incorporation of an advanced land-surface model into the ETA meteorological model by Professor Dragutin Mihailovic.
- Dr. Gang Liu applied non-linear time series methods to evaluate the temperature predictions from two different meteorological models.
- Professor Dragutin Mihailovic developed new approaches to account for sub-grid scale variability of surface roughness and albedo in atmospheric models. He also incorporated his advanced land-surface model into the ETA meteorological model.
- Professor P. Steven Porter helped compare different statistical techniques for the evaluation of photochemical modeling systems. He further participated in the development of a methodology for integrating the observations and model predictions into a probabilistic regulatory framework.
- Professor Somaraju Vempaty applied different statistical techniques for evaluating photochemical modeling systems.
- Professor Igor Zurbenko developed several statistical techniques for the spectral decomposition of time series of atmospheric variables in observations and model outputs.

ADMINISTRATIVE STAFF

- Ms. Sally Marsh provided administrative support to this research project.

Appendix A

Evaluation and Intercomparison Studies of the Land-Air Parameterization Scheme (LAPS) Using a 1-D Model and FIFE Observations

by

Kiran Alapaty

*MCNC– Environmental Modeling Center
Research Triangle Park, North Carolina*

Revised Technical Report

June 20, 2003

Corresponding author address: *Dr. Kiran Alapaty, MCNC–Environmental Modeling Center, P.O. Box 12889, 3021 Cornwallis Road, Research Triangle Park, NC 27709-2889. E-mail: kiran_alapaty@unc.edu; Ph: (919) 966-2223; FAX: (919) 843-3113*

Disclaimer

The comments, recommendations, and suggestions included in this document are based solely on Dr. Alapaty's experience in atmospheric modeling. His views do not necessarily reflect those of MCNC.

SUMMARY

The Land-Air Parameterization Scheme (LAPS), a sophisticated land surface parameterization formulation, was implemented into a 1-D atmospheric boundary layer model and evaluated utilizing the special observational data collected during summer of 1987 from the First International Satellite Land Surface Climatology Project (ISLSCP) Field Experiment (FIFE) over Manhattan, Kansas. The LAPS simulation results were compared with the results obtained from using another sophisticated but relatively simpler land surface parameterization scheme (referred to as NPJS) that is already available in the 1-D model. Results from two case studies were analyzed during which boundary layer processes dominated the lower atmospheric processes.

Both the LAPS and NPJS use simple but different formulations estimating outgoing and incoming radiation fluxes resulting in minor differences in the estimated net radiation reaching the surface. We found that an underestimation of net radiation and estimation of higher stomatal resistance in LAPS have triggered many of the differences in results between LAPS and NPJS in the first case study. In the NPJS negative sensible heat fluxes that exists after late evening hours occurred an hour before than that in LAPS and the observations. LAPS underestimated latent heat fluxes in first case more than in the second case when compared to observations and NPJS. Trends in soil heat flux are very similar in LAPS and NPJS. In the second case only minor differences existed between respective net radiation and stomatal resistance fields, leading to similar boundary layer structures. Diagnostic results indicate that in both cases direct evaporation fluxes are significantly different while transpiration fluxes are somewhat similar. Growth rates of and depths of atmospheric boundary layer in both schemes are also very similar. Vertical profiles of virtual potential temps, water vapor mixing ratio, horizontal winds are also found to be very similar in LAPS and NPJS. Differences in concentrations of various chemical species are mainly due to differences in depths of boundary layer resulted from using different land surface models.

There were some general features that were associated with each of the schemes in both the simulations. Simulated direct evaporation fluxes are higher in LAPS while they are significantly lower in NPJS. Further, diurnal variation in direct evaporation fluxes is significant in NPJS while it is absent in the LAPS. Also, transpiration fluxes are lower in both the simulations in LAPS compared to those in the NPJS.

In our future studies, we propose to perform sensitivity studies for further evaluation of LAPS in simulating boundary layer structures. Finally, we will move to the mesoscale model, Version 5 (MM5) to evaluate LAPS in simulating mesoscale circulations influenced by surface processes.

INTRODUCTION

Land surface processes play important role in boundary layer and other atmospheric processes at local- to global-scales. Due to the lack of computer resources and detailed observational data for use and verification in numerical models, these processes are represented using highly simplified formulations in the past generation of numerical models. Ever increasing availability of computer resources and traditional land-based observations as well as satellite measurements of various land surface parameters led to the development and refinement of land surface models (LSM). During the past decade many land surface models were developed and these are being refined to improve model simulations. Special measurements such as those from the **F**irst **I**nternational **S**atellite **L**and **S**urface **C**limatology **P**roject (ISLSCP) **F**ield **E**xperiment (FIFE) (Sellers et al., 1992) provide a unique opportunity to improve our understanding of surface-atmosphere interactions and also use these measurements for specification of initial conditions and evaluation of land surface models. One of these sophisticated land surface models is the Land-Air Parameterization Scheme (LAPS) developed by Mihailovic et al. (1993) and Mihailovic and Ruml (1996) and Mihailovic and Kallos (1997). Advantages of this scheme over many other schemes are that LAPS (1) estimates of canopy temperature as well as ground/skin temperature, and (2) it has ability to take account of subgrid-scale land use variability and thereby many surface parameters in a grid cell are represented more accurately than in other schemes where only dominant land use and related parameters are used.

Our overall objectives are to (1) to study the performance of the LAPS using the FIFE measurements, and (2) compare LAPS simulations with a relatively simpler land surface model. These two objectives are accomplished by using a one-dimensional soil-vegetation-boundary layer-chemistry model. In the near future we plan to implement the LAPS into the fifth-generation mesoscale model MM5 (Grell et al. 1994) for further evaluation by simulating mesoscale circulations that are dominated by land surface processes.

BRIEF DESCRIPTION OF MODEL

We used a three-dimensional windowed model developed by Alapaty et al., (1997) to study the effects of different representations of soil-vegetation-atmosphere interactions on predicted boundary layer parameters using a turbulent kinetic energy (TKE) scheme. The windowed model has 35 vertical sigma layers and 3X3 grid cells in the horizontal. Essentially, this model is a one-dimensional boundary layer model in which predictions are made only at the central grid cell for all vertical layers. The eight horizontal grid cells surrounding the computational grid cell in each layer assume the same meteorological characteristics as those of the central/computational grid cell. Modular models like this one offer several advantages: they can be used efficiently for one-dimensional simulation and diagnostic studies, they can be used on any computer system, and they can easily be implemented into any two- or three-dimensional model without major modifications. The governing equations and the parameterization schemes used are described below.

The governing equations

The general forms of the dynamic and thermodynamic equations used in the model are

$$\frac{\partial u}{\partial t} = -u \frac{\partial u}{\partial x} - v \frac{\partial u}{\partial y} - \frac{\partial}{\partial z} (\overline{u'w'}) - f(v_g - v) \quad (1)$$

$$\frac{\partial v}{\partial t} = -u \frac{\partial v}{\partial x} - v \frac{\partial v}{\partial y} - \frac{\partial}{\partial z} (\overline{v'w'}) + f(u_g - u) \quad (2)$$

$$\frac{\partial T}{\partial t} = -u \frac{\partial T}{\partial x} - v \frac{\partial T}{\partial y} - \frac{\partial}{\partial z} (\overline{w'T'}) \quad (3)$$

$$\frac{\partial q_v}{\partial t} = -u \frac{\partial q_v}{\partial x} - v \frac{\partial q_v}{\partial y} - \frac{\partial}{\partial z} (\overline{w'q'_v}) \quad (4)$$

where u and v are the eastward and northward components of the wind, respectively; z is the altitude; the quantities in the parentheses are turbulent fluxes; f is the Coriolis parameter; T is temperature; and q_v is the mixing ratio of water vapor, and u_g and v_g are the eastward and northward geostrophic winds, respectively.

Land Surface Models

Accurate representation of surface characteristics is very important because these control surface processes that affect the surface energy budget and hence the atmospheric boundary layer (ABL) processes. We have implemented the LAPS, a sophisticated soil-vegetation parameterization scheme, developed by Mihailovic et al. (1993), Mihailovic and Ruml (1996) and Mihailovic and Kallos (1997) into the 1-D model. The 1-D model has already an option to use another sophisticated land surface model developed by Noilhan and Planton (1989) and Jacquemin and Noilhan (1990). The 1-D model is configured with two different surface and subsurface configurations according to the land surface schemes. These details are given below.

With the Noilhan and Planton (1989) and Jacquemin and Noilhan (1990) scheme (hereafter referred to as NPJS), the 1-D model configuration has two soil layers, representing surface and subsurface processes; the first layer is 0.01 m thick and the second layer is 1 m thick, and the prognostic equations to calculate the temperatures and soil moisture contents of the two soil layers are shown in Eq. (5) through (8). The rate of change of the mean temperature of soil layer 1 can be written as

$$\frac{\partial T_{g1}}{\partial t} = C_T (R_n - S_{hf} - L_{hf}) - \frac{2\pi}{\tau} (T_{g1} - T_{g2}) \quad (5)$$

where t is time, T_{g1} and T_{g2} are the temperatures of layers 1 and 2; C_T is the inverse of thermal capacity of a particular type of soil; R_n is the net radiation at the surface; S_{hf} and L_{hf} are the surface sensible and latent heat

fluxes; and τ is the number of seconds in a day. The mean temperature of layer 2 is given by (Blackadar 1976):

$$\frac{\partial T_{g2}}{\partial t} = \frac{1}{\tau} (T_{g1} - T_{g2}) \quad (6)$$

Prognostic equations for the soil moisture for the two layers are given as

$$\frac{\partial W_{g1}}{\partial t} = \frac{C_1}{\rho_w d_1} (P_g - E_g) - \frac{C_2}{\tau} (W_{g1} - W_{geq}) \quad (7)$$

$$\frac{\partial W_{g2}}{\partial t} = \frac{1}{\rho_w d_2} (P_g - E_g - E_{tr}) \quad (8)$$

where W_{g1} and W_{g2} are the volumetric soil moisture contents for the two soil layers, C_1 and C_2 are functions of soil type and its water retention characteristics, ρ_w is the density of liquid water, d_1 and d_2 are the thicknesses of the two soil layers, P_g is the flux of rain water reaching the soil surface, E_g is the evaporation at the soil surface after interception and runoff, E_g is the evaporation at the soil surface, W_{geq} is the layer 1 soil moisture when gravity balances the capillary forces, and E_{tr} is the transpiration rate.

The water content on the wet parts of the canopy due to rainfall and/or dew formation on the foliage is represented by W_r . The prognostic equation for W_r is based on Deardorff's (1978) formulation and can be written as

$$\frac{\partial W_r}{\partial t} = (V_c P_r) - E_r - R_r \quad (9)$$

where V_c is the vegetation cover in fractional units, P_r is the precipitation rate at the top of the vegetation, E_r is the evaporation rate from the wet parts of the canopy, and R_r is the runoff rate from canopy interception reservoir.

With the Mihailovic et al. (1993), Mihailovic and Ruml (1996) and Mihailovic and Kallos (1997) land surface scheme, the Land-Air Parameterization Scheme (hereafter referred to as LAPS), there are three soil layers. The LAPS scheme uses the morphological and physiological characteristics of the vegetation community for deriving the coefficients and resistances that govern all the fluxes between the surface and atmosphere. The prognostic equations for the canopy temperature, T_p and the soil surface temperature, T_g and deep soil temperature T_d , are

$$C_f \frac{\partial T_f}{\partial t} = R_f^{net} - H_f - \lambda E_f \quad (10)$$

$$C_g \frac{\partial T_g}{\partial t} = R_g^{net} - H_g - \lambda E_g - G \quad (11)$$

$$\frac{\partial T_d}{\partial t} = 2 C_g (R_g^{\text{net}} - H_g - \lambda E_g) / \sqrt{365\pi} \quad (12)$$

where C is the heat capacity, R^{net} the absorbed short wave and long wave radiation, λ is latent heat of evaporation, H the sensible heat transpiration rate, G the soil heat flux, and C_g is ground thermal capacity. The subscript f refers to the canopy, g to the soil surface. The soil heat flux is parameterized using "force-restore" method. The third soil layer temperature is governed by a simple diffusion equation. The prognostic equations for the water stored on the canopy, w_p is

$$\frac{\partial w_f}{\partial t} = P_f - E_{wf} / \rho_w \quad (13)$$

where ρ_w is the density of water, P_f the water amount retained on the canopy, E_{wf} the evaporation of water from the wetted fraction of canopy. When the conditions for dew formation are satisfied, the condensed moisture is added to the interception store, w_p . The parameterization of the soil water content is based on the concept of the three-layer model (Mihailovic, 1993). The governing equations take the form

$$\frac{\partial w_1}{\partial t} = \frac{1}{D_1} \left\{ P_1 - F_{1,2} - \frac{E_g + E_{tf,1}}{\rho_w} - R_0 - R_1 \right\} \quad (14)$$

$$\frac{\partial w_2}{\partial t} = \frac{1}{D_2} \left\{ F_{1,2} - F_{2,3} - E_{tf,2} / \rho_w - R_2 \right\} \quad (15)$$

$$\frac{\partial w_3}{\partial t} = \frac{1}{D_3} \left\{ F_{2,3} - F_3 - R_3 \right\} \quad (16)$$

where w_i is the volumetric soil moisture content in i th layer, P_1 the infiltration rate of precipitation into the upper soil moisture store, D_i the thickness of the i th soil layer, $F_{i,i+1}$ the water flux between i and $i+1$ soil layer, F_3 the gravitational drainage flux from recharge soil moisture store, $E_{tf,1}$ and $E_{tf,2}$ the canopy extraction of soil moisture by transpiration from the first and the second soil layer, respectively, R_0 the surface runoff and R_i the subsurface runoff from the i th soil layer.

The radiation model

Two simple radiation models are used in this study. In both the land surface models (i.e., LAPS and NPJS) the net radiation at the surface is calculated as the sum of incoming solar radiation absorbed at the surface, atmospheric longwave back-scattering radiation, and outgoing longwave surface radiation. However, both the schemes use different physical formulations in estimating the net radiation reaching the ground. In general, in these formulations solar radiation reaching the surface is a function of solar zenith angle, surface albedo, and atmospheric turbidity. Surface albedo is computed as the sum of minimum albedo with a solar zenith angle of

zero and albedo changes due to the variation in the solar zenith angle (Idso et al., 1975; Pielke et al., 1992; Pleim and Xiu, 1995). Upward and downward longwave radiation are calculated as suggested by Anthes et al. (1987), which are functions of soil emissivity, ground temperature, atmospheric longwave emissivity, and atmospheric temperatures.

Surface layer formulation

The lower boundary layer (surface layer) is parameterized based on similarity theory suggested by Monin and Yaglom (1971) using the nondimensional stability parameters Φ_m , Φ_h , and Φ_q , for momentum, heat, and moisture, respectively. Turbulent sensible heat fluxes are computed using the relation given by

$$S_{hf} = u_* \Theta_*$$

where u_* is friction velocity, and Θ_* is the scale for temperature. Latent heat fluxes are computed from the soil-vegetation model discussed above, where bare-ground evaporation and evaporation from transpiring canopies and the wet parts of the canopies (due to dew formation and/or rainfall interception) are estimated. Thus, the total latent heat fluxes at the surface in NPJS and LAPS, respectively, can be written as

$$L_{hf} = E_g + E_{tr} + E_r \quad \text{and} \quad L_{hf} = E_g + (E_{tf,1} + E_{tf,2}) + E_{wf}$$

Boundary Layer Scheme

In our study, we used a scheme based on turbulent kinetic energy (TKE) and its dissipation rate that is already implemented and well tested in the 1-D and a 3-D mesoscale model (MM5) by Alapaty et al. (1997) and Alapaty et al., (1999). The prognostic equations used in this scheme to explicitly calculate the turbulent kinetic energy (E) and its dissipation rate (ϵ) are those suggested by Yamada and Mellor (1975). This TKE scheme is often called a one-and-a-half-order closure scheme in which the unknown terms in the prognostic equations are parameterized in terms of local gradients of dynamic and thermodynamic parameters. The coefficient of vertical eddy diffusivity is calculated from the ratio of E and ϵ . Surface layer similarity profiles (Businger et al. 1971) are used for obtaining boundary conditions for the prognostic equations for E and ϵ , while for the mixed layer the E- ϵ scheme is used. For further details, the reader is referred to Alapaty et al. (1994). The coefficients of eddy diffusivity for momentum and heat can be written as

$$K_m = \frac{c_2 E^2}{\epsilon} \quad \text{and} \quad K_h = K_m \frac{\Phi_m(z/L)}{\Phi_h(z/L)} \quad (17)$$

where c_2 is used as a constant though it was originally formulated as function of friction velocity and E by Detering and Etling (1985), Φ_m and Φ_h are nondimensional functions for momentum and heat (Businger et al. 1971).

Free Atmospheric Turbulent Mixing

In the free atmosphere, turbulent mixing is parameterized using the formulation suggested by Blackadar (1979) in which vertical eddy diffusivities are functions of the Richardson number and wind shear in the vertical. This formulation can be written as

$$K_z = K_0 + S (kt)^2 \frac{R_c - R_i}{R_c} \quad (18)$$

where K_0 is the background value ($1 \text{ m}^2 \text{ s}^{-1}$), S is the vertical wind shear, t is the characteristic turbulent length scale (100 m), R_c is the critical Richardson number, and R_i is the Richardson number:

$$R_i = \frac{g}{\Theta_v S^2} \frac{\partial \Theta_v}{\partial z}$$

where g is the acceleration due to gravity and Θ_v is virtual potential temperature.

NUMERICAL SIMULATIONS AND SYNOPTIC CONDITIONS

We have performed two numerical case studies using the special measurements available from the FIFE. In each of these case studies, we performed two numerical simulations for a period of 12 hours using the NPJS and the LAPS land surface models. The starting time of simulations in the first and second cases respectively is 0700 LT 06 June 1987 and 0700 LT 11 July 1987. These two days are referred to as “golden days” in the literature because boundary layer processes dominated the lower atmospheric structure over the FIFE region. The FIFE site is located near Manhattan, KS, covering a $15 \times 15 \text{ km}$ area where grass prairie is the predominant vegetation. Various initial conditions used in the simulations are shown in the Table 1. Measured surface fluxes (sensible and latent heat and net radiation fluxes) are available for every 30 minutes time interval while vertical profiles of temperature, winds, and humidity obtained using slow ascent balloons are available for every $\sim 10 \text{ m}$ vertical altitude intervals for various hours during each day of the observations.

Initial meteorological conditions (0700 LT) for the two FIFE cases have indicated the presence of the remnants of a nocturnal jet with a maximum wind speed located at about 500 m above ground level. Up to the altitude of about 500 m water vapor mixing ratio showed very weak vertical gradients. Virtual potential temperature indicated stable lapse rates. Observations at later time periods indicated that during the daytime evolution of the ABL, the nocturnal jet had dissipated, leading to decreased wind shear within the ABL. Observed water vapor mixing ratio and virtual potential temperature profiles (estimated from temperature, dew point temperature and pressure) at different periods during daytime indicated the presence of well-mixed layers in the ABL. In the July case clouds were observed at about 1600 LT causing changes in the land surface and boundary layer processes. Since the 1-D model is not configured with a cumulus cloud convection option, cloud-induced processes could not be simulated in the present model simulations.

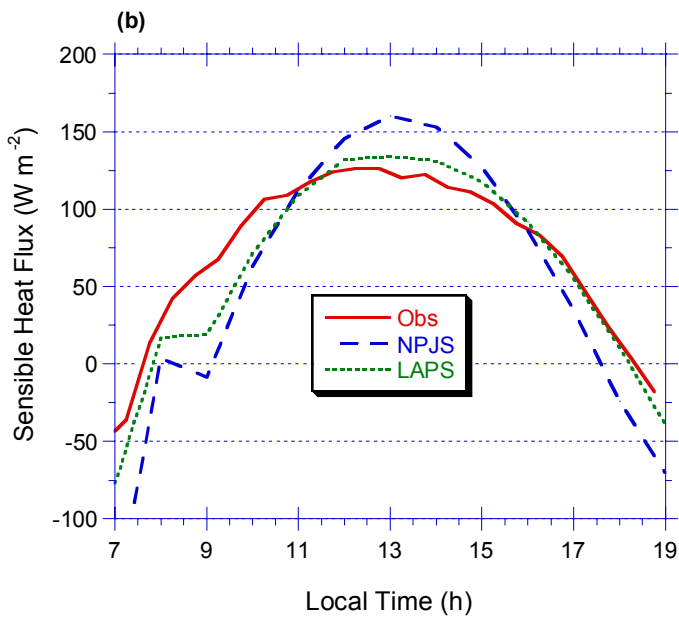
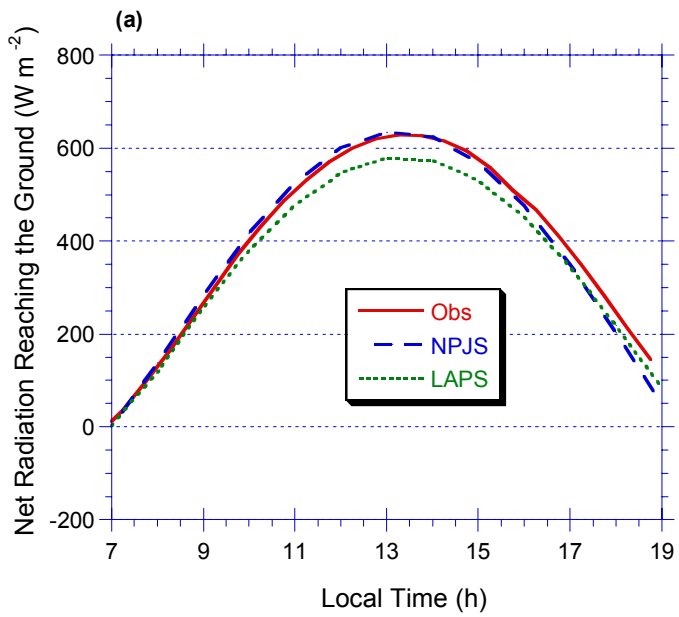
RESULTS AND DISCUSSION

In all illustrations measurements are referred to as “Obs” and model results obtained from using the land surface parameterization developed by Noilhan and Planton (1989) and Jacquemin and Noilhan (1990) are referred to as NPJS while those from using the land surface parameterization developed by Mihailovic et al. (1993), Mihailovic and Ruml (1996) and Mihailovic and Kallos (1997) are referred to as LAPS.

The 06 June 1987 case study

During this first case study period (which is the first intensive field campaign of the FIFE) clear sky conditions were observed during the entire day. Thus, comparing measured radiation and surface heat fluxes with the model estimates will reveal effects of approximations in the land surface model formulations. Temporal variation of measured (available at every 30-minute intervals from 0700 to 1900 LT) and modeled net radiation reaching the ground surface is shown in Figure 1a. As mentioned earlier, both the LAPS and NPJS use simple but different formulations estimating outgoing and incoming radiation fluxes. As a result, minor differences in the estimated net radiation can be attributed mostly to the difference in the formulations. It can be seen that LAPS underestimates the peak in net radiation by about 50 W m^{-2} compared to observations and NPJS. Major portion of surface energy is partitioned between sensible, latent, and soil heat fluxes. Of these three, a land surface model determines latent heat fluxes, then most of the remaining energy is partitioned into sensible and soil heat fluxes. Thus, an underestimation in the net radiation can lead to differences in model estimation of other meteorological variables.

Figure 1b shows temporal variation of measured and predicted sensible heat fluxes. In general, fluxes predicted by LAPS are in very good agreement with measurements. With NPJS, peak in the sensible heat flux is overestimated by about 30 W m^{-2} . Also, from the late afternoon hours to the end of the simulation (1900 LT), LAPS predictions are much closer to observations. Though the initial conditions and the formulation used to represent surface layer processes are the same in both the simulations, the slight differences among the predictions indicate the effects of different representations of surface and subsurface processes. In the NPJS the onset of negative sensible heat fluxes happens an hour before than that in LAPS and the observations. If one uses an ABL scheme such as one based on K-theory, sign reversal in surface sensible heat flux leads to differing estimates of eddy diffusivity values as compared to a TKE-based scheme. Our experience (Alapaty et al., 1997) indicated that this early reversal of sign of the sensible heat flux led to early collapse of ABL compared to that in observations. Since the present study uses a TKE-based scheme, early collapse of ABL will not show up in the simulations.



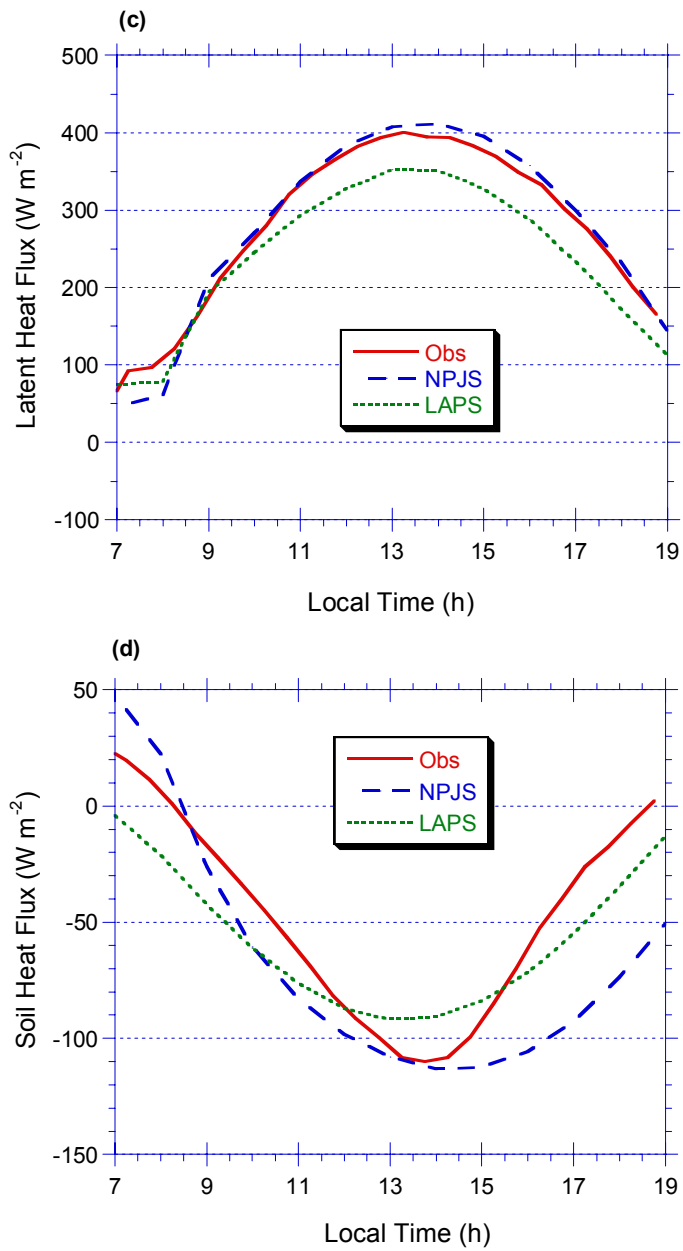
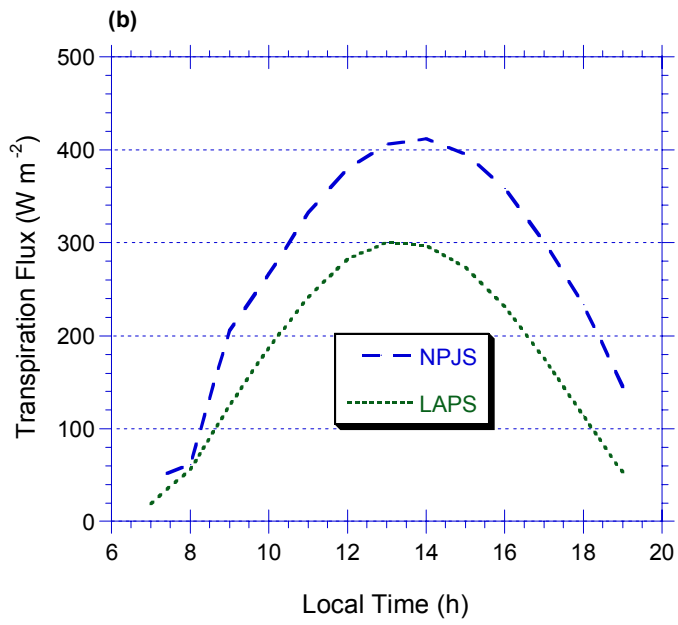
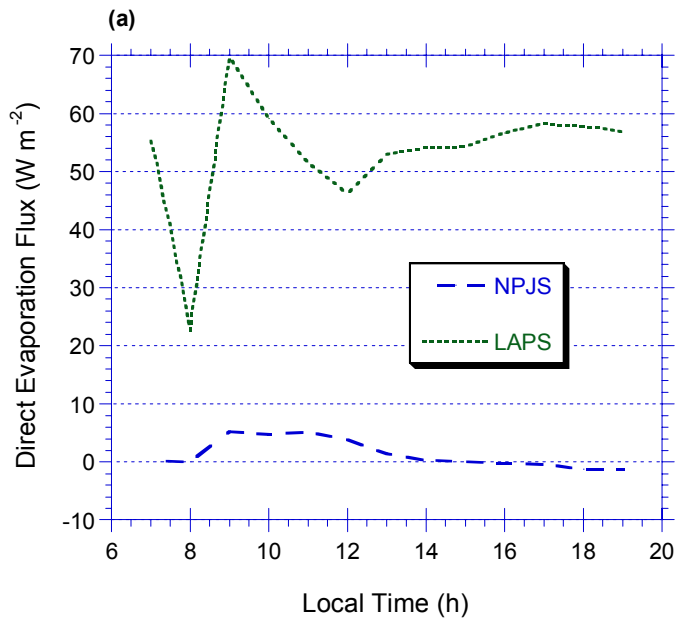


Figure 1. Temporal variation of measured and modeled (a) Net radiation reaching the surface (b) Sensible heat flux, (c) Latent heat flux, and (d) Soil heat flux for the 06 June 1987 FIFE case study. All measurements are available at 30-minute time interval.

Predicted latent heat fluxes (Fig. 1c) by NPJS are very close to observations while LAPS underestimated latent heat fluxes with a maximum difference of about $\sim 45 \text{ W m}^{-2}$. The remaining component in the surface energy budget is the soil heat flux, i.e., heat flux due to conduction between soil layers. Temporal variation of measured and modeled soil heat flux between soil layers 1 and 2 is shown in Figure 1d. Positive values indicate heat conduction from soil layer 2 to 1 (i.e., soil layer 2 is warmer than layer 1), which is typical during late night through morning hours. During daytime, typical to this type of case study, soil heat fluxes should be negative (i.e., heat is lost to soil layer 2 from layer 1). The initial soil layer temperatures and moistures in LAPS and NPJS are exactly same while formulations in the prognostic equations for these variables are different, there exists some differences among the measurements and model estimates. However, the trend is very similar in all of them. An underestimation of net radiation reaching the surface in LAPS has triggered many of the differences discussed above.

To further diagnose differences between estimated surface latent heat fluxes in LAPS and NPJS, we present temporal variation of predicted direct evaporation and transpiration fluxes in Figs. 2a and 2b. The sum of these two components makes up most of the total surface latent heat fluxes. Interestingly, large differences exist. NPJS estimates very negligible amounts (-2 to 5 W m^{-2}) of direct evaporation fluxes (Fig. 2a) compared to LAPS which on average is about $\sim 50 \text{ W m}^{-2}$. On the other hand, transpiration fluxes in NPJS are higher than those in LAPS with a peak difference by about $\sim 110 \text{ W m}^{-2}$. To further study nature of these differences, we present the temporal variation of volumetric soil moisture for layers 1 and 2 in Figures 2c and 2d. Despite larger direct evaporation fluxes in LAPS compared to NPJS, layer-1 soil moisture is higher than that in NPJS, probably due to transport of water from layer 2. Also, diurnal variation of layer-1 soil moisture is absent in LAPS. Since the soil layer-1 is only 10 cm thick, one would expect diurnal variation in such a thin soil layer. Since we don't have access to soil moisture measurements, it can't be readily verified. Since the transpiration fluxes in LAPS are lower than those in NPJS, root zone soil moisture (soil layer-2) in LAPS is consistently higher to that of it in NPJS.

Temporal variation of depth of atmospheric boundary layer (ABL) from the measurements (LIDAR-based) and from LAPS and NPJS (based on the predicted TKE profiles) are shown in Figure 3a. Though both the LAPS and NPJS underestimated the ABL depths but the magnitude differences between measurements and modeled depths are within the uncertainty in the measured depths. Importantly, the growth rate of ABL starting from 0800 LT in LAPS and NPJS is very similar to that in measurements. Further, both the LAPS and NPJS show very similar ABL depths with time. Since the estimated turbulent sensible heat fluxes are slightly higher in NPJS compared to that in LAPS, its effect is reflected in the simulated depths of the ABL. Alapaty et al. (1997b) showed that stomatal resistance is one of key parameter that influences the surface latent heat fluxes and hence the depth of the ABL. Figure 3b shows the temporal variation of modeled stomatal resistance in LAPS and NPJS. Note that we have used the same value of minimum stomatal resistance (available from FIFE measurements) in both the simulations (i.e., LAPS and NPJS) and both LAPS and NPJS use Jarvis-type



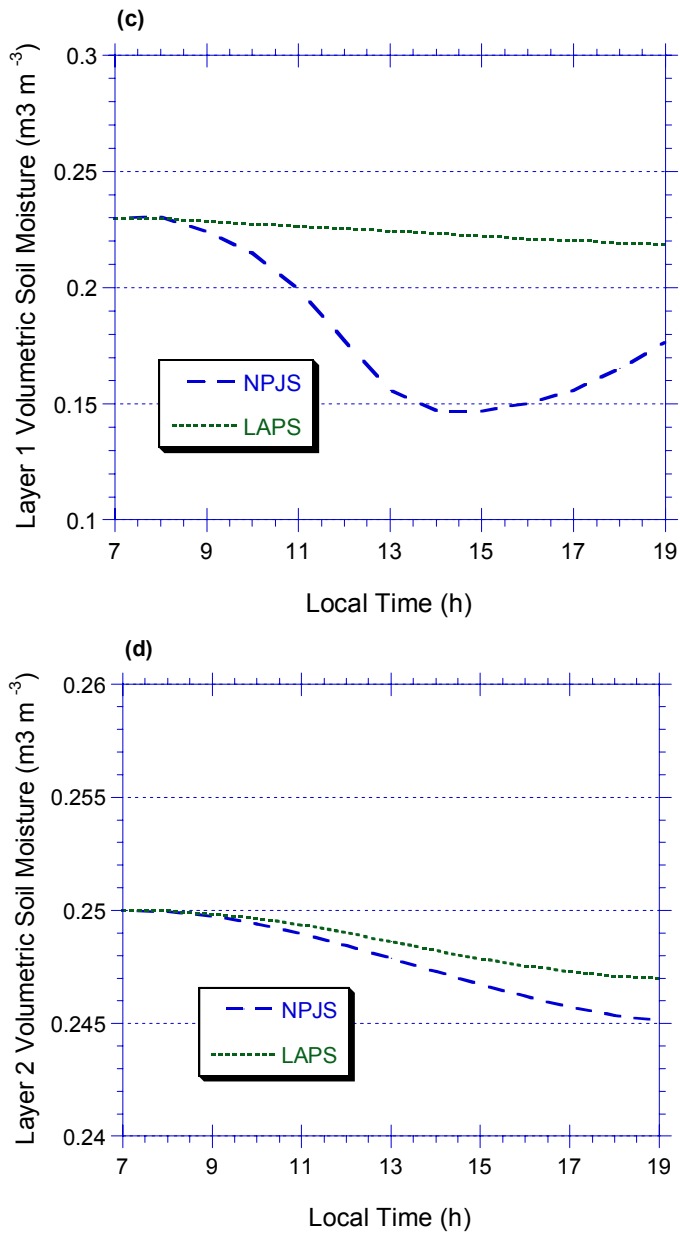


Figure 2. Temporal variation of modeled (a) Direct evaporation, and (b) Transpiration fluxes, and soil moisture for (c) layer 1, and (d) layer 2 for the 06 June 1987 FIFE case study.

formulations to estimate stomatal resistance. However, NPJS uses a slightly different version of Jarvis-type formulation compared to that in LAPS, resulting in differences in the estimation of stomatal resistance. Since estimated stomatal resistance in LAPS is higher by about $\sim 40 \text{ s m}^{-1}$ compared to that in NPJS during convective conditions in ABL, it resulted in lower estimation of transpiration fluxes as shown in Figure 1c and hence in higher root zone soil moisture (for soil layer-2). Thus, differences in surface sensible and latent heat fluxes in LAPS and NPJS are mostly due to differences in estimated net radiation and stomatal resistance, which influenced other processes and parameters.

Of interest to meteorological and air quality simulation modelers is better prediction of near-surface winds, temperature, and moisture. This is because these parameters can affect the estimation of surface turbulent fluxes of thermodynamic parameters and chemical species, biogenic emission rates, chemical reactions that are strongly influenced by H_2O_2 concentrations. We compare surface observations of temperature, water vapor mixing ratio, u- and v-winds (eastward and northward components of horizontal wind) with corresponding modeled values from LAPS and NPJS. Since the lowest level in the model is located at about 10.9 m AGL, predicted winds, temperature, and water vapor mixing can be directly compared to the measurements made at 10 m AGL.

Figure 4a shows the temporal variation of near-surface air temperature from measurements and from LAPS and NPJS. Both the schemes result in very similar temperatures and are similar to that in observations. Similarly, water vapor mixing ratio (Fig. 4b) also shows some minor differences, but in general they both follow observations. Trends in the predicted zonal winds (Fig. 4c) in both simulations follow the observations closely until 1400 LT after which observations and modeled zonal winds deviated by about a maximum of 3 m/s. Note that the zonal winds are very weak both in observations as well as in simulations, ranging from 1-4 m s^{-1} . Strong meridional winds (Fig. 4d) as observed are well simulated by LAPS and NPJS. In general, differences in between LAPS and NPJS are very insignificant. We now compare observed and predicted thermodynamic and dynamic profiles. Figures 5a, 5b, 5c, and 5d show the vertical variation in virtual potential temperature (Θ_v) obtained from the observations at different hours and corresponding model simulations using LAPS and NPJS. Initial conditions (0700 LT) indicate that the depth of the stable boundary layer could be about 300 m AGL (Fig. 5a). Also, the Θ_v profile between 300 m and 1400 m indicates the presence of the previous day's ABL, the residual boundary layer. At 1000 LT (Fig. 5b) both LAPS and NPJS very similar Θ_v profiles and by 1300 LT (Fig. 5c) both schemes show very similar results except that both are potentially cooler than observations by about 1-1.5 K. Though simulated surface sensible heat fluxes are slightly higher (by about 10-50 W m^{-2}) than in observations, depth of the ABL (inferred from the altitude of inversion) is shallow in LAPS and NPJS compared to that in observations (inferred from observed Θ_v and from Fig. 3a). Cooler temperatures in LAPS and NPJS are probably due to unaccounted advection processes happening at the FIFE site. Similar cooler temperatures (by about 2 K) and shallower ABL depths in LAPS and NPJS are persistent even at 1600 LT (Fig. 5d) compared to respective observations.

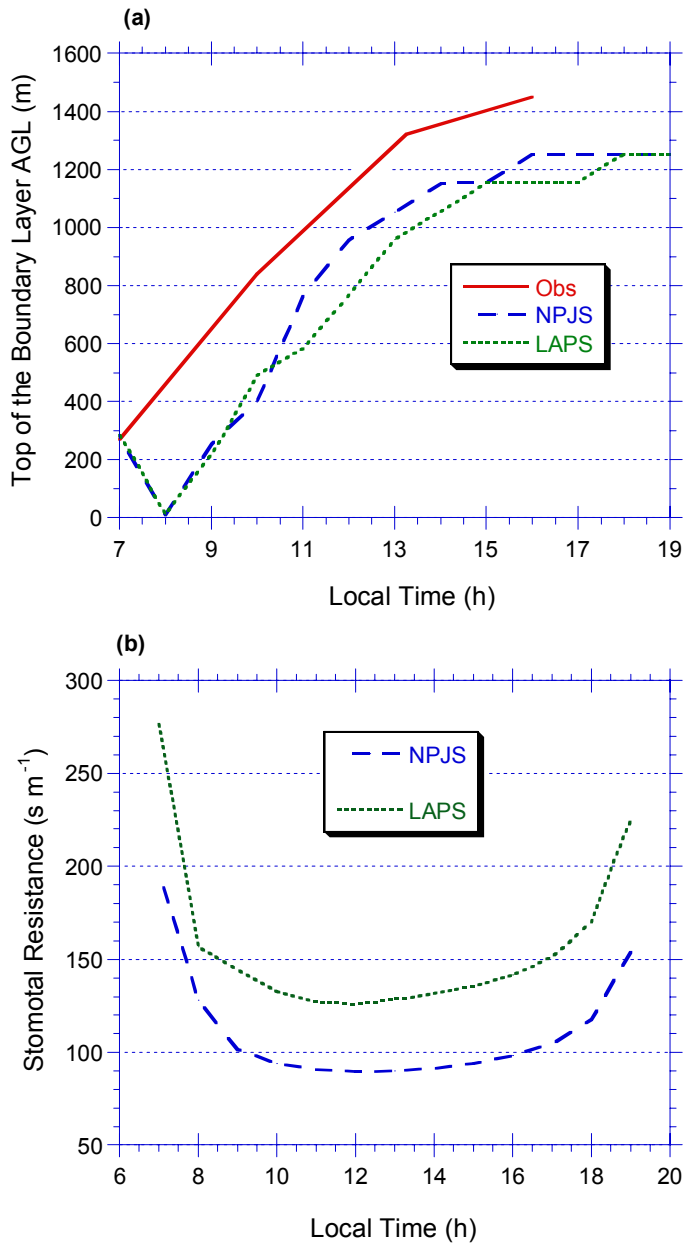
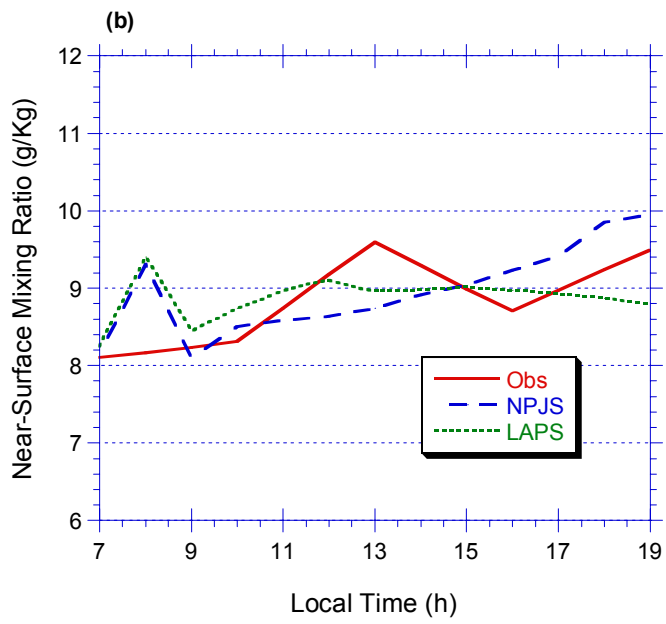
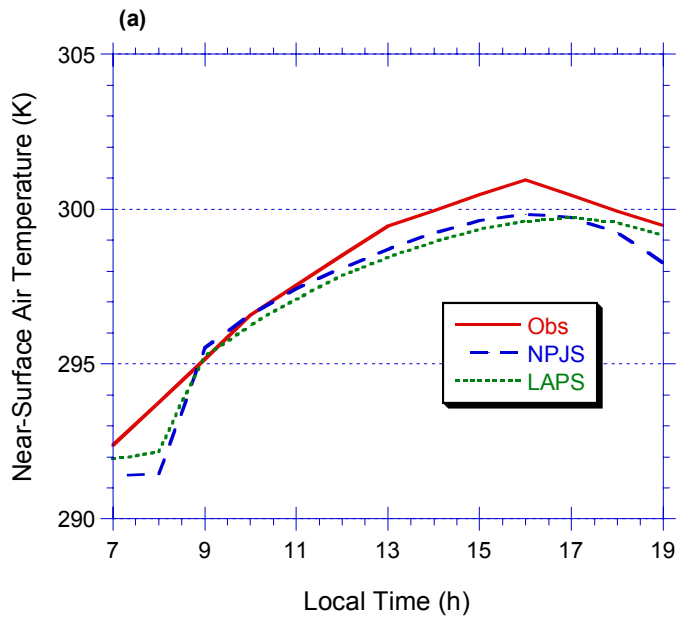


Figure 3. Temporal variation of (a) measured and modeled depth of the boundary layer, and (b) modeled stomatal resistance for the 06 June 1987 FIFE case study.



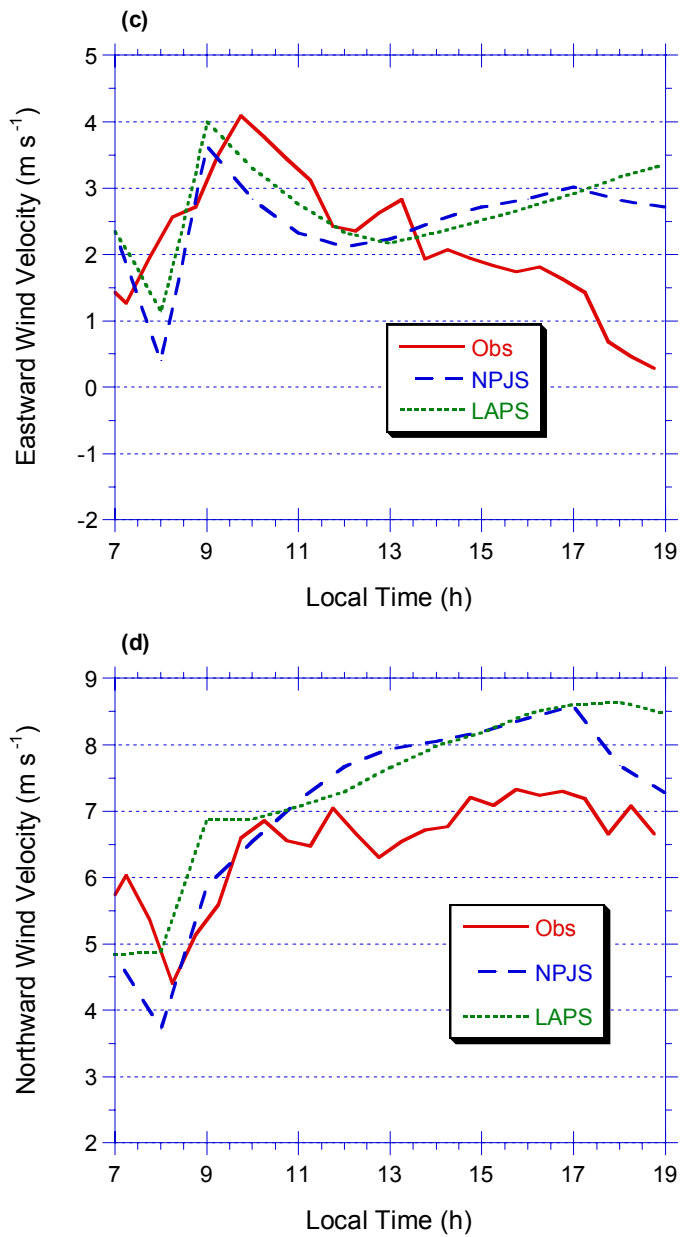
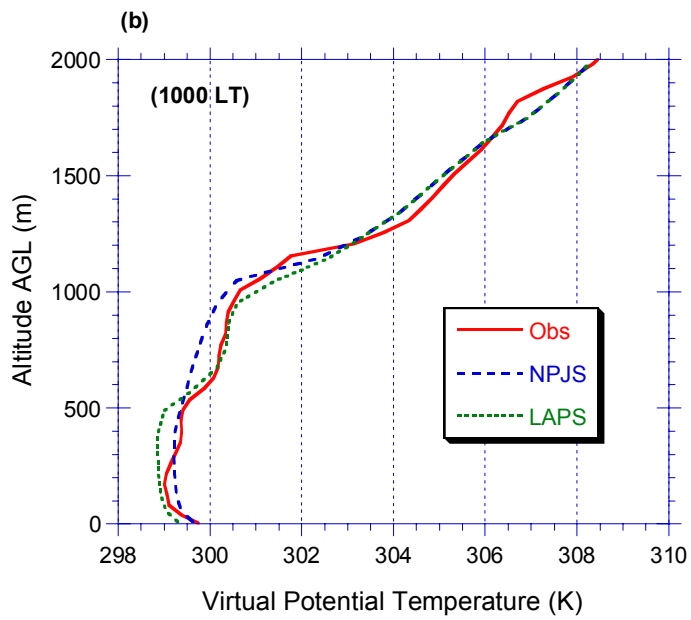
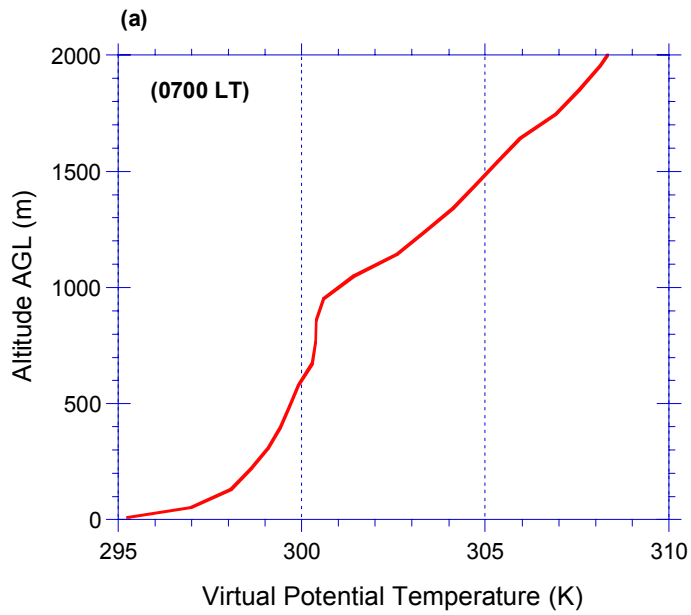


Figure 4. Temporal variation of measured and modeled near-surface (10.5 m AGL) (a) Air temperature, (b) Water vapor mixing ratio, (c) Eastward horizontal wind velocity, and (d) Northward horizontal wind velocity for the 06 June 1987 FIFE case study.



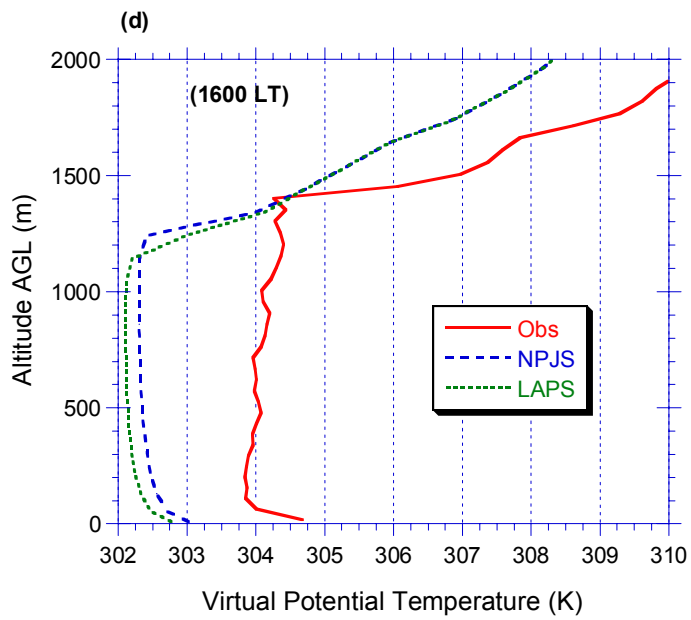
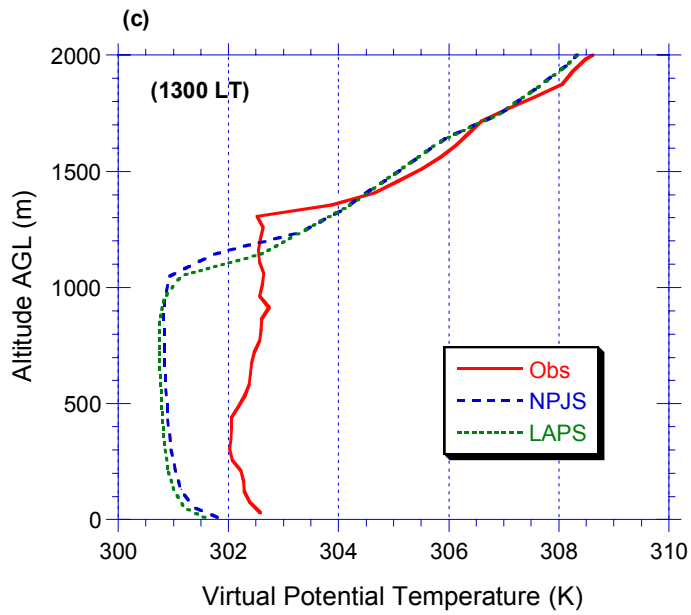


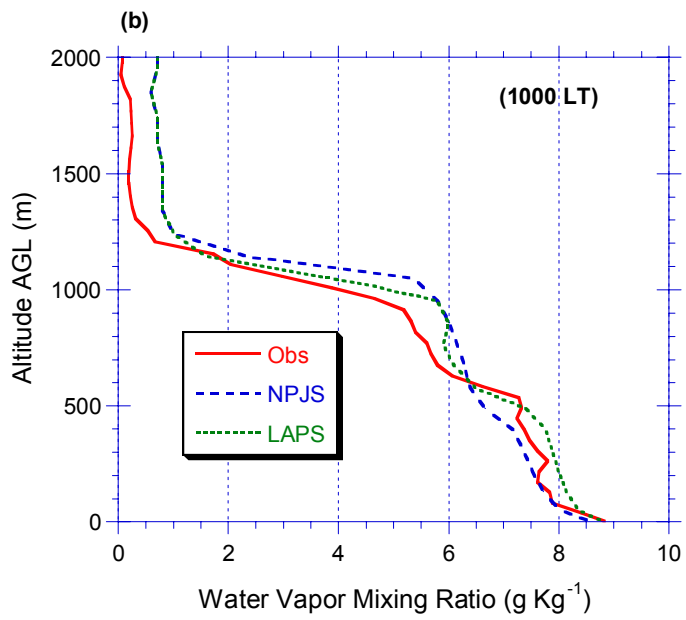
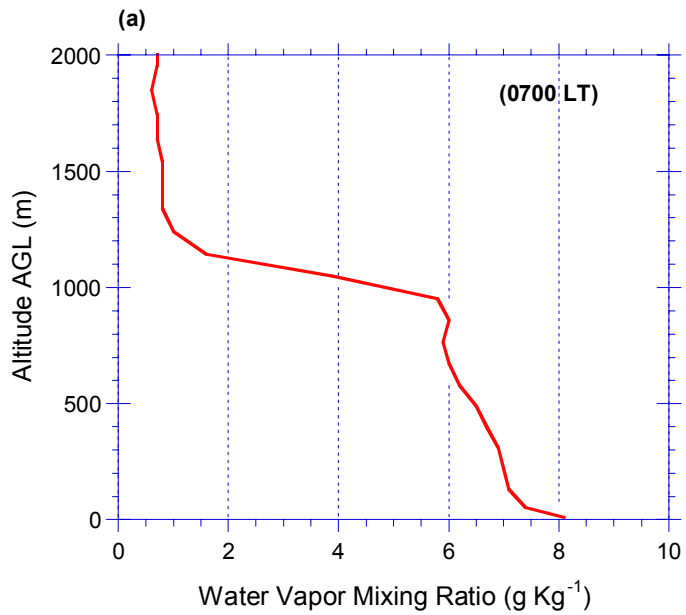
Figure 5. Vertical variation of “measured” and modeled virtual potential temperature at (a) 0700, (b) 1000, (c) 13000, and (d) 1600 LT for the 06 June 1987 FIFE case study.

Modeled and observed vertical variations of water vapor mixing ratio at different times are presented in Figs. 6a-6d. At 0700 LT (Fig. 6a; initial conditions) show the effects of stable boundary layer's stratification on mixing ratio. At altitude of about 1000 m, sharp vertical gradient indicates the presence of very dry air in the free atmosphere and is an indicative of depth of the previous day's ABL. At 1000 LT (Fig. 6b), like in q_v profiles, modeled and observed mixing ratios are very similar to each other. At 1300 LT (Fig. 6c) both LAPS and NPJS indicate relatively drier and shallow ABL compared to observations. Though surface latent and sensible heat fluxes at 1300 LT simulated by LAPS are relatively lower than those in NPJS dilution of fluxes through a relatively shallow ABL in LAPS leads to relatively humid ABL compared to NPJS (Fig. 6c). At 1600 LT (Fig. 6d) both LAPS and NPJS very similar mixing ratios and are comparable to observations. Though observations indicate a well-mixed profiles for water vapor mixing ratio (at 1300 and 1600 LT), both schemes are unable to produce such a well mixed ABL.

Predictions of the horizontal winds in a one-dimensional model can be very sensitive to the prescribed geostrophic wind profiles. In all of our simulations we prescribed geostrophic wind profiles that were used by Alapaty et al. (1997). Since horizontal pressure gradients are not readily available, they used a qualitative procedure to estimate temporally evolving geostrophic winds. Vertical variation in the u-wind (eastward component) obtained from observations and model simulations are shown in Figs 7a-7d. Presence of a nocturnal jet at 0700 LT is evident from the u-wind profile between the surface and 1000 m altitude; the core of the jet is located at about 400 m AGL. At 1000 LT (Fig. 7b), observations still indicate the presence of nocturnal jet while in LAPS and NPJS it is weakened due to strong vertical diffusion. At 1300 LT (Fig. 7c) observations indicate a strong vertical u-wind shear within the ABL while LAPS and NPJS indicate a relatively well-mixed ABL. Best agreements between NPJS, LAPS and observations are found at 1600 LT (Fig. 7d).

Vertical variation in the v-wind (northward component) obtained from observations and model simulations is shown in Figs. 8a-8d. The presence of the nocturnal jet is somewhat evident (0700 LT) in the lower altitudes of the atmosphere. Interestingly, observed v-winds do not show the signs of remnants of nocturnal jet at 1000 LT unlike in the u-winds (Fig. 7b). In general, observed v-winds are more uniform with altitude and corresponding simulations with LAPS and NPJS are in general agreement with observations.

To summarize differences between LAPS and NPJS simulations, most of the differences in prognostic variables (Temperature, mixing ratio, and horizontal winds) are very minor and compare with observations very well as seen in the respective figures. The diagnostic parameters also show similar signature. However, the relative magnitudes of sub-processes (surface evaporation verses transpiration) are different in LAPS and NPJS. These differences can be attributed mostly to differences in the formulations estimating net radiation reaching the surface and stomatal resistance.



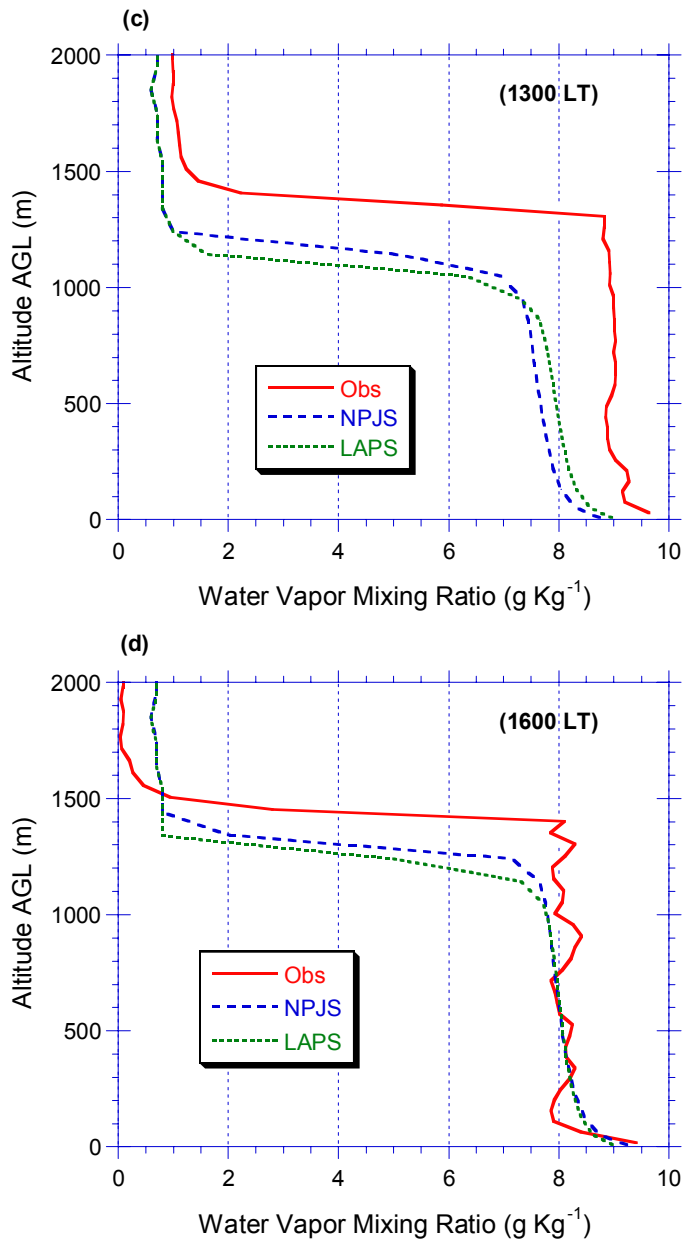
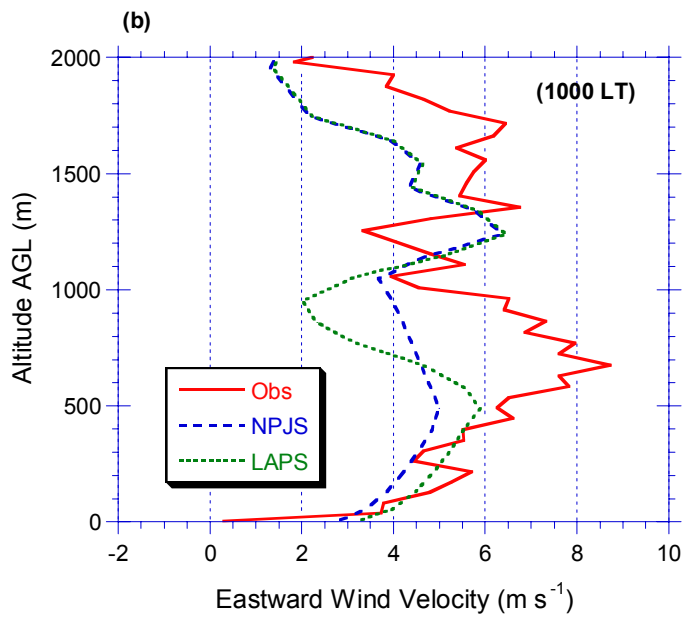
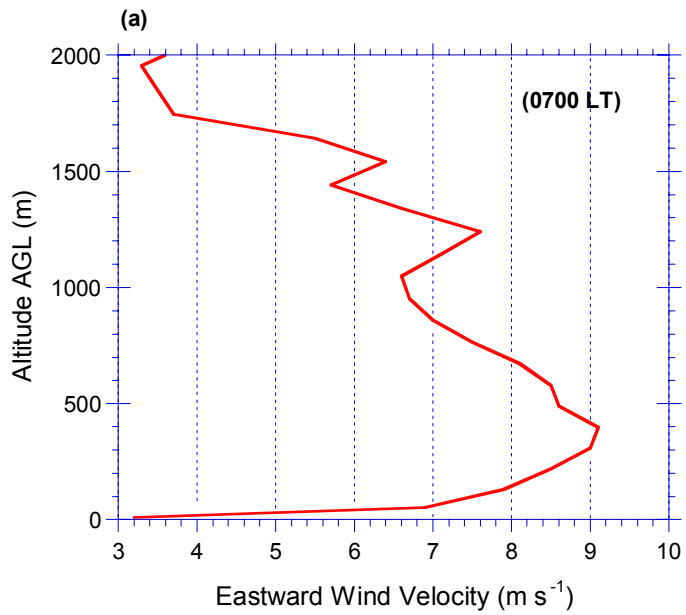


Figure 6. Vertical variation of “measured” and modeled water vapor mixing ratio at (a) 0700, (b) 1000, (c) 13000, and (d) 1600 LT for the 06 June 1987 FIFE case study.



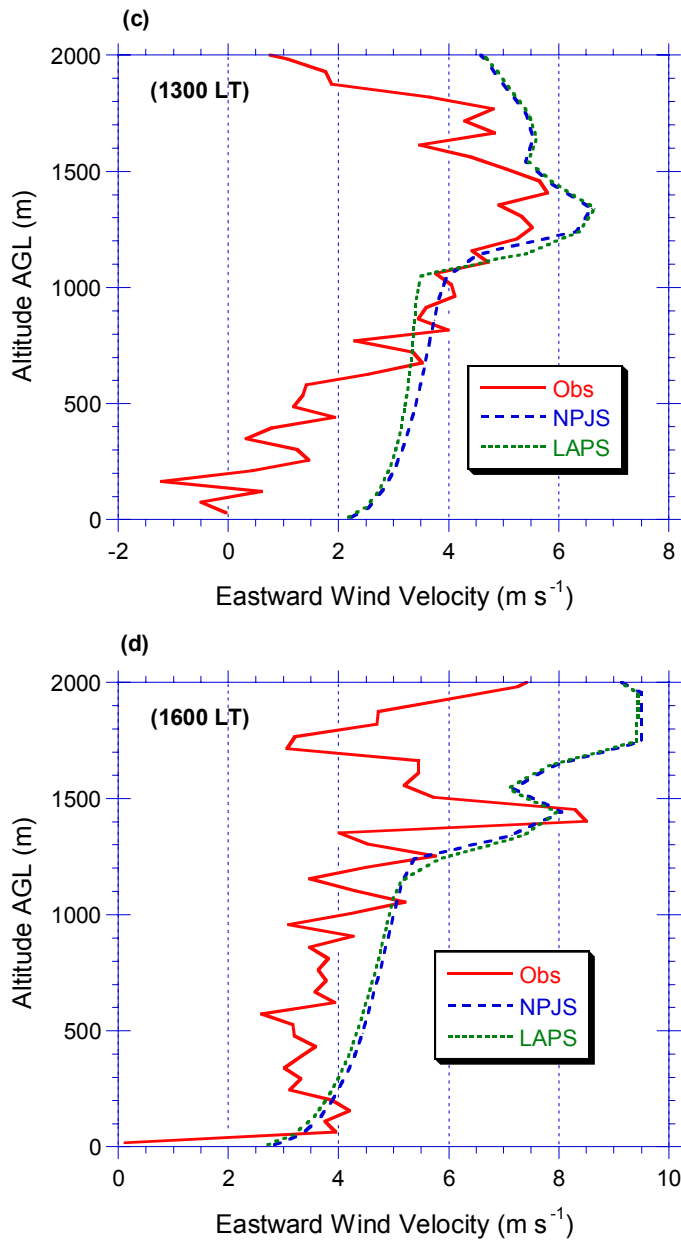
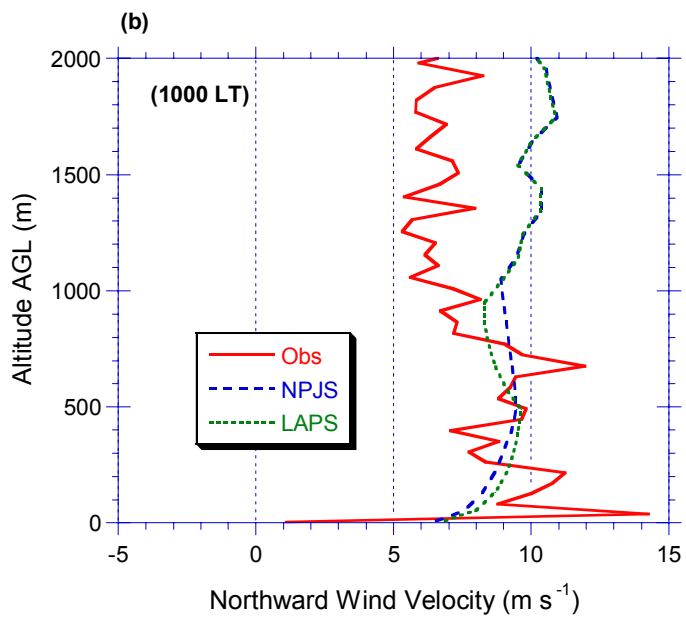
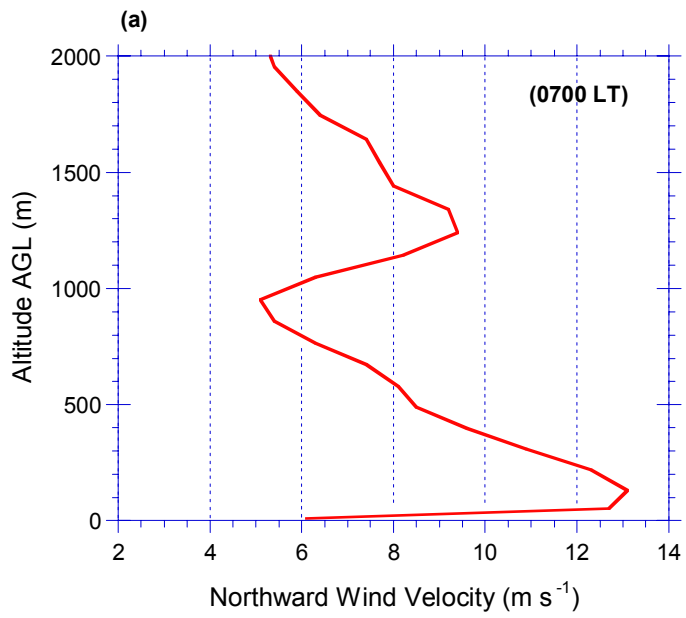


Figure 7. Vertical variation of “measured” and modeled eastward horizontal wind velocity at (a) 0700, (b) 1000, (c) 1300, and (d) 1600 LT for the 06 June 1987 FIFE case study.



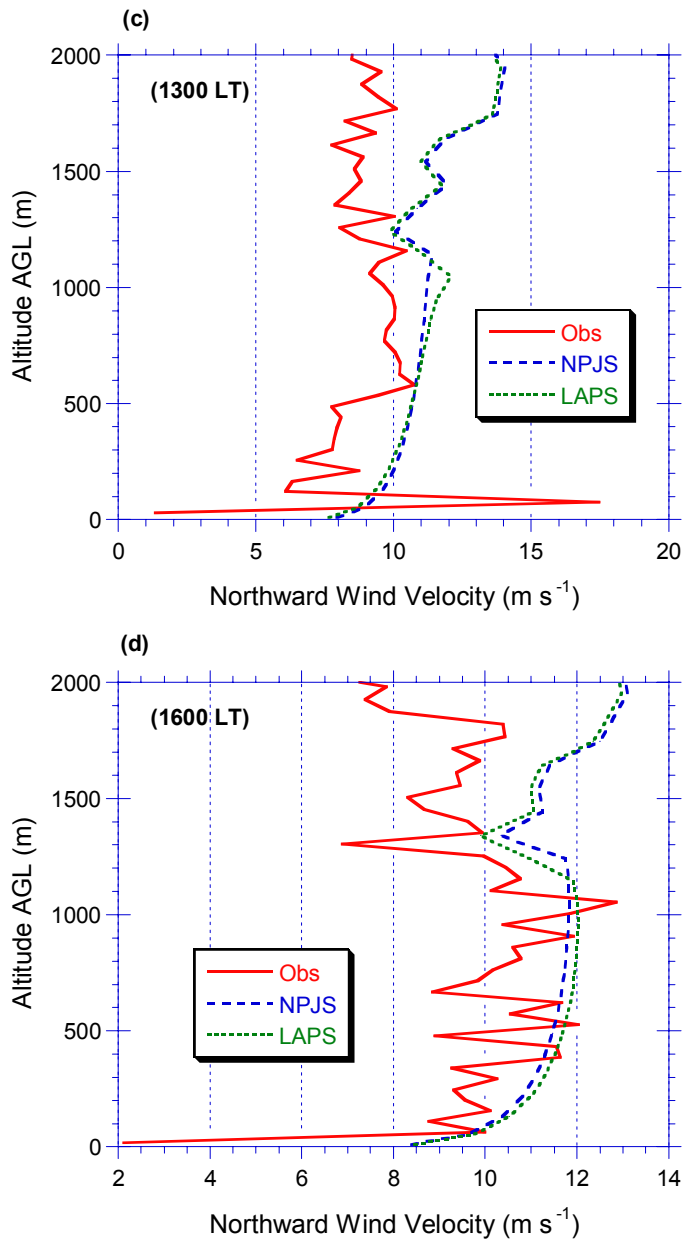


Figure 8. Vertical variation of “measured” and modeled northward horizontal wind velocity at (a) 0700, (b) 1000, (c) 1300, and (d) 1600 LT for the 06 June 1987 FIFE case study.

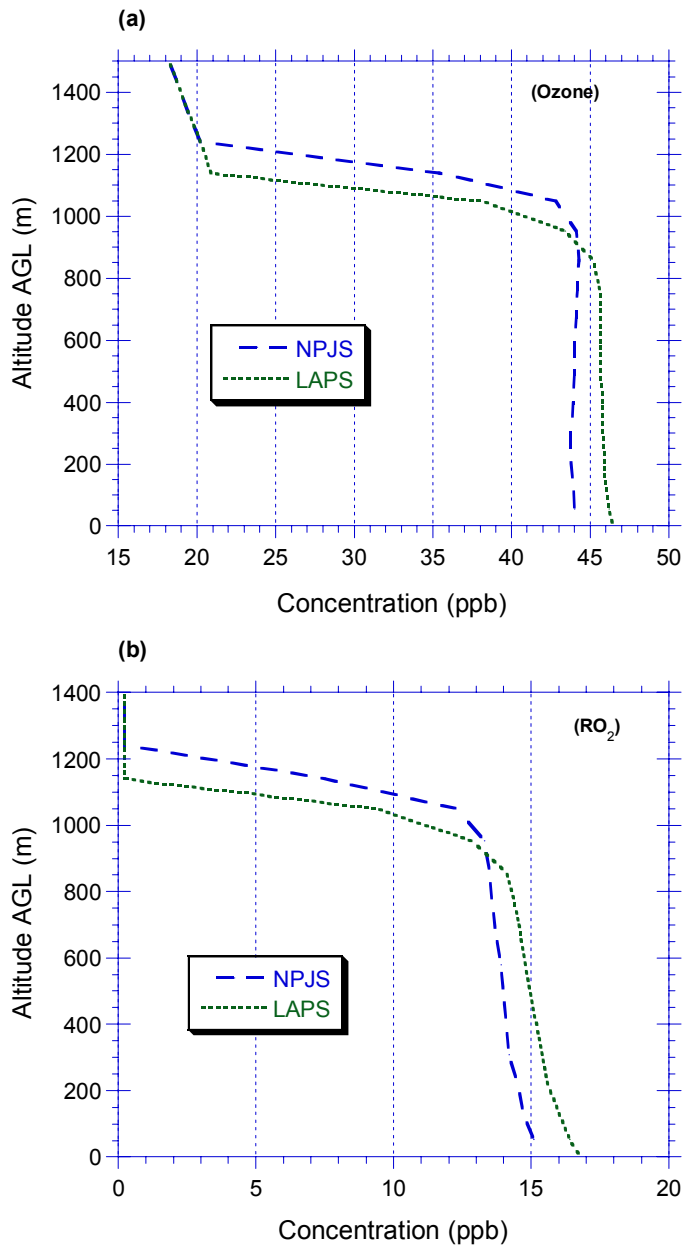
Simulation of Trace Gas Species Concentrations

Since the 1-D model is capable of simulating boundary layer-chemistry interactions, we present some of the results obtained from the above-described case study. The chemical reaction set used in this study is based on Hov et al. (1989). The set of reactions (Table 2) consists of ten chemical reactions representing the nonlinear chemical pathways related to NO_x -VOC chemistry and has been previously used to test, compare and contrast the performance of various advection schemes coupled with chemistry (e.g., Odman and Russell, 1991; Chock and Winkler, 1994). The chemistry in the experiments described in this study, was defined to be simple to keep the number of equations to a minimum, while representing the nonlinear chemical pathways that characterize tropospheric chemistry (Hov et al., 1989). Though this chemical scheme is too simple to represent complex chemical reactions that occur in atmosphere, it is sufficient for a preliminary investigation of the effects of different land surface schemes on simulated concentrations of chemical species. Since solar zenith angle is a function of time, rate constants k_2 , k_5 , and k_7 , shown in the Table 2, also vary temporally. Initial chemical conditions used in the numerical experiments are shown in Table 3. All species had maximum concentrations in the lowest model layer closer to the ground (Table 3) and then decreased smoothly to specified background values in the sixth and higher layers, representing the conditions similar to that of a stable boundary layer typical during early morning.

Four reactive chemical species (HC, HCHO, NO, and NO_2) are continuously released in these layers. In all simulations we have used idealized emission rates for simplicity in analyzing the impact of differing mixing representations. Temporal patterns of emission sources are specified such that from the starting time of simulation (0700 LT) emission rates for each of these species at each vertical level increase linearly to a maximum value at 1300 LT (local time) after which these rates decrease linearly to the starting value at the end of the 12 h simulation (1900 LT). In all of the simulations dry deposition is neglected.

Since the surface sensible heat fluxes are very similar to each other in LAPS and NPJS, hence the TKE and associated vertical mixing is very similar in both the LAPS and NPJS. Thus, differences in the predicted depths of the ABL alone contribute to differences in the concentrations (excluding the effects of resulting nonlinearity in chemical reactions). Figures 9a-9d show time-height sections of O_3 , RO_2 , NO_2 , and HCHO, respectively, at 1300 LT. Since chemical timescales of O_3 are relatively longer than those of the turbulence, a well-mixed ABL for O_3 is simulated (Fig. 9a). On the other hand, since the chemical timescale of RO_2 is almost comparable (slightly smaller) to that of turbulence, simulated weak vertical gradients (Fig. 9b) are due to Damkohler number (ratio of timescales of turbulence to chemical reaction) close to unity (moderate chemistry). For fast reacting species like NO_2 , strong vertical gradients (Fig. 9c) are expected due to a large Damkohler number. For this reason, in the case of NO_2 , it is also expected that the differences in simulated concentrations in LAPS and NPJS be minimal as seen in Fig. 9c. Simulated HCHO in LAPS and NPJS show differences similar to that in RO_2 . Note that the depth of the ABL in the NPJS is slightly higher than that in the LAPS, increased dilution through a deeper ABL in NPJS leads to lower concentration profiles as compared to those in LAPS. Figures

10a and 10b show the vertical profiles of simulated OH and HO₂ in LAPS and NPJS at 1300 LT indicating effects of differences depths of the ABL. In general this analysis indicates that all species having large Damkohler number results in strong vertical gradients while for others, such as O₃, it results in uniform vertical variation.



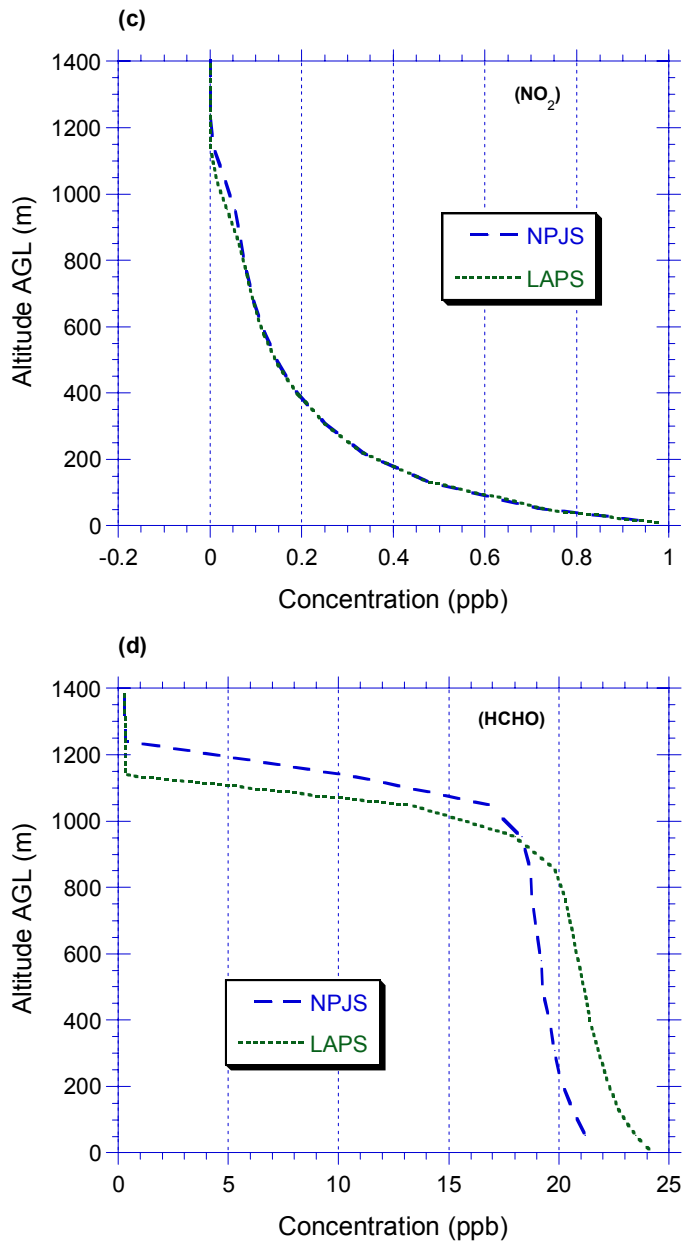


Figure 9. Vertical variation of modeled concentration of (a) O₃, (b) RO₂, (c) NO₂, and (d) HCHO at 1300 LT for the 06 June 1987 FIFE case study.

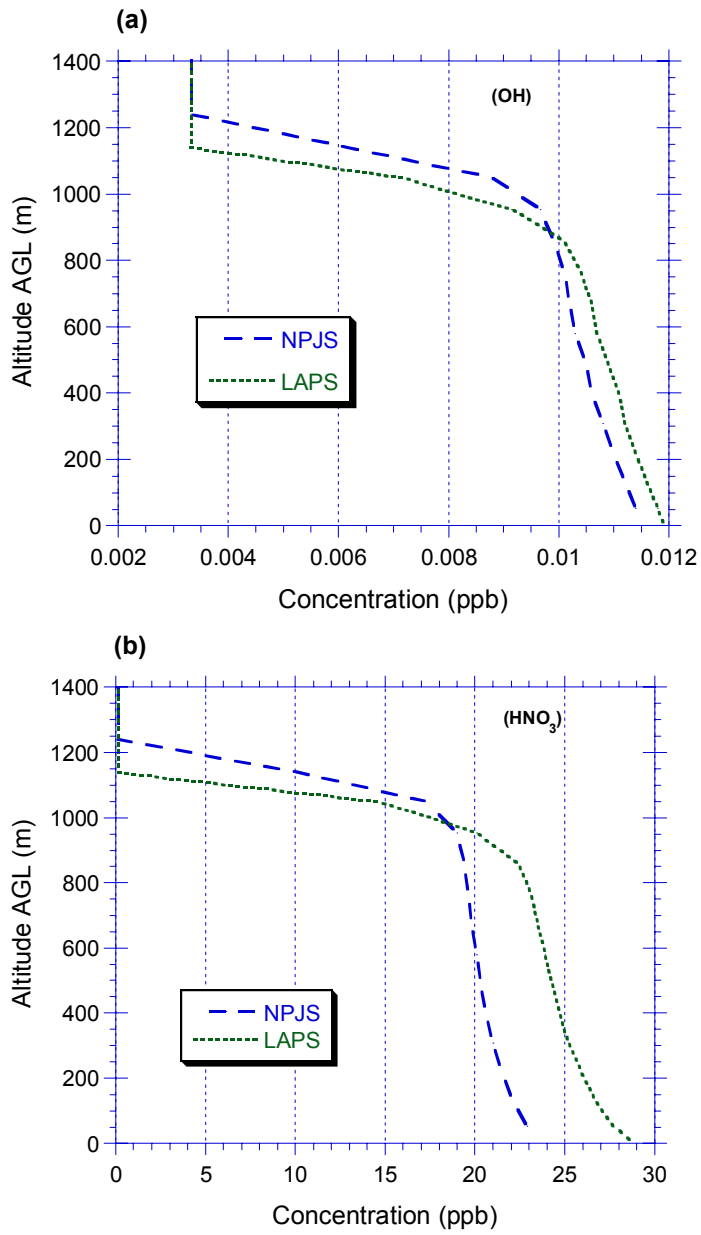


Figure 10. Vertical variation of modeled concentration of (a) OH, (b) HO₂, (c) CO, and (d) HNO₃ at 1300 LT for the 06 June 1987 FIFE case study.

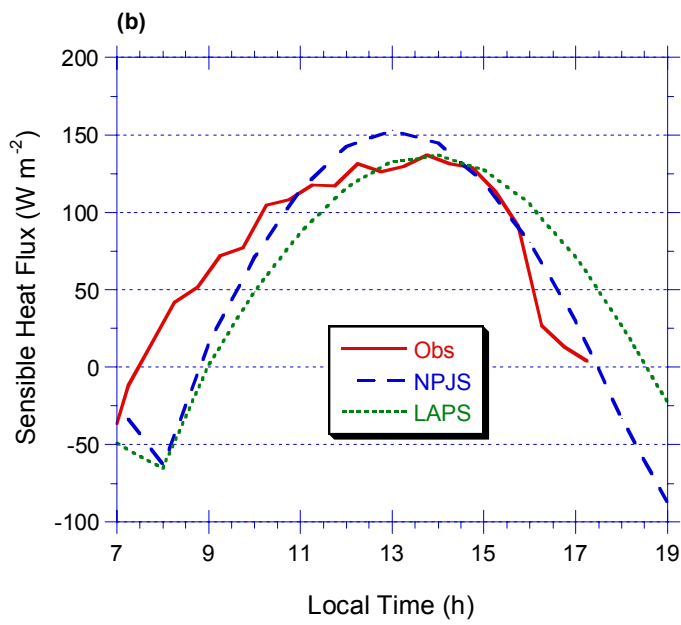
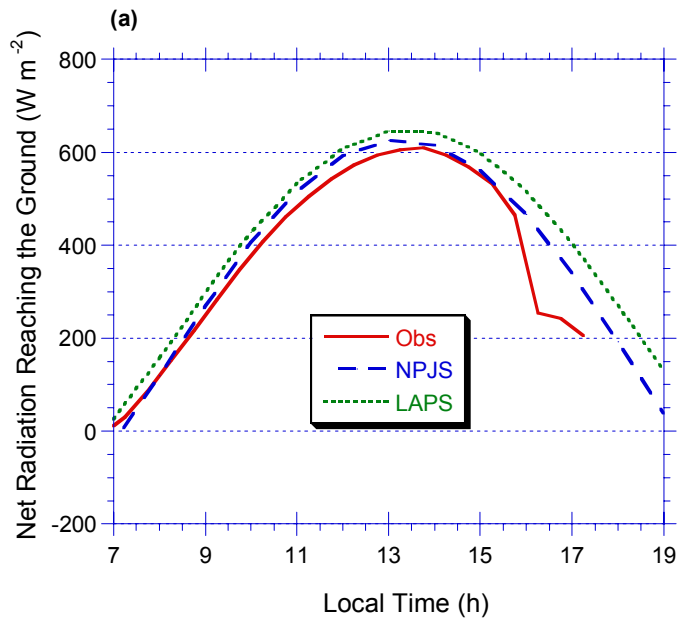
The 11 July 1987 case study

During this day, the second IFC of the FIFE, clear sky conditions were observed until afternoon. Cloud-camera observations indicated overcast sky conditions after 1500 LT. Because the current version of our model does not consider processes related to cloud formation and its effects on atmospheric radiation and surface processes, model predictions after 1500 LT may not be comparable to observations. The temporal variations in the net radiation reaching the ground estimated by the model and from the observations are shown in Fig. 11a. Interestingly, throughout the simulation period LAPS overestimates net radiation by about $5\text{-}20\text{ W m}^{-2}$ unlike in the earlier case where LAPS underestimated it. This behavior indicates that estimated upward and downward long wave radiation in two schemes using different formulation may not always yield exactly same results. Net radiation estimated by NPJS is very close to LAPS as well as observations. As mentioned earlier, after 1530 LT LAPS and NPJS estimations deviated from observations because the present version of our 1-D model does not consider dynamic and thermodynamic processes related to cloud formation. Figure 11b shows the temporal variation in the measured and estimated sensible heat fluxes from using the two land surface schemes. In general, both LAPS and NPJS follow observations with a noticeable difference during evening hours consistent with the results from the earlier case study.

Figure 11c compares measured surface latent heat fluxes with those obtained using LAPS and NPJS. Unlike in the earlier case, LAPS slightly overestimates latent heat fluxes by about $5\text{-}35\text{ W m}^{-2}$ until noon. Note that the differences in latent heat fluxes between the LAPS and NPJS is much smaller as compared to that in the earlier case study. After 1500 LT, estimated latent heat fluxes deviate greatly from the measurements due to exclusion of cloud effects in the model. Figure 11d shows the temporal variation of observed and modeled soil heat flux. Even though the initial soil layer temperatures and moistures in LAPS and NPJS are exactly same while formulations in the prognostic equations for these variables are different, the two schemes adjust soil layers' temperatures quite rapidly (in less than five minutes of simulation time), leading to differing solutions during the initial spin-up time. However, the trend is very similar in all of them.

In order to further explore the partition of total evaporation flux, we show the temporal variation of direct evaporation and transpiration fluxes in Figs. 12a and 12b. Consistent with the earlier case study, the direct evaporation flux in NPJS is significantly lower compared to that in the LAPS. However, the transpiration flux in LAPS, now in this case study, is much closer to NPJS. In the earlier case study, the maximum difference in transpiration flux between LAPS and NPJS is about $\sim 100\text{ W m}^{-2}$ while in the present case it is only about 50 W m^{-2} . This decreased difference in the transpiration flux resulted in improved estimation of latent heat flux in LAPS.

Figures 12c and 12d show the temporal variation of layers 1 and 2 soil moistures. Again, LAPS does not show any diurnal curvature in layer-1 soil moisture consistent with that in the earlier case study while the layer 2 soil moisture distributions are very similar. Note that soil moistures (Fig. 12c and 12d) are lower in NPJS compared to respective values in LAPS while direct evaporation is lower and transpiration is higher in NPJS compared to



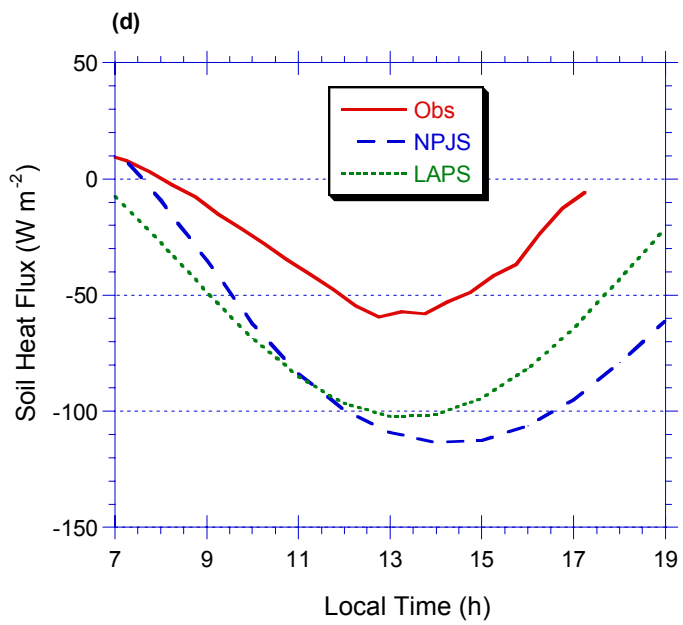
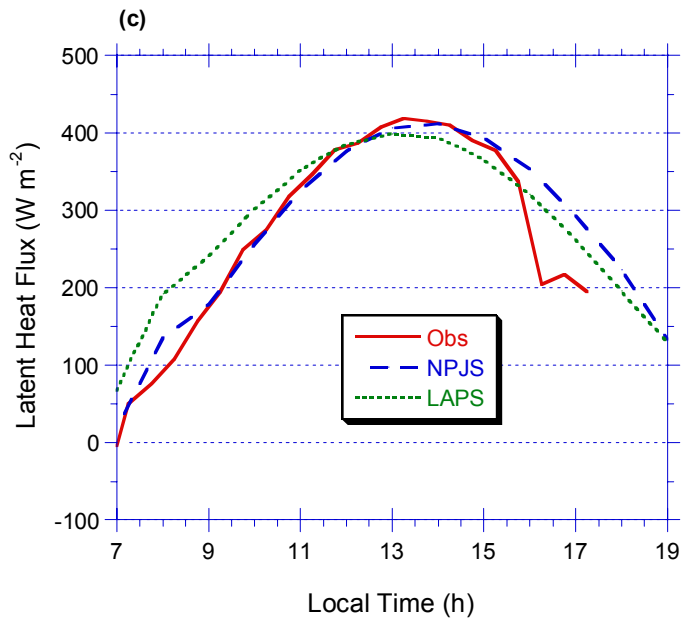
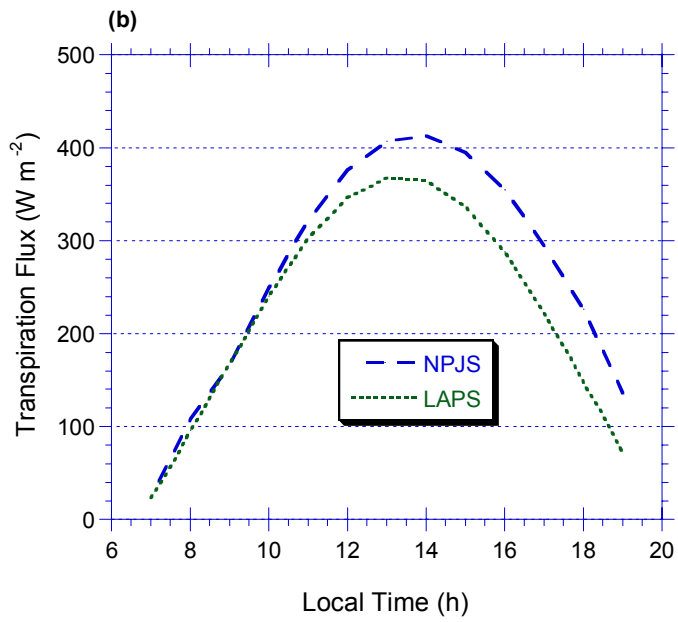
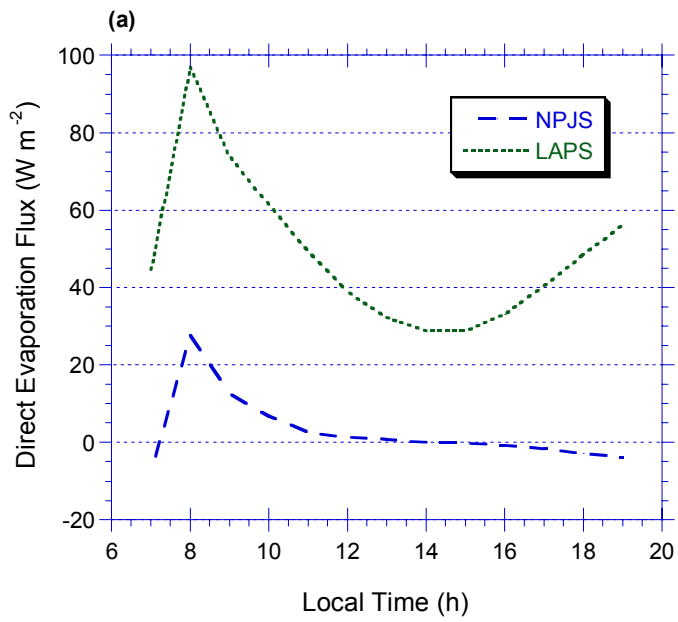


Figure 11. Temporal variation of measured and modeled (a) Net radiation reaching the surface (b) Sensible heat flux, (c) Latent heat flux, and (d) Soil heat flux for the 11 July 1987 FIFE case study. All measurements are available at 30-minute time interval.

those in LAPS. It seems that diffusion of soil moisture through interface of soil layers 1 and 2 seems to be different in direction as well as in magnitudes in LAPS and NPJS. In our future studies, we will explore this issue in detail.

We now present temporal variation of depth of the ABL, near-surface (lowest layer) temperature, and stomatal resistance in Figures 13a, 13b, and 13c, respectively. The growth rate of the ABL is well captured in NPJS as well as in LAPS and is comparable to that in observations (Fig. 13a). Also, near-surface air temperatures in LAPS and NPJS are very close to each other and observations. The maximum difference between estimated stomatal resistances (Fig. 13c), in this case study, is only about 15 s m^{-1} while it is about 50 s m^{-1} in the earlier case study. This result is consistent with the predicted transpiration fluxes in LAPS and NPJS. It is interesting to note that even though the stomatal resistance formulation used in LAPS and NPJS are very similar, their estimation differed significantly between two cases. Figure 14a shows the vertical variation in observed virtual potential temperature, Θ_v , (initial conditions). Stable lapse rates are present at this time (0700 LT) with an indication of ABL depth being about 300-400 m. Model simulations using LAPS and NPJS and observations of Θ_v at 0900 LT are shown in Fig. 14b. In LAPS and NPJS modeled mean Θ_v of the ABL is warmer compared to observations by about 0.5 K. However, at 1200 LT Θ_v in LAPS and NPJS indicate potentially cooler ABL and shallow ABL depths (Fig. 14c) compared to observations. This trend continues even at 1500 LT (Fig. 14c). Presence of superadiabatic lapse rates, a typical feature during the daytime near the surface, is evident starting from 0900 LT in observations. This feature is well simulated by LAPS and NPJS at 1200 and 1500 LT. The stronger vertical gradient (inversion) present at higher altitudes indicates the approximate altitude of the top of the mixed layer in each Θ_v profile. The Θ_v profile at 1500 LT (Fig. 14d) contain the influence of dynamic and thermodynamic processes related to the reported cloud activity. Also, a stable-type of ABL has evolved in observed Θ_v due to cloud processes, which cannot be simulated with the current model version.

In the absence of cloud formation and advection processes, the vertical distribution of trace gas species in the lower troposphere is largely controlled by ABL processes. The water vapor mixing ratio can be considered as a surrogate for the trace gas species (nonreactive) (just as latent heat fluxes at the surface can be viewed as a surrogate for surface emission fluxes). Thus, the temporal behavior and vertical distribution of the water vapor mixing ratio (q_v) can provide some insight on the probable behavior of a surface emitted nonreactive trace gas species. Vertical profiles of observed q_v at different hours are shown in Figs. 15a-15d. At 1200 and 1500 LT, q_v profiles indicate a uniform distribution within the mixed layer with a large gradients in the surface layer.



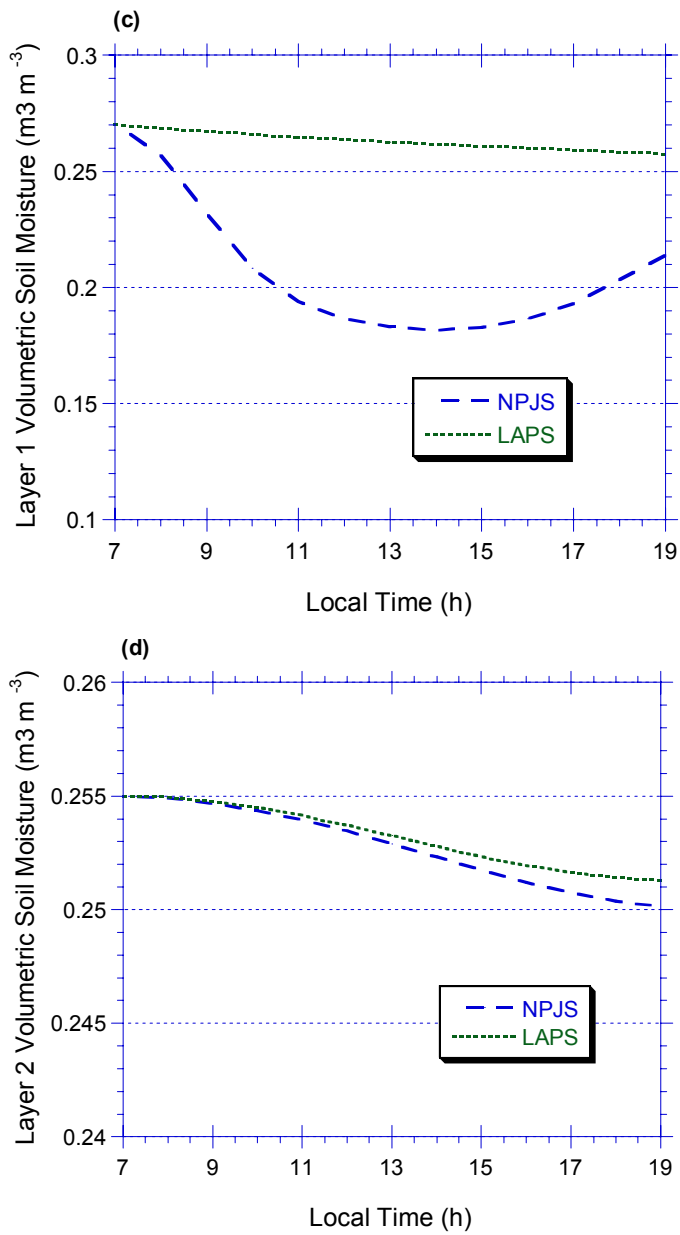
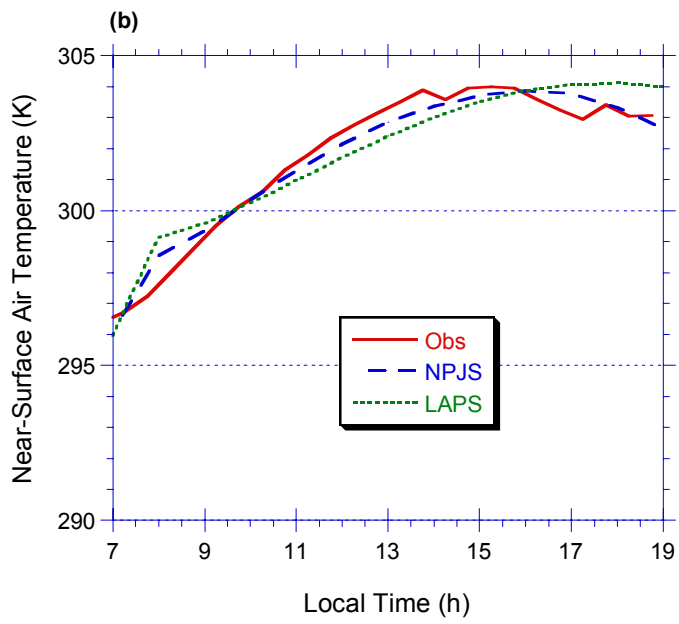
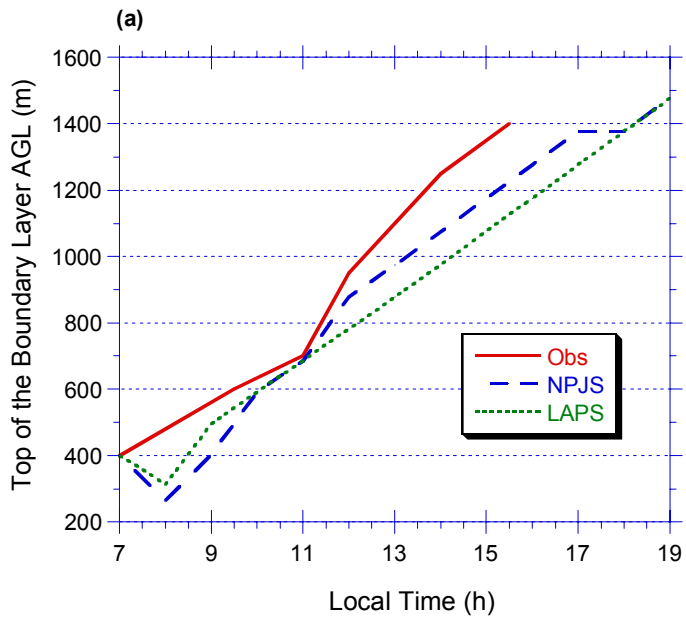


Figure 12. Temporal variation of modeled (a) Direct evaporation, and (b) Transpiration fluxes, and soil moisture for (c) layer 1, and (d) layer 2 for the 11 July 1987 FIFE case study.



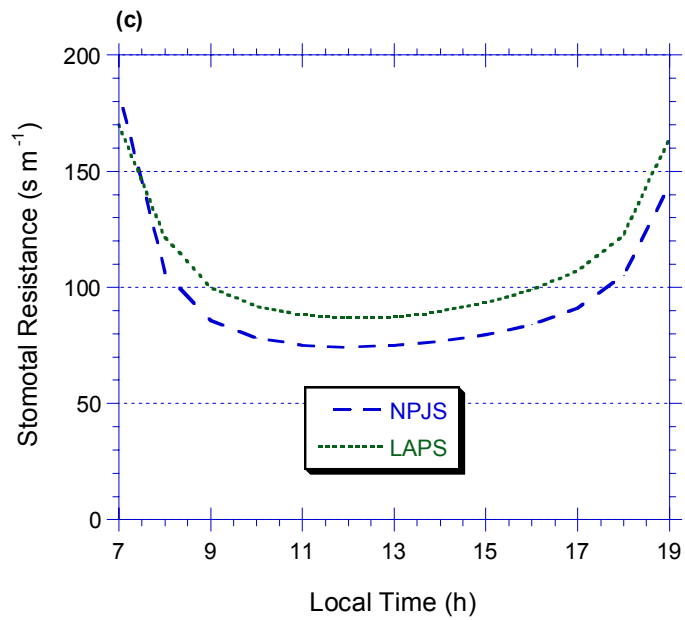
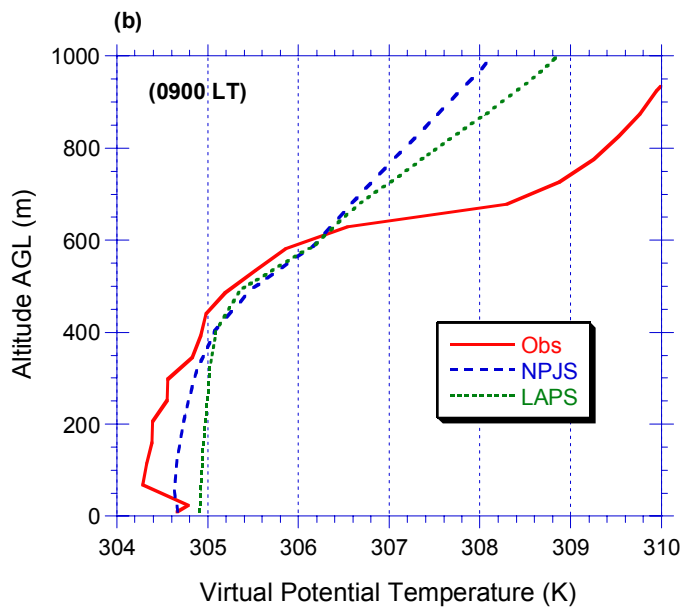
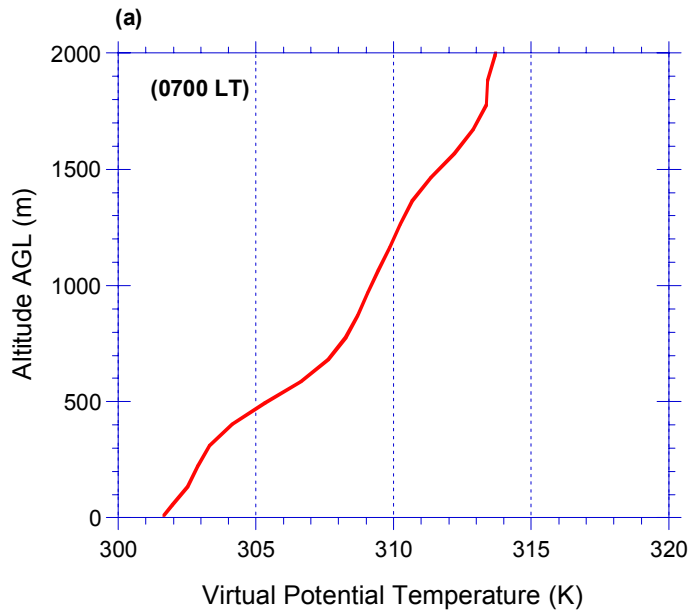


Figure 13. Temporal variation of measured and modeled (a) Boundary layer depth, (b) Near-surface (10.5 m AGL) air temperature, and (c) Northward horizontal wind velocity for the 06 June 1987 FIFE case study.



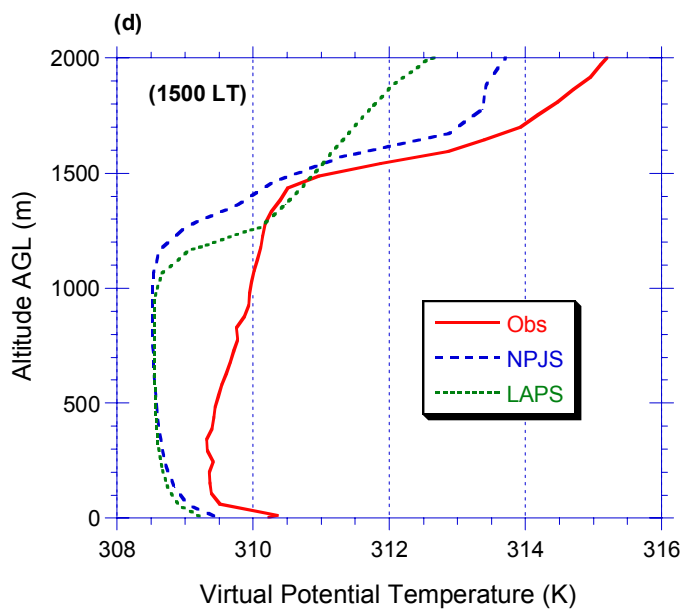
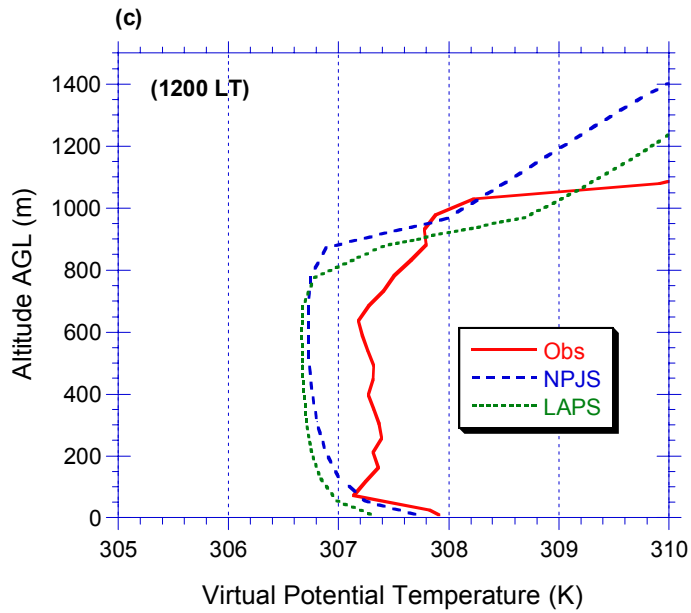


Figure 14. Vertical variation of “measured” and modeled virtual potential temperature at (a) 0700, (b) 0900, (c) 12000, and (d) 1500 LT for the 11 July 1987 FIFE case study.

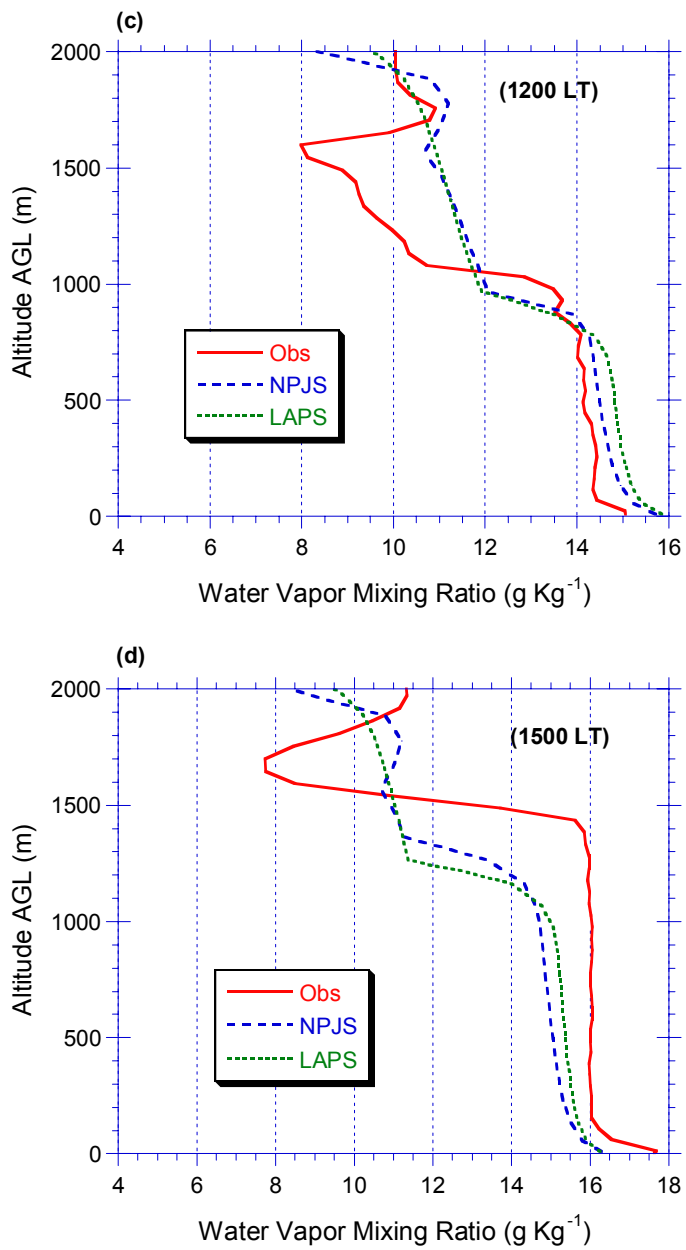
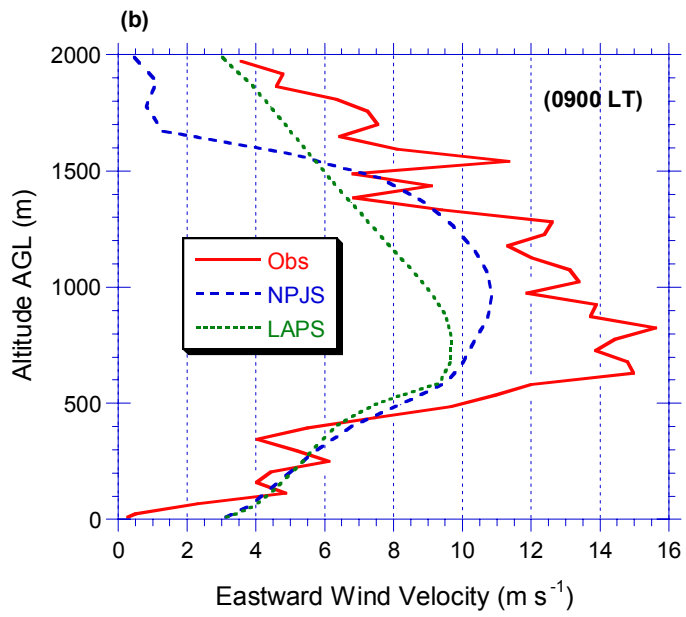
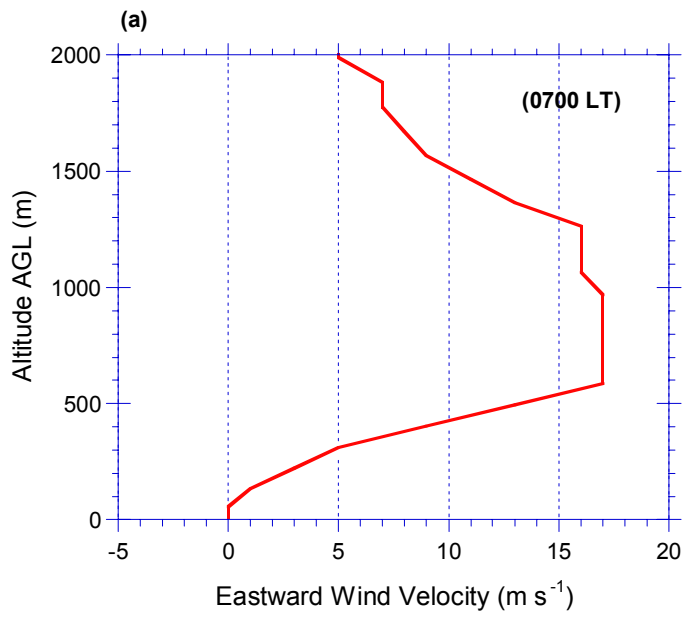


Figure 15. Vertical variation of “measured” and modeled water vapor mixing ratio at (a) 0700, (b) 0900, (c) 12000, and (d) 1500 LT for the 11 July 1987 FIFE case study.



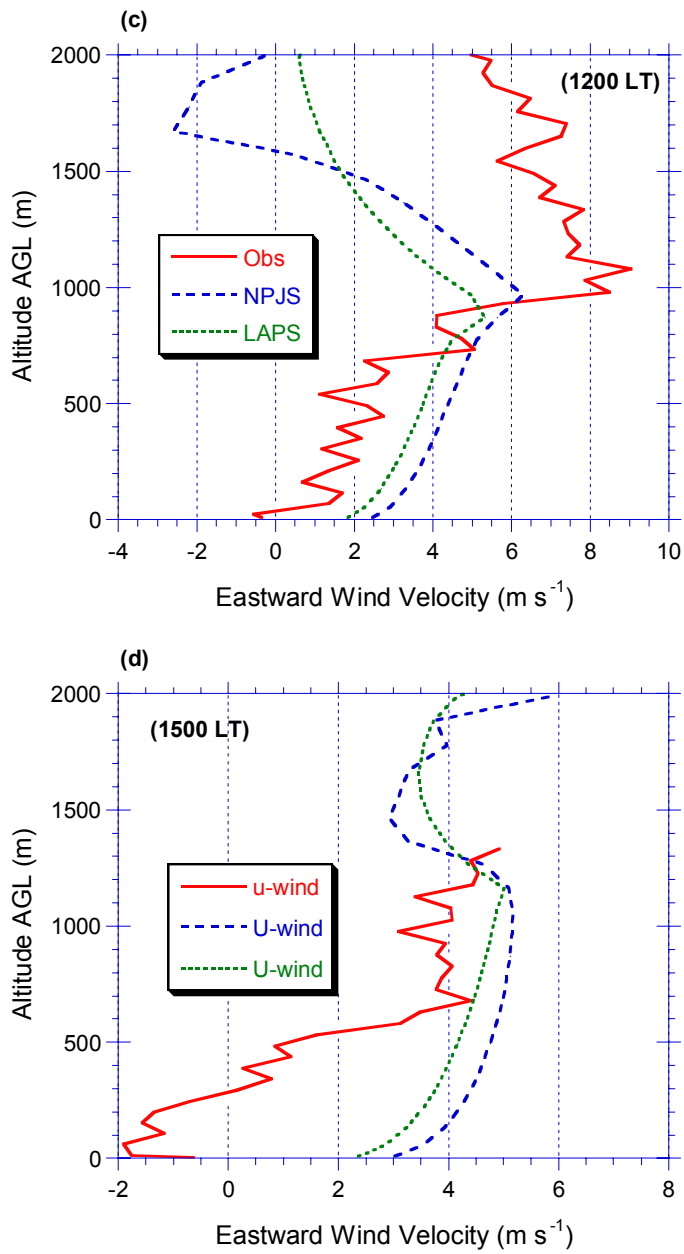
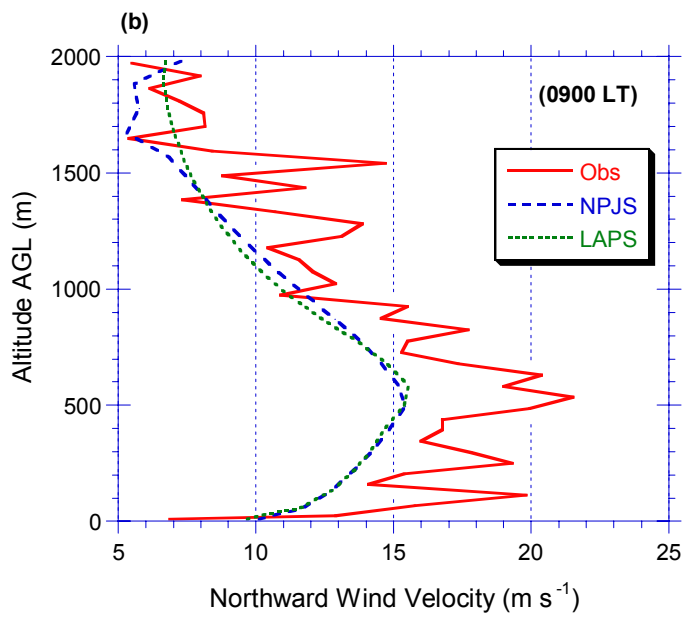
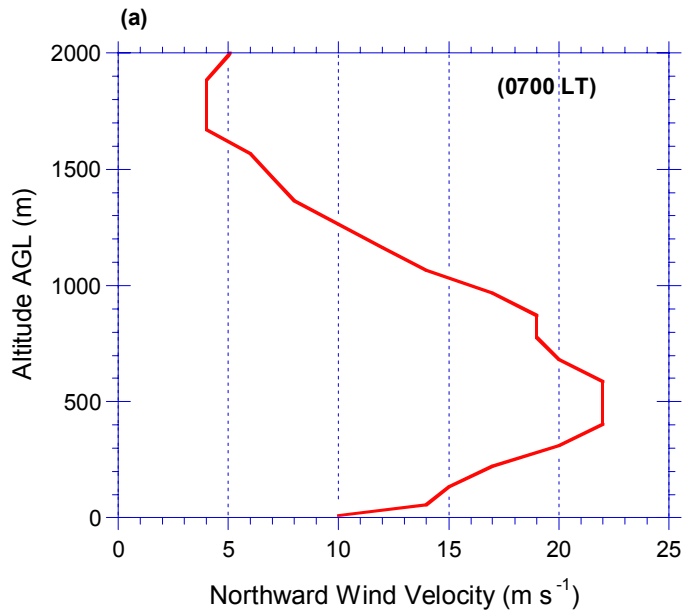


Figure 16. Vertical variation of “measured” and modeled eastward horizontal wind velocity at (a) 0700, (b) 0900, (c) 1200, and (d) 1500 LT for the 11 July 1987 FIFE case study.



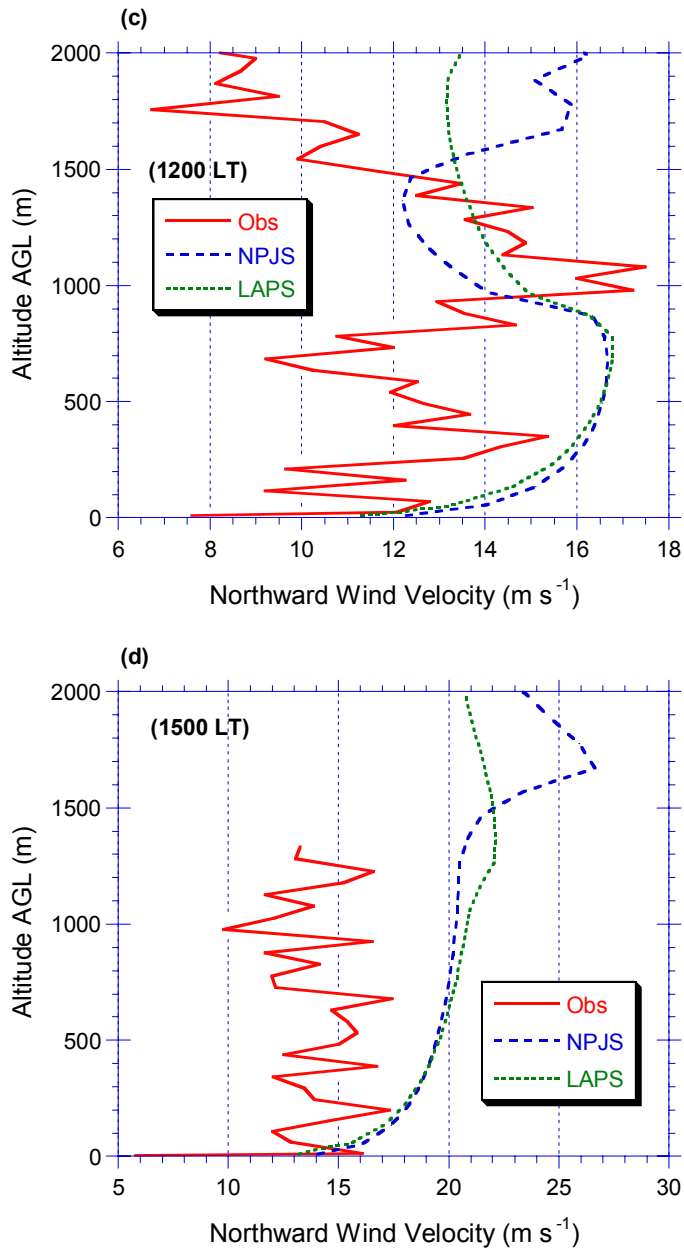


Figure 17. Vertical variation of “measured” and modeled northward horizontal wind velocity at (a) 0700, (b) 0900, (c) 12000, and (d) 1500 LT for the 11 July 1987 FIFE case study.

Observed and modeled eastward wind velocity profiles at different times are shown in Figs. 16a-16d. Initial conditions (Fig. 16a) indicate the presence of remnants of a nocturnal jet in the lower altitudes in the initial conditions (0700 LT). Presence of vertical wind shear in the ABL is an indication of weaker vertical mixing. Due to presence of cloud processes at 1500 LT (Fig. 16d) both LAPS and NPJS could not simulate strong vertical wind shear as observed. Observed and modeled northward wind velocity profiles at different times are shown in Figs. 17a-17d. Initial conditions (Fig. 17a) also indicate the presence of remnants of a nocturnal jet in the lower altitudes in the v-wind field. Compared to u-winds, vertical wind shear in the ABL is weaker in observations. In general, insignificant differences are present in LAPS and NPJS simulations of horizontal winds.

ACKNOWLEDGMENTS

The research work described in this document has been funded by the University at Albany under a contractual agreement CR-823628 to MCNC. The Investigator would like to thank Dr. Guta Mihailovic for his help during the course of this project.

REFERENCES

- Alapaty, K., S. Raman, and R.V. Madala, 1994: Investigation of the role of the boundary layer processes in an active monsoon using a mesoscale model. *Bound.-Layer Meteor.* **67**, 407-426.
- Alapaty, K., J. Pleim, S. Raman, D.S. Niyogi, and D.W. Byun, 1997: Simulation of Atmospheric Boundary Layer Processes using Local- and Nonlocal-Closure Schemes. *Journal of Applied Meteorology*, **36**, 214-233.
- Alapaty, K., S. Raman, and D.S. Niyogi, 1997b: Uncertainty in the Specification of Surface Characteristics: A Study of Prediction Errors in the Boundary Layer. *Boundary-Layer Meteorology*, **82**, No. 3, 473-500.
- Alapaty, K., and R. Mathur, 1998: Effects of Atmospheric Boundary Layer Mixing Representations on Vertical Diffusion of Passive and Reactive Tracers. *Meteorology and Atmospheric Physics*, **69**, 101-118.
- Alapaty, K., M. Alapaty, 1999: Development and Testing of an E- \square scheme using the MM5. The 9th Penn State/NCAR MM5 Users' workshop, 25-27 June 1999, Boulder, Colorado, USA.
- Anthes, R.A., E.-Y. Hsie, and Y.-H. Kuo, 1987: Description of the Penn State/NCAR Mesoscale Model Version 4 (MM4). NCAR Tech. Note, NCAR/TN-282+STR, 66 pp.
- Blackadar, A.K., 1976: Modeling the nocturnal boundary layer. Preprints, *Third Symposium on Atmospheric Turbulence, Diffusion and Air Quality*, Raleigh, Amer. Meteor. Soc., 46-49.
- Blackadar, A.K., 1979: Modeling pollutant transfer during daytime convection. Preprints, *4th Symposium on Turbulence, Diffusion and Air Pollution*, Reno, Amer. Meteor., Soc., 443-447.
- Businger, J.A., J.C. Wyngaard, Y. Izumi and E.F. Bradley, 1971: Flux-profile relationship in the atmospheric surface layer. *J. Atmos. Sci.*, **28**, 181-189.
- Chock, D.P., and S.L. Winkler, 1994: A particle grid air quality modeling approach, 2. Coupling with Chemistry, *J. Geophys. Res.*, **99**(D1), 1033-1041.
- Deardorff, J., 1978: Efficient prediction of ground surface temperature and moisture, with inclusion of a layer of vegetation. *J. Geophys. Res.*, **83**, 1889-1903.
- Detering, H.W., and D. Etling, 1985: Application of E- \square turbulence model to the atmospheric boundary layer. *Bound.-Layer Meteor.*, **33**, 113-133.
- Grell, G.A., J. Dudhia, and D.R. Stauffer, 1994: A description of the Fifth-Generation Penn State/NCAR Mesoscale Model (MM5). NCAR/TN-398 + STR, 138 pp.
- Hov, O., Z. Zlatev, R. Berkowicz, A. Eliassen, and L.P. Prahm, 1989: Comparison of numerical techniques for use in air pollution models with nonlinear chemistry. *Atmos. Environ.*, **23**, 967-983.
- Idso, S., R. Jackson, B. Kimball, and F. Nakayama, 1975: The dependence of bare soil albedo on soil water content. *J. Appl. Meteor.*, **14**, 109-113.
- Jacquemin, B., and J. Noilhan, 1990: Sensitivity study and validation of land surface parameterization using the HAPEX-MOBILHY data set. *Bound.-Layer Meteor.*, **52**, 93-134.
- Monin, A.S., and A.M. Yaglom, 1971: *Statistical Fluid Mechanics. Vol. I*, MIT Press, 468-504.

- Mihailovic, D.T., R.A. Pielke, B. Rajković, T.J. Lee and M. Jeftić, 1993: A resistance representation of schemes for evaporation from bare and partly plant-covered surfaces for use in atmospheric models. *J. Appl. Meteor.*, **32**, 1038-1054.
- Mihailovic, D.T. and Ruml, M., 1996. Design of land-air parameterization scheme (LAPS) for modeling boundary layer surface processes. *Meteorol. Atmos. Phys.*, **58**, 65-81.
- Mihailovic, D.T. and Kallos, G., 1997: A sensitivity study of a coupled soil-vegetation boundary-layer scheme for use in atmospheric modeling. *Boundary-Layer Meteorol.*, **82**, 283-315.
- Noilhan, J., and S. Planton, 1989: A simple parameterization of land surface processes for meteorological models. *Mon. Wea. Rev.*, **117**, 536-549.
- Odman, M.T., and A.G. Russell, 1991: Multiscale modeling of pollutant transport and chemistry, *J. Geophys. Res.*, **96**, 7363-7370, 1991.
- Pielke, R.A., W.R. Cotton, R.L. Walko, C.J. Tremback, W.A. Lyons, L. Grasso, M.E. Nicholls, M.D. Moran, D.A. Wesley, T.J. Lee, and J.H. Copeland, 1992: A Comprehensive Meteorological Modeling System-RAMS. *Meteorol Atmos. Phys.*, **49**, 69-91.
- Pleim, J.E., and A. Xiu, 1994: Development and testing of a surface flux planetary boundary layer model with explicit soil moisture parameterization for applications in mesoscale models. *J. Appl. Meteor.*, **34**, 16-32.
- Sellers P. J., F. G. Hall, G. Asrar, D. E. Strebel, and R. E. Murphy. 1992: An overview of the First International Satellite Land Surface Climatology Project (ISLSCP) Field Experiment (FIFE). *J. Geophys. Res.* **97**, 18,345-18,371.
- Yamada, T., and C.L. Mellor, 1975: A hierarchy of turbulence closure models for planetary boundary layers. *J. Atmos. Sci.*, **31**, 1791-1806.

TABLE 1. Surface parameter values used in all numerical simulations.

Parameter	FIFE-IFC2	FIFE-IFC1
R_{smin} ($s\ m^{-1}$)	60.0	60.0
LAI	2.80	1.90
Veg	0.99	0.99
Texture	Silty clay loam	Silty clay loam
W_{g1} ($m^3\ m^{-3}$)	0.270	0.230
W_{g2} ($m^3\ m^{-3}$)	0.255	0.250
Z_0 (m)	0.065	0.045
T_{g1} (K)	296.0	289.15
T_{g2} (K)	297.0	293.35

R_{smin} : minimum stomatal resistance; LAI: leaf area index; Veg: vegetation cover;

W_{g1} : layer 1 volumetric soil moisture; W_{g2} : layer 2 volumetric soil moisture;

Z_0 : surface roughness length; T_{g1} : layer 1 soil temperature; T_{g2} : layer 2 soil temperature

TABLE 2. CHEMICAL SCHEME USED IN MODEL SIMULATIONS*

Reaction	Rate
(1) $\text{HC} + \text{OH} \rightarrow 4\text{RO}_2 + 2\text{HCHO}$	$k_1 = 6 \times 10^{-12}$
(2) $\text{HCHO} + \text{h}\nu \rightarrow 2\text{HO}_2 + \text{CO}$	$k_2 = 7.8 \times 10^{-5} \exp(-0.87/\cos \theta)$
(3) $\text{RO}_2 + \text{NO} \rightarrow \text{NO}_2 + \text{HCHO} + \text{HO}_2$	$k_3 = 8 \times 10^{-12}$
(4) $\text{NO} + \text{HO}_2 \rightarrow \text{NO}_2 + \text{OH}$	$k_4 = 8.3 \times 10^{-12}$
(5) $\text{NO}_2 + \text{h}\nu \rightarrow \text{NO} + \text{O}_3$	$k_5 = 1 \times 10^{-2} \exp(-0.39/\cos \theta)$
(6) $\text{NO} + \text{O}_3 \rightarrow \text{NO}_2 + \text{O}_2$	$k_6 = 1.6 \times 10^{-14}$
(7) $\text{O}_3 + \text{h}\nu \rightarrow \text{O}_2 + \text{O}^1\text{D}$	$k_7 = 1.9 \times 10^{-4} \exp(-1.9/\cos \theta)$
(8) $\text{O}^1\text{D} + \text{H}_2\text{O} \rightarrow 2\text{OH}$	$k_8 = 2.3 \times 10^{-10}$
(9) $\text{NO}_2 + \text{OH} \rightarrow \text{HNO}_3$	$k_9 = 1.0 \times 10^{-11}$
(10) $\text{CO} + \text{OH} \rightarrow \text{CO}_2 + \text{HO}_2$	$k_{10} = 2.9 \times 10^{-13}$

* θ is the solar zenith angle; rate constants are in units of $\text{cm}^3 \text{ molecule}^{-1} \text{ s}^{-1}$ (converted to $\text{ppm}^{-1} \text{ s}^{-1}$ when performing computations); photolysis rate constants are in s^{-1} .

TABLE 3. INITIAL MAXIMUM CONCENTRATIONS (PPB)

HC = 4.3	HCHO = 5.2	NO = 4.3	NO ₂ = 4.3
OH = 0.42×10^{-5}	HO ₂ = 0.42×10^{-4}	RO ₂ = 0.42×10^{-4}	O ₃ = 63
O(¹ D) = 0.42×10^{-13}	CO = 42	HNO ₃ = 0	



UNIVERSITY OF ATHENS

SCHOOL OF PHYSICS, DIVISION OF APPLIED PHYSICS
ATMOSPHERIC MODELING & WEATHER FORECASTING GROUP
University Campus, Bldg PHYS-V
Athens 15784, Greece

Appendix B

IMPLEMENTATION OF THE LAND AIR-PARAMETERIZATION SCHEME (LAPS) IN A LIMITED AREA MODEL

FINAL REPORT

Prepared by

D.T. Mihailovic

FACULTY OF AGRICULTURE, UNIVERSITY OF NOVI SAD,
CENTER FOR METEOROLOGY AND ENVIRONMENTAL MODELLING
NOVI SAD, SERBIA AND MONTENEGRO

February 27, 2003

SUMMARY

The Land-Air Parameterization Scheme (LAPS), having a sophisticated land surface parameterization formulation, was implemented into the NCEP Eta Mesoscale Model used both operationally in the NCEP and for research purposes at many places. Two types of numerical experiments were performed. Firstly, the sensitivity tests were made using three different scenarios for the underlying surface including the Control surface, crop, tall grass and mixed woodland. In the second set of experiments the quality of linking done was evaluated utilizing the 24- hour forecast with boundary conditions for the 05 June 2002 assimilated from the global NCEP model. The LAPS-NCEP Eta Mesoscale Model (referred to as Eta-LAPS) simulation results for the air temperature at 2 m and extreme temperatures were compared with the corresponding observed values taken from the SYNOP data set for a domain selected including different type of vegetation. In the sensitivity tests the differences between the hourly mean air temperatures at 2m, spatially averaged, were significant. Particularly, the highest differences were between the surfaces covered by crop and mixed woodland reaching a maximum of about 4 °C. We found that the Eta-LAPS underestimates air shelter temperature in the early morning hours comparing with the SYNOP data, while the shelter air temperatures simulated for the around noon and early night periods are in a good agreement with the observations. The simulated values obtained for daily extreme temperatures show better agreement with the observations in the case of maximum value rather than for the minimum.

In our future studies, we propose to perform more sensitivity and case studies for further evaluation of quality of the Eta-LAPS linking in simulating mesoscale circulations influenced by surface processes.

INTRODUCTION

Land surface processes play important role in boundary layer and other atmospheric processes at local- to global-scales. Due to the lack of computer resources and detailed observational data for use and verification in numerical models, these processes are represented using highly simplified formulations in the past generation of numerical models. Ever increasing availability of computer resources and traditional land-based observations as well as satellite measurements of various land surface parameters led to the development and refinement of land surface models (LSM). During the past decade many land surface models were developed and refined to improve numerical model simulations. One of these sophisticated land surface models is the Land-Air Parameterization Scheme (LAPS) developed by Mihailovic (1996), Mihailovic and Ruml (1996), Mihailovic and Kallos (1997) and Mihailovic et al. (1998). Advantages of this scheme over many other schemes are that LAPS (1) estimates canopy temperature as well as ground/skin temperature, and (2) it has ability to take account of subgrid-scale land use variability and thereby many surface parameters in a grid cell are represented more accurately than in other schemes where only dominant land use and related parameters are used.

In making the choice of the limited area model that would be used to implementing the LAPS surface scheme we were governed by the following reason. The last version of the RAMS model already has the land surface scheme that is quite similar to the LAPS scheme. So we did not expect significant differences in the case of implementing the LAPS. Instead we decided to implement it in the NCEP Eta Mesoscale Model broadly since it is used both for scientific and operational purposes at many university centers and federal agencies including the EPA.

Our overall objectives are to (1) show the complete feature of the last version of the LAPS including a new specification of input biophysical parameters as well the parameterization of the processes when the rock as a underlying surface is presented; (2) implement the LAPS scheme in an advanced non hydrostatic model and (3) compare the performance of this linking using data from the SYNOP of 05 June 2002. In the near future we plan to make more tests with the model indicated for further evaluation by simulating mesoscale circulations that are dominated by land surface processes.

BRIEF DESCRIPTION OF THE NCEP ETA MESOSCALE MODEL

The basic characteristics of the NCEP Mesoscale Model having hydro/nonhydrostatic switch (Janjic, 2002) can be grouped into the following parts: model geometry and governing equations, schemes for horizontal nonlinear advection, pressure gradient and omega-alpha terms and physics consisting of surface processes, turbulent mixing in the vertical, cumulus convection, large scale condensation, lateral diffusion and radiation. In the horizontal, the semi-staggered Arakawa E grid is used. For simulation of the slowly changing quasi-geostrophic motion the corresponding numerical scheme, controlling energy cascade toward smaller scales on the E grid developed by Janjic (1984), is used. For the vertical coordinate model allows two options. The standard terrain following σ coordinate and the quasi horizontal coordinate surface arrangement the so-called η coordinate (Mesinger et al., 1988). The governing model equations, following Simmons and Burridge (1981), for frictionless and adiabatic motion, are written in the form which can be found in Mesinger et al. (1988). A horizontal advection scheme for the semi-staggered E grid designed by Janjic (1984), following principles of Arakawa (1966) in designing schemes free of numerical problems, is implemented. The scheme

leading to the conservation of energy in energy transformations between the momentum and thermodynamic equations (Janjic, 1977; Janjic, 1980) is applied in the model.

A comprehensive physical package has been developed for the model by Janjic (1990). The package includes parameterization of the following processes: surface processes, turbulent mixing in the vertical, cumulus convection, large scale condensation, lateral diffusion and radiation. Currently, the Oregon State University (OSU) scheme (Ek and Mahrt, 1991). is available for use in the model. The Level 2.5 turbulence closure model in the Mellor-Yamada hierarchy improved/modified by Janjic 1990, 1994, 1996) is used for simulation of turbulence in the free atmosphere. This choice was motivated by the theoretical soundness of the closure model and by high performances shown in atmospheric models. The turbulence closure model is applied to all model layers except to the surface layer. To take into account the effect of the molecular mixing just above the surface, additional parameterization techniques are applied over the sea points in the model (Janjic 1994, 1996). Parameterization of deep convective precipitation in the model is done using Betts-Miller-Janjic scheme (Betts, 1986; Bets and Miller, 1986; Janjic, 1990; Janjic, 1994). For the models radiation schemes is used GFDL well known radiation package for simulating the processes of the radiation in atmosphere based on Fels and Schwarzkopf (1975).

DESCRIPTION OF LAND-AIR PARAMETERIZATION SCHEME (LAPS)

A land-air parameterization scheme (LAPS), developed through the joint efforts of the Faculty of Agriculture, and Center for Meteorology and Environmental Modelling, University of Novi Sad and University of Belgrade (Serbia and Montenegro), describes mass, energy and momentum transfer between the land surface and the atmosphere. The scheme is designed as a software package, and can be run as part of an atmospheric model or as a stand-alone model. A single layer approach is chosen for the physical and biophysical scheme background. The scheme has seven prognostic variables: three temperature variables (the canopy vegetation, soil surface and deep soil), one interception storage variable, and three soil moisture storage variables. In the scheme upper boundary conditions are used: air temperature, water vapor pressure, wind speed, radiation and precipitation at a reference level within the atmospheric boundary layer. The sensible and latent heat are calculated using resistance representation. The evaporation from the bare soil is parameterized using an " α " scheme. The soil model part is designed as a three-layer model which is used to describe the vertical transfer of water in the soil.

The LAPS scheme describes the interaction of the land surface and the atmosphere, under processes which can be divided into three sections: subsurface thermal and hydraulic processes, bare soil transfer processes and canopy transfer processes. They are: Interaction of vegetation with radiation, evaporation from bare soil, evapotranspiration which includes transpiration and evaporation of intercepted precipitation and dew, conduction of soil water through the vegetation layer, vertical water movement in the soil, runoff, heat conduction in the soil and momentum transport. The design of the scheme is based on papers by: Sellers et al. (1986), Dickinson et al. (1986), Mihailovic (1990), Mihailovic (1991), Mihailovic et al. (1992), Mihailovic et al. (1993), Mihailovic and Jeftic (1994), Dekic et al. (1995), Mihailovic et al. (1995a), Mihailovic et al. (1995b), Mihailovic and Ruml (1996), Mihailovic and Kallos (1997), Mihailovic et al. (1997) and Mihailovic et al. (2000).

Scheme Structure and Basic Equations

The LAPS scheme uses the morphological and physiological characteristics of the vegetation community for deriving the coefficients and resistances that govern all the fluxes between the surface and atmosphere. The prognostic equations for the canopy temperature, T_f , and the soil surface temperature, T_g and deep soil temperature T_d , are

$$C_f \frac{\partial T_f}{\partial t} = R_f^{\text{net}} - H_f - \lambda E_f \quad (1)$$

$$C_g \frac{\partial T_g}{\partial t} = R_g^{\text{net}} - H_g - \lambda E_g - G \quad (2)$$

$$\frac{\partial T_d}{\partial t} = 2 C_g (R_g^{\text{net}} - H_g - \lambda E_g) / \sqrt{365\pi} \quad (3)$$

where C is the heat capacity, R^{net} the absorbed short wave and long wave radiation, H the sensible heat transpiration rate, λ the latent heat of vaporization and G the soil heat flux. The subscript f refers to the canopy, g to the soil surface. The soil heat flux is parameterized using "force-restore" method. The ground heat capacity C_g is parameterized following Zhang and Anthens (1982).

The prognostic equations for the water stored on the canopy, w_p is

$$\frac{\partial w_f}{\partial t} = P_f - E_{wf} / \rho_w \quad (4)$$

where ρ_w is the density of water, P_f the water amount retained on the canopy, E_{wf} the evaporation of water from the wetted fraction of canopy. When the conditions for dew formation are satisfied, the condensed moisture is added to the interception store, w_f .

The parameterization of the soil content is based on the concept of the three-layer model (Mihailovic, 1991).

The governing equations take the form

$$\frac{\partial w_1}{\partial t} = \frac{1}{D_1} \left\{ P_1 - F_{1,2} - \frac{E_g + E_{tf,1}}{\rho_w} - R_0 - R_1 \right\} \quad (5)$$

$$\frac{\partial w_2}{\partial t} = \frac{1}{D_2} \{ F_{1,2} - F_{2,3} - E_{tf,2} / \rho_w - R_2 \} \quad (6)$$

$$\frac{\partial w_3}{\partial t} = \frac{1}{D_3} \{ F_{2,3} - F_3 - R_3 \} \quad (7)$$

where w_i is the volumetric soil moisture content in i th layer, P_1 the infiltration rate of precipitation into the upper soil moisture store, D_i the thickness of the i th soil layer, $F_{i,i+1}$ the water flux between i and $i+1$ soil layer, F_3 the gravitational drainage flux from recharge soil moisture store, $E_{tf,1}$ and $E_{tf,2}$ the canopy extraction of soil moisture by transpiration from the first and the second soil layer, respectively, R_0 the surface runoff and R_1 the subsurface runoff from the i th soil layer.

Detailed description of the foregoing terms will be given in the next sections. Eq. (4)-(7) are solved by using an explicit time scheme.

Representation of Energy Fluxes

Our treatment of the energy fluxes may be classified as the so-called "resistance" representation. This formulation is often used to describe the energy fluxes in an Ohm's law analog form:

$$\text{flux} = \frac{\text{potential} - \text{difference}}{\text{resistance}} \quad (8)$$

Potential difference for sensible and latent heat fluxes can be expressed in terms of chosen prognostic variables, atmospheric boundary layer reference temperature and water vapor pressure in the canopy air space. The LAPS schematic diagram of transfer pathways for latent and sensible heat fluxes is shown in Figure 1.

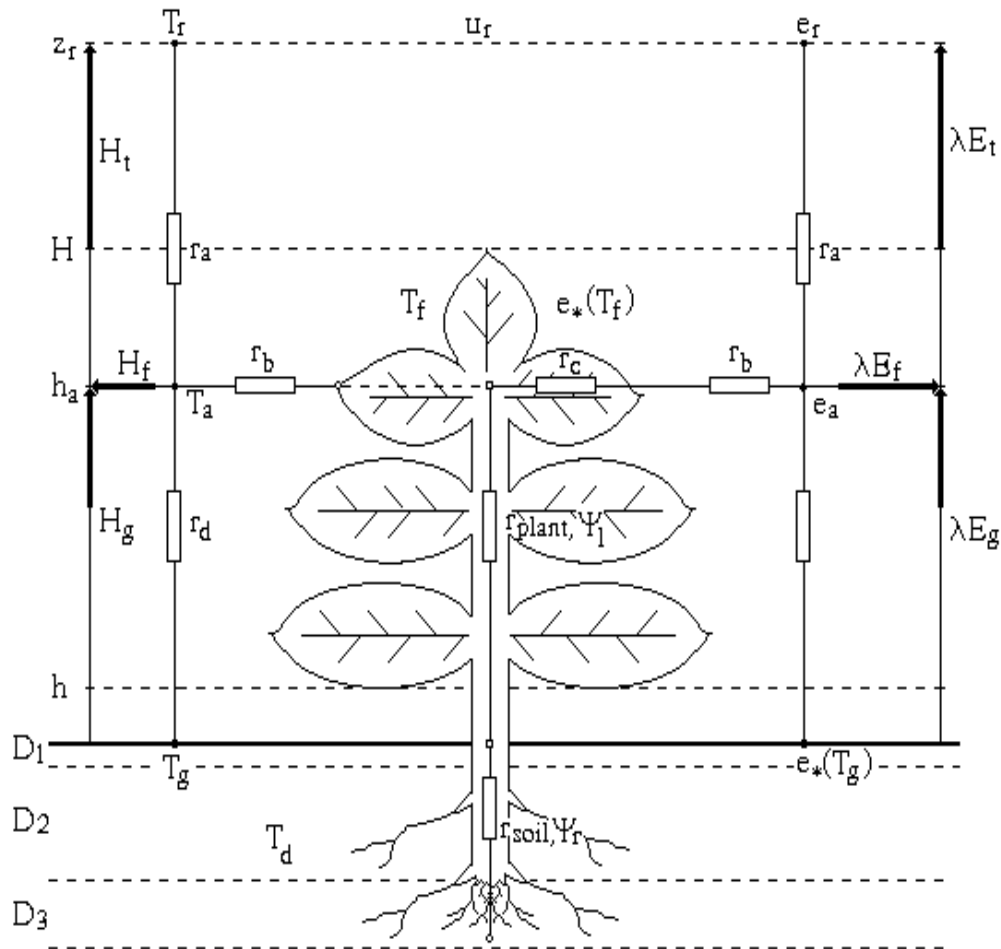


Figure 1. LAPS schematic diagram of transfer pathways for latent and sensible heat fluxes

The latent heat flux from canopy vegetation to canopy air space is given by

$$\lambda E_f = [e^*(T_f) - e_a] \left(\frac{W_w}{r_b} + \frac{1 - W_w}{r_b + r_c} \right) \frac{\rho c_p}{\lambda} \quad (9)$$

where $e^*(T_f)$ is the saturation water vapor pressure at the canopy temperature T_f , e_a the water vapor pressure of the air at the canopy source height, W_w the wetted fraction of canopy, r_b the bulk boundary layer resistance for the canopy leaves, r_c the bulk stomatal resistance of the canopy leaves, ρ the density of air, c_p the specific heat of air at constant pressure and γ the psychrometric constant. The sensible heat flux from canopy vegetation to canopy air space is given by

$$H_f = 2(T_f - T_a) \frac{\rho c_p}{r_b} \quad (10)$$

where T_a is the temperature of air at the canopy source height. The latent and sensible heat fluxes from soil surface are parameterized as

$$\lambda E_g = \frac{\rho c_p}{\gamma} \frac{[\alpha e^*(T_g) - e_a]}{r_1 + r_d} \quad (11)$$

and

$$H_g = \rho c_p \frac{T_g - T_a}{r_d} \quad (12)$$

where $e^*(T_g)$ is the saturation water vapor pressure at the soil surface temperature T_g , r_1 is the bare soil surface resistance and r_d the aerodynamic resistance between the soil surface and the canopy source height. Parameter α is calculated as a function of the volumetric soil moisture content of the top layer, w_1 , and field capacity, w_{fc} ,

$$\alpha = \begin{cases} 1 - [(w_{fc} - w_1) / w_{fc}]^2 & w_1 \leq w_{fc} \\ 1 & w_1 > w_{fc} \end{cases} \quad (13)$$

The flux λE_{wf} from the wetted portion of foliage, with wetted fractions denoted by W_w according to Eq. (9) is

$$\lambda E_{wf} = [e^*(T_f) - e_a] \frac{W_w}{r_b} \frac{\rho c_p}{\gamma} \quad (14)$$

The fraction of the foliage that is wet, W_w , is parameterized according to Deardorff (1978) and Dickinson (1984).

Transpiration occurs only from dry leaf and it is only outward. This physiological process is parameterized with the equation

$$\lambda E_{tf} = [e^*(T_f) - e_a] \frac{1 - W_w}{r_b + r_c} \frac{\rho c_p}{\gamma} \quad (15)$$

where E_{tf} is the transpiration rate from foliage. Dew formation occurs when $e^*(T_f) \leq e_a$. In that case the condensed

moisture is added to the surface interception store, w_f . The transpiration rate is zero under this condition. Air within the canopy has negligible heat capacity, so the sensible heat flux from the canopy, H_p , and from the soil surface, H_g , must be balanced by the sensible heat flux to the atmosphere, H_t

$$H_t = H_f + H_g = (T_f - T_r) \frac{\rho c_p}{r_a} \quad (16)$$

where T_r is the air temperature at the reference level within the atmospheric boundary layer and r_a the aerodynamic resistance between canopy air space and reference level. Similarly, the canopy air is assumed to have zero capacity for water storage so that the latent heat flux from canopy air space to reference level in atmospheric boundary layer, λE_g

$$\lambda E_t = \lambda E_f + \lambda E_g \frac{(e_a - e_r) \rho c_p}{r_a \gamma} \quad (17)$$

where e_r is the water vapor pressure of the air at the reference level within the atmospheric boundary layer. Diagnostic variables T_a and e_a were calculated from Eqs. (16) and (17), using corresponding expressions for H_p , H_g , λE_f and λE_g .

Parameterization of Fluxes

The net radiation absorbed by the canopy, R_f^{net} , and the soil surface, R_g^{net} , is calculated as a sum of short and long wave radiative flux,

$$R_f^{net} = R_f^s + R_f^l \quad (18)$$

and

$$R_g^{net} = R_g^s + R_g^l \quad (19)$$

The short wave radiation absorbed by the canopy, R_f^s , and the soil surface, R_g^s , is

$$R_f^s = R_o^s (\sigma_f - \alpha_f) [1 + (1 - \sigma_f) \alpha_g] \quad (20)$$

and

$$R_g^s = R_o^s (1 - \sigma_f) (1 - \alpha_g + \alpha_f \alpha_g) \quad (21)$$

where R_o^s is the incident downward directed short wave flux, assumed to be known as the forcing variable, α_g and α_f are the soil surface albedo and the foliage albedo, respectively, and σ_f is the vegetation fraction cover. The variability of ground albedo with soil wetness is parameterized in accordance with Idso et al. (1975). There is no distinction between direct and diffuse radiation and it is assumed that albedo does not vary with zenith angle. Both short wave and long wave radiation are reflected once between the soil surface and canopy.

The long wave radiative fluxes absorbed by the canopy, R_f^l , and the soil surface, R_g^l , are

$$R_f^l = R_o^l \sigma_f \epsilon_f - 2 \sigma_f \epsilon_f \sigma_B T_f^4 + \sigma_f \epsilon_f [R_o^l (1 - \epsilon_g) \sigma_B T_f^4 + \epsilon_g \sigma_B T_g^4] \quad (22)$$

and

$$R_g^1 = \epsilon_g \left[R_o^1 (1 - \sigma_f) + \epsilon_f \sigma_f \sigma_B T_f^4 + \sigma_f \epsilon_g (1 - \epsilon_f) \sigma_B T_g^4 - \sigma_B T_g^4 \right] \quad (23)$$

where σ_B is the Stefan-Boltzman constant, ϵ_f and ϵ_g the emissivities of the foliage and the soil surface respectively, and R_o^1 the incident downward long wave radiation prescribed as the forcing variable.

Aerodynamic Canopy Characteristics and Resistances

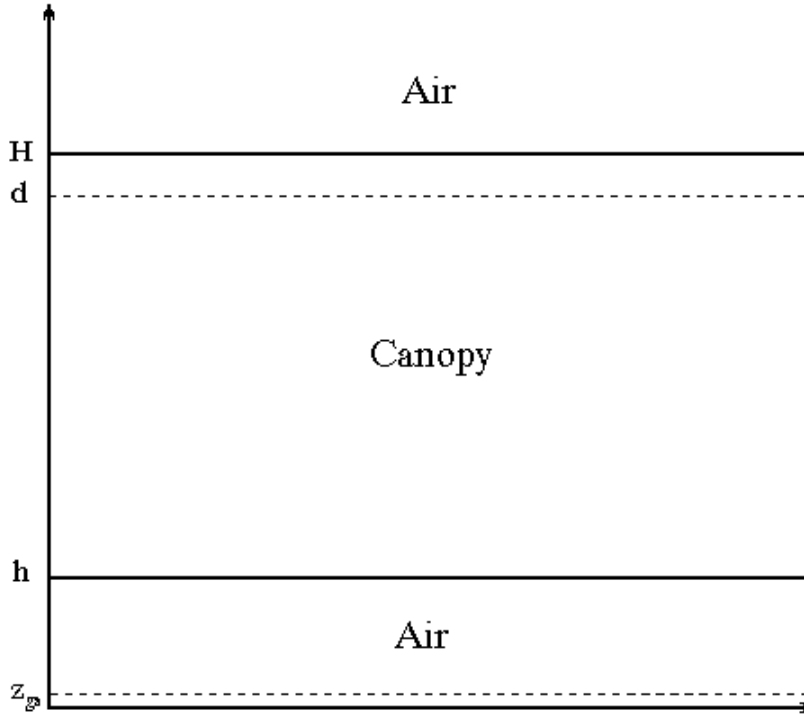


Figure 2. The single layer “sandwich” approach of the canopy vegetation used in the LAPS.

In the model the vegetation is represented as a block of constant density porous material sandwiched between two constant stress layers, the height of the canopy top, H and the height of the canopy bottom, h (Figure 2). The shear stress τ above the canopy was calculated according to the Monin-Obuhov theory where it has the form

$$\tau = \rho \left\{ k u_r / \left[\left((z - d) / z_o \right) + \Psi_M \right] \right\}^2 \quad (24)$$

where ρ is the air density, u_r the wind speed at a reference height, z_r , within the atmospheric boundary layer, $k=0.35$ the von Karman’s constant, d the zero plane displacement height, z_o the roughness length and Ψ_M the stability adjustment

function for momentum transport.

The shear stress within the canopy using the "K-theory" is expressed as

$$\tau = \rho K_m \frac{\partial u}{\partial z} \quad (25)$$

where K_m is the momentum transfer coefficient which is parameterized as

$$K_m = \sigma_s u \quad (26)$$

where σ_s is a constant and u the wind speed within the canopy. The constant σ_s is defined following Goudriaan (1977)

$$\sigma_s = i_w \left[\frac{4 w_d}{\pi L_d} \right]^{1/2} \quad (27)$$

where i_w is the relative turbulence intensity, w_d is the width of the square leaves and L_d the stem and leaf area density related to leaf area index, LAI, as $LAI=L_d(H - h)$. The wind speed inside the canopy is given by

$$u = u_H \left[\sinh(\beta z / H) / \sinh \beta \right]^{1/2} \quad (28)$$

where u_H is the wind speed at the canopy top. The extinction factor, β , depends on the plant morphology and is defined as

$$\beta = \left(\frac{C_d LAI H}{2 \sigma_s} \right)^{1/2} \quad (29)$$

where C_d is the leaf drag coefficient. The zero plane displacement height, d and roughness length, z_0 , are calculated according to Goudriaan (1977),

$$d = H - \frac{1}{k} \left(\frac{\sigma_s H}{\beta} \right)^{1/2} \quad (30)$$

and

$$z_0 = (H - d) \exp \left\{ - \frac{H}{\beta(H - d)} \right\}. \quad (31)$$

The fluxes in the model are calculated using aerodynamic and surfaces resistances. Corresponding electrical circuits with resistances are shown in Figure 1. The resistances r_a , r_b and r_d are usually called aerodynamic resistances and they are equivalent to the integrals of inverse conductances over a specified length. In the case of the aerodynamic resistances, the conductances correspond to the turbulent transfer coefficient for heat and water vapor. Surface resistances r_c and r_l control water transfer through the plant-soil system.

The aerodynamic resistance r_a represents the transfer of heat and moisture from the canopy to reference level, z_r , and is calculated as

$$r_a = \frac{1}{k u_*} \ln \frac{z_r - d}{H - d} \quad (32)$$

where u_* is the friction velocity.

The area-averaged bulk boundary layer resistance, r_b , is calculated as

$$r_b = \frac{1}{u_H^{1/2}} P_s C_t \beta (\sinh \beta)^{1/4} / (L_d H) \int_{\alpha_w \beta}^{\beta} (\sinh y)^{1/4} dy \quad (33)$$

where $\alpha_w = h/H$, $y = \beta_z/H$, C_t is the transfer coefficient and P_s is the leaf shelter factor.

In the model physics we considered r_b as the total resistance, what implicitly includes an assumption that both forms free and forced convection equally contribute to convection over the whole unstable region.

The resistance to water vapor and heat flow from the soil surface to air space within the canopy is represented by an aerial resistance r_d , which is parameterized as

$$r_d = \int_{h_0}^h \frac{1}{K_m} dz = \frac{1}{k^2 u_H} \left[\frac{\sinh(\beta)}{\sinh(\alpha_w \beta)} \right]^{1/2} \ln^2 \left(\frac{h}{h_0} \right) \quad (34)$$

where h_0 is the effective roughness length. The aerodynamic resistances are modified taking into account the effect of non-neutrality (Businger et al., 1971).

In the LAPS scheme stomatal resistance, r_s , depends both upon the atmospheric factors and water stress. This dependence is given in the form

$$r_s = r_{smin} \Phi_1 \Phi_2^{-1} \Phi_3^{-1} \Phi_4^{-1} \quad (35)$$

where r_{smin} is the minimum of stomatal resistance.

The factor Φ_1 gives the dependence on the solar radiation. It is parameterized by using the expression suggested by Dickinson (1984)

$$\Phi_1 = (1 + f)(f + r_{smin} / r_{smax})^{-1} \quad (36)$$

where

$$f = 1.1. R_o^s / (R_{gl} LAI) \quad (37)$$

where LAI is the leaf area index, R_o^s the incoming short wave radiation and R_{gl} the limit value of 30 W m^{-2} for a forest and 100 W m^{-2} for crops. The value of 5000 s m^{-1} for r_{smax} is used. The factors Φ_2 , Φ_3 and Φ_4 are limited to a range from 0 to 1. The factor Φ_2 takes into account the effect of the water stress on the stomatal resistance and it is parameterized in the following way

$$\Phi_2 = \begin{cases} 1 & w_a > w_{fc} \\ 1 - \left(\frac{w_{wil}}{w_a} \right)^{1.5} & w_{wil} \leq w_a \leq w_{fc} \\ 0 & w_a < w_{wil} \end{cases} \quad (38)$$

where w_a is the mean volumetric water content in the first and second soil layer, w_{wil} the volumetric soil moisture content at wilting point and w_{fc} volumetric soil moisture content at field capacity. The factor Φ_3 gives the dependence of stomatal resistance on the air temperature. This factor is calculated, according to Dickinson et al. (1986), as

$$\Phi_3 = 1.0 - 0.0016(298 - T_r)^2 \quad (39)$$

where T_r is the air temperature at the reference level.

The factor Φ_4 represents the effect of atmospheric water vapor pressure deficit. It is parameterized following Jarvis (1976) who suggested the form

$$\Phi_4 = 1 - \eta [e^*(T_f) - e_r] \quad (40)$$

where $e^*(T_f)$ is the saturation water vapor pressure for the canopy temperature T_f , e_r the water vapor pressure at some reference level and η the species-dependent empirical parameter that is equal to 0.025 hPa^{-1} . The bulk stomatal resistance, r_c , represents the effective stomatal resistance per unit ground surface area and it is given by

$$r_c = r_s / LAI. \quad (41)$$

The leaf water potential Ψ_l describing the water transfer pathway from root zone to leaf is calculated following Van der Honert (1948),

$$\Psi_l = \Psi_r - z_t - E_{tf} (r_{plant} + r_{soil}) / \rho_w \quad (42)$$

where Ψ_r is the soil moisture potential in the root zone, z_t the height of the transpiration source (equal to canopy source height, h_a), E_{tf} the transpiration rate, r_{plant} the plant resistance imposed by the plant vascular system prescribed as a variable, r_{soil} , the resistance of the soil and root system. The canopy source height, h_a , is defined as a center of action of bulk aerodynamic resistance within the canopy. An estimation for h_a is suggested by Mihailovic and Rajkovic (1993) in the following form

$$h_a = H \left\{ 1 + 2 / \beta \ln \left[0.5 \left[1 + \exp(\beta(h / H - 1)) \right] \right] \right\}. \quad (43)$$

The soil water potential in the root zone, Ψ_r , is parameterized as an average term obtained by summing the weighted soil water potentials of the soil layers from the surface to the rooting depth, z_d ,

$$\Psi_r = \sum_0^{z_d} (\Psi_i D_i) / z_d \quad (44)$$

where Ψ_i is the soil water potential of the i th soil layer and D_i the depth of the i th soil layer. The soil water potential, Ψ_i , is parameterized as it is usually done, after Clapp and Horberger (1978),

$$\Psi_i = \Psi_s (w_i / w_s)^{-B} \quad (45)$$

where Ψ_s is the soil water potential at saturation, w_i and w_s are volumetric soil moisture content of the i th soil layer and its value at saturation and B the soil type constant. The depth-averaged resistance r_{soil} to water flow from soil to roots, is parameterized according to Federer (1979)

$$r_{\text{soil}} = (R / D_d + \alpha_j / K_r) / z_d \quad (46)$$

where

$$\alpha_j = \left\{ V_r - 3 - 2 \ln \left[V_r / (1 - V_r) \right] \right\} / (8\pi D_d) \quad (47)$$

and where R is the resistance per unit root length, D_d the root density, V_r the volume of root per unit volume of soil and K_r the mean soil hydraulic conductivity in the root zone expressed as function of Ψ_r

$$K_r = K_s (\Psi_s / \Psi_r)^{(2B+3)/B} \quad (48)$$

where K_s is the saturated hydraulic conductivity.

The bare soil surface resistance, r_1 , governs moisture flux from the top soil layer into the atmosphere. This surface resistance is parameterized following the empirical expression given by Sun (1982),

$$r_1 = p_1 + p_2 (w_1 / w_s)^{-p_3} \quad (49)$$

where p_1 , p_2 and p_3 are empirical constants obtained from the data, equal to 30, 3.5 and 2.3, respectively (Sellers et al., 1989).

Hydrology Parameterization

Moving from top to bottom of the soil water column, the LAPS has the three layers (Figure 3). The governing equations for the three volumetric soil moisture content are given by Eq. (5)-(7).

The precipitation P_1 that infiltrates into the top soil layer is given by

$$P_1 = \begin{cases} \min(P_o, K_s) & w_1 < w_s \\ 0 & w_1 = w_s \end{cases} \quad (50)$$

where K_s is the saturated hydraulic conductivity and P_o the effective precipitation rate on the soil surface given by

$$P_o = P - (P_f - D_f). \quad (51)$$

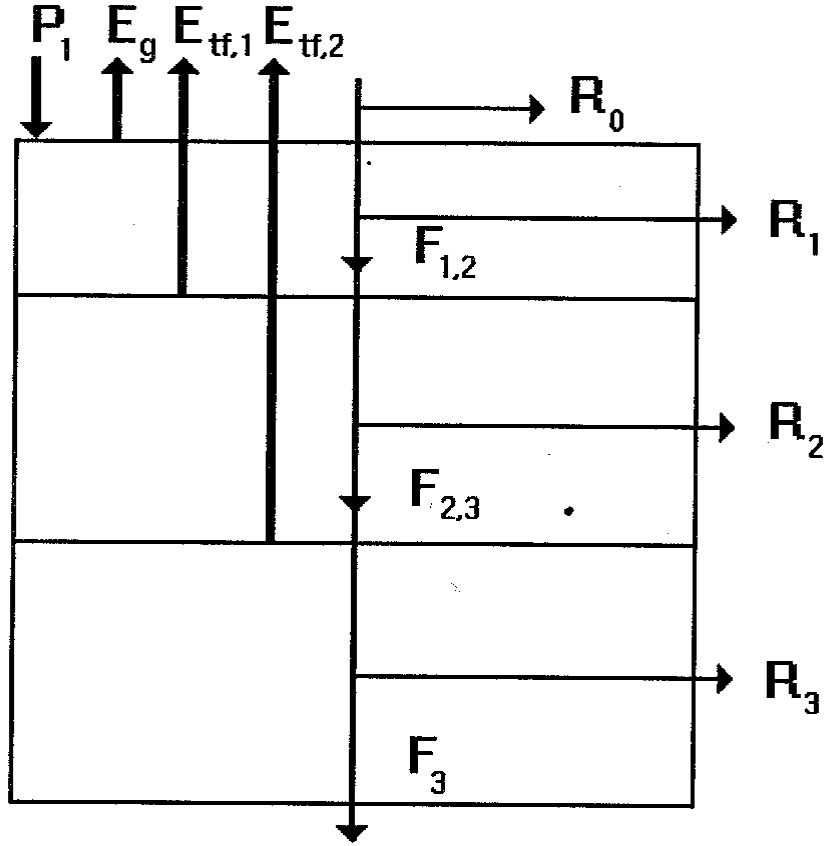
The rate of interception (inflow) for the canopy, P_f is given by

$$P_f = P(1 - e^{-\alpha_{if}}) \sigma_f \quad (52)$$

where P is the precipitation rate above the canopy, α_{if} a constant depending on the leaf area index. It is assumed that the interception can be considered via the expression describing the exponential attenuation (Sellers et al., 1986). The rate of drainage of water stored on the vegetation (outflow) for the canopy, D_f is given by

$$D_f = \begin{cases} 0 & w_f < w_{max} \\ P_f & w_f = w_{max} \end{cases} \quad (53)$$

The transfer of water between adjacent layers $F_{i,i+1}$, is given by



$$F_{i,i+1} = K_{ef} [2(\Psi_i - \Psi_{i+1}) / (D_i + D_{i+1}) + 1] \quad (54)$$

Figure 3. Representation of runoff and drainage for LAPS scheme

where Ψ_i is the soil moisture potential of the i th layer, obtained by Eq. (45) and K_{ef} the effective hydraulic conductivity between soil layers given by

$$K_{ef} = (D_i K_i + D_{i+1} K_{i+1}) / (D_i + D_{i+1}) \quad (55)$$

where K_i is the hydraulic conductivity of the i th soil layer determined by the empirical formula

$$K_i = K_{si} (w_i / w_s)^{2B+3} \quad (56)$$

where K_{si} is the hydraulic conductivity at saturation of the i th soil layer.

The gravitational drainage from the bottom soil layer is defined by

$$F_3 = K_{si} (w_3 / w_s)^{2B+3} \sin x \quad (57)$$

where x is the mean slope angle (Sellers et al., 1986; Abramopoulos et al., 1988).

The schematic diagram representing the drainage and runoff in the LAPS is shown in Figure 3. The surface runoff R_0 is computed as

$$R_0 = P_1 - \min(P_1, K_s). \quad (58)$$

The subsurface runoff is calculated for each soil layer using the expressions

$$R_1 = F_{1,2} - \min(F_{1,2}, K_s) \quad (59)$$

$$R_2 = F_{2,3} - \min(F_{2,3}, K_s) \quad (60)$$

$$R_3 = F_3 - \min(F_3, K_s). \quad (61)$$

At the end of time step, Δt , the value Γ_i is calculated as

$$\Gamma_i = \frac{D_i}{\Delta t} [w_i^k + A_i \Delta t - w_{fc}] \quad (62)$$

where w_i^k is the volumetric soil moisture content at the beginning of k time step while A_i representing the terms on the right side of Eqs. (5)-(7). If the condition Γ_i becomes runoff which is added to corresponding subsurface runoff R_i .

Consequently, at the end of the time step, the calculated value of the volumetric soil moisture content w_i^{k+1} takes the value w_{fc} .

BIOPHYSICAL INPUT PARAMETERS IN THE LAPS SCHEME

Recently, in the land surface schemes offered by the meteorological community there is a growing demand for a finer treatment of vegetation, soil textures and solid surfaces because of their pronounced impact on thermal circulation as well as synoptically induced mesoscale systems. The LAPS scheme operates with 18 land covers according to Dickinson et al. (1986), which are presented in Table 1a, and 11 textural classes according to the USDA soil texture classification (Table 1b). These types of covers are classified into the three groups for: (a) vegetative, (b) bare and (c) solid (Table 1c) surfaces. Since the LAPS scheme has a sophisticated land surface parameterization formulation it includes 22 different morphological, physiological, photometric and aerodynamic characteristics for vegetative covers. The values of these parameters are derived following Dickinson et al. (1986), Lalic and Mihailovic (1998) and Mihailovic et al. (1998). They are shown in Table 2. The corresponding values of 10 thermal and water soil characteristics for 11 soil textural types are listed in Table 3. These values are obtained according to Clapp and Hornberger (1978), Cosby et al. (1984), Dickinson et al. (1986) and Mihailovic et al. (1998). However, calculation of the surface temperature and corresponding fluxes is more complicated for the rocks than for other solid materials, due their particular thermal and physical properties.

Although the rocks are often the dominant type of ground on the interface between the Earth and atmosphere or celestial objects in space or the atmosphere if it exists, a very limited number of papers in planetary space science (Simpson and Lucas, 1972; Jones et al., 1975) as well as in geophysical sciences (Mihailovic et al., 1996; Arsenic et al., 1997), is devoted to this problem. In the LAPS scheme we added an additional type of the underlying surface, i.e., solid surface representing mostly surfaces consisting of different types of the rock. Let us note that the LAPS is the only scheme, among others, considering this type of the surface in modelling of the land-air interaction. To demonstrate an advantage when this type of the surface is introduced in surface modelling, we will show a result from the paper by Papadopoulos et al. (1999). In this paper he presented the simulations over the Sahara Desert, using a simple parameterization of rocky ground instead of coarse texture commonly employed in land surface schemes. In design of the experiment the classification of rocks was done according to Mihailovic et al. (1996). The 5-day time integration was performed using the comprehensive SKIRON forecasting system based on the NCEP Eta Model (Mesinger 1988; Janjic, 1994) which has been integrated at the University of Athens (Kallos et al., 1997). In Figure 4a is shown a comparison of 2m air temperature observations with the values simulated by the ROCK and SAND runs. It shows that the ROCK simulations agree closer with available observations than those coming from the SAND run. This is more emphasized for station A and partly for station D. Also it is seen that for the ROCK case the 2 m air temperatures, during the night, are systematically higher than ones obtained when sand was an underlying surface. It comes from the fact that the surface temperature over the rocky ground, during the night, was higher than sand surface temperature (Figure 4b). Because of the sand thermal properties it seems that the sand surface cools much more rapidly than the rocky surface does, sometime resulting in significantly lower surface temperature and air temperature as is seen (stations C and D) at the end of the 4th day of integration (Figure 4). The nine types of rocks currently used in the LAPS and their corresponding 5 physical properties are shown in Tables 1c and 4, respectively.

Table 1a. Land covers used in the LAPS. The values of their parameters listed in Table 2 are obtained from different sources (Dickinson et al., 1986; Lalic and Mihailovic, 1998; Mihailovic et al., 1998)

COVER TYPE	NUMBER
CROP	(1)
SHORT GRASS	(2)
EVERGREEN NEEDLE LEAF	(3)
DECIDUOUS NEEDLE LEAF TREE	(4)
DECIDUOUS BROADLEAF TREE	(5)
EVERGREEN BROADLEAF TREE	(6)
TALL GRASS	(7)
DESERT	(8)
TUNDRA	(9)
IRRIGATED CROP	(10)
SEMI-DESERT	(11)
ICE-CAP-GLACIER	(12)
BOG AND MARSH	(13)
INLAND WATER	(14)
OCEAN	(15)
EVERGREEN SHRUB	(16)
DECIDUOUS SHRUB	(17)
MIXED WOODLAND	(18)

Table 1b. The soil textures, following the USDA soil texture classification, used in the LAPS. The values of their parameters listed in Table 3 are obtained according to Clapp and Hornberger (1978), Cosby et al. (1984), Dickinson et al. (1986) and Mihailovic et al. (1998)

TYPE	NUMBER
SAND	(1)
LOAMY SAND	(2)
SANDY LOAM	(3)
SILT LOAM	(4)
LOAM	(5)
SANDY CLAY LOAM	(6)
SILT CLAY LOAM	(7)
CLAY LOAM	(8)
SANDY CLAY	(9)
SILTY CLAY	(10)
CLAY	(11)

Table 1c. The rock types used in the LAPS. The values of their parameters listed in Table 4 are used from Mihailovic et al. (1996), Arsenic et al. (1997) and Arsenic et al. (2000)

TYPE	NUMBER
LIME	(1)
BASALT	(2)
DOLOMITE	(3)
SANDSTONE	(4)
DIABASE	(5)
GABBRO	(6)
GRANITE-GNEISS	(7)
MARBLE	(8)
GRANITE	(9)

Indicator for surface type	1	2	3	4	5	6	7	8	9	10	11	12	13	14	15	16	17	18
Albedo of foliage	0.18	0.18	0.16	0.17	0.18	0.13	0.18	0.18	0.18	0.16	0.2	0.12	0.12	0.	0.	0.16	0.16	0.14
Canopy height (m)	1.	0.8	17.	14.	20.	35.	2.3	0.	0.6	1.5	2.8	0.	2.2	0.	0.	2.5	2.5	13.
Canopy bottom height (m)	0.02	0.01	8.5	7.	8.	1.	0.22	0.	0.01	0.16	0.16	0.	0.16	0.	0.	0.3	0.28	5.
Emissivity of foliage	0.95	0.95	0.97	0.97	0.97	0.97	0.95	0.	0.95	0.94	0.94	0.	0.95	0.	0.	0.95	0.95	0.95
Maximum stomatal resistance 10^3 ($s\ m^{-1}$)	5.	5.	5.	5.	5.	5.	5.	0.	5.	5.	5.	0.	5.	0.	0.	5.	5.	5.
Minimum stomatal resistance ($s\ m^{-1}$)	150.	152.	250.	250.	300.	252.	150.	0.	152.	150.	150.	0.	152.	0.	0.	152.	149.	248.
Leaf shelter factor	2.9	3.4	1.1	1.1	1.3	1.1	3.	0.	2.4	2.5	1.6	0.	1.4	0.	0.	1.5	1.9	1.4
Value in stomatal resistance calculations ($W\ m^{-2}$)	100.	100.	30.	30.	30.	30.	100.	0.	100.	100.	100.	0.	100.	0.	0.	30.	30.	30.
Fractional cover for canopy	0.85	0.85	0.8	0.8	0.9	0.99	0.9	0.	0.5	0.85	0.1	0.	0.75	0.	0.	0.75	0.75	0.87
Averaged leaf area density ($m^2\ m^{-2}$)	3.9	4.7	0.2	0.3	0.5	0.2	2.	0.	2.8	3.	1.2	0.	0.7	0.	0.	0.9	1.8	0.8
Volume of root per unit volume of soil 10^{-3} ($m^3\ m^{-3}$)	15.	15.	20.	20.	20.	35.	15.	0.	3.75	18.5	3.	0.	18.5	0.	0.	17.	20.	20.
Root density for canopy 10^3	4.	14.	8.	8.	8.	10.	4.	0.	1.	5.	2.	0.	5.	0.	0.	3.	3.5	8.
Root resistance per unit length 10^{12} ($s\ m^{-1}$)	4.	4.	4.	4.	4.	4.	4.	0.	4.	4.	4.	0.	4.	0.	0.	4.	4.	4.
Root depth for canopy (m)	1.	1.	1.5	2.	1.5	2.	1.	0.	1.	1.	1.	0.	1.	0.	0.	1.	1.	2.
Extinction coefficient for interception by canopy 10^{-3}	103.	117.	260.	260.	33.	68.	96.	0.	462.	103.	231.	0.	295.	0.	0.	255.	60.	55.
Plant resistance imposed by the plant vascular system 10^8 (s)	2.5	2.5	2.5	2.5	2.5	2.5	2.5	0.	2.5	2.5	2.5	0.	2.5	0.	0.	2.5	2.5	2.5
Heat capacity of canopy ($J\ m^{-2}\ K^{-1}$)	870.	870.	870.	870.	870.	870.	870.	0.	870.	870.	870.	0.	870.	0.	0.	870.	870.	870.
Identifier for surface type	1	2	3	4	5	6	7	8	9	10	11	12	13	14	15	16	17	18
Canopy drag coefficient	0.2	0.2	0.2	0.2	0.2	0.2	0.2	0.	0.2	0.2	0.2	0.	0.2	0.2	0.2	0.2	0.2	0.2
Transfer coefficient ($m^{-1/2}\ s^{1/2}$)	50.	50.	50.	50.	50.	50.	50.	0.	50.	50.	50.	0.	50.	0.	0.	50.	50.	50.
Width of square leaves (m^2)	0.03	0.02	0.28	0.27	0.55	0.8	0.05	0.	0.01	0.05	0.05	0.	0.02	0.	0.	0.05	0.08	0.6
Relative turbulence intensity	0.5	0.5	0.5	0.5	0.5	0.5	0.5	0.	0.5	0.5	0.5	0.	0.5	0.	0.	0.5	0.5	0.5
Effective ground roughness length (m)	0.002	0.002	0.3	0.3	0.3	0.3	0.01	0.	0.001	0.002	0.01	0.	0.002	0.	0.	0.01	0.01	0.03

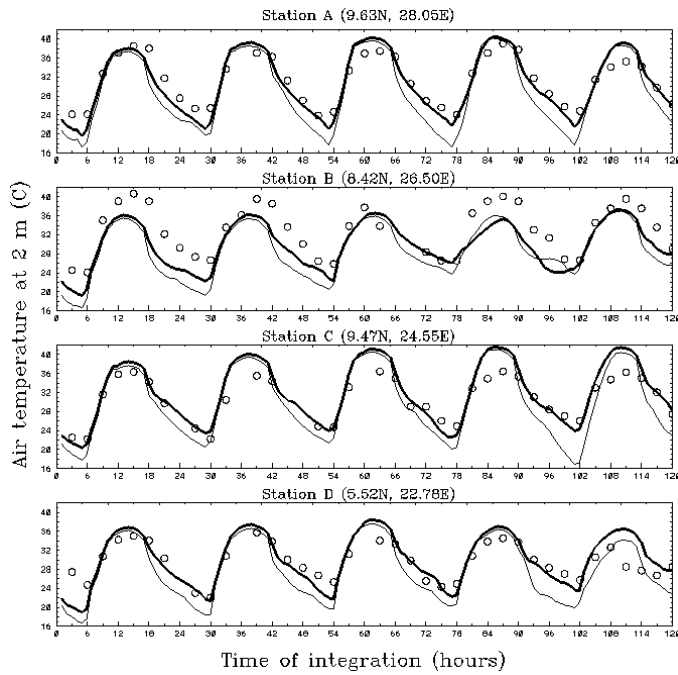
Table 3. Parameters for the following soil textures: sand (1), loamy sand (2), sandy loam (3), silt loam (4), loam (5), sandy clay loam (6), silt clay loam (7), clay loam (8), sandy clay (9), silty clay (10), clay (11)

Indicator for soil type	1	2	3	4	5	6	7	8	9	10	11
Exponent "B"	4.05	4.38	4.90	5.30	5.39	7.12	7.75	8.52	10.40	10.401	11.40
Emissivity of the ground	0.95	0.95	0.95	0.95	0.95	0.95	0.95	0.95	0.95	0.95	0.95
Heat capacity of soil fraction ($J m^{-3} K^{-1}$)	916.	879.	840.	796.	759.	736.	824.	767.	736.	719.	680.
Saturated hydraulic conductivity $10^{-6} (m s^{-1})$	176.00	156.30	34.67	7.20	6.95	6.30	1.70	2.45	2.167	1.033	1.283
Soil moisture potential at saturation (m)	-0.121	-0.090	-0.218	-0.786	-0.478	-0.299	-0.356	-0.630	-0.153	-0.490	-0.405
Soil density ($J kg m^{-3}$)	1200.	1250.	1300.	1400.	1350.	1350.	1500.	1450.	1450.	1650.	1700.
Ratio of saturated thermal conductivity to that of loam	1.7	1.5	1.3	1.2	1.1	1.0	0.95	0.90	0.85	0.80	0.75
Volumetric soil moisture at saturation ($m^3 m^{-3}$)	0.395	0.410	0.435	0.485	0.451	0.420	0.477	0.476	0.426	0.482	0.482
Soil moisture content at field capacity ($m^3 m^{-3}$)	0.112	0.192	0.218	0.259	0.236	0.241	0.311	0.303	0.284	0.334	0.346
Wilting point volumetric soil moisture at saturation ($m^3 m^{-3}$)	0.013	0.047	0.068	0.16.	0.089	0.111	0.183	0.165	0.177	0.209	0.229

Table 4 Parameters for the following rock types: lime (1), basalt (2), dolomite (3), sandstone (4), diabase (5), gabbro (6), granite-gneiss (7), marble (8) and granite (9)

Indicator for type of rock	1	2	3	4	5	6	7	8	9
Volumetric heat capacity $10^6 (J m^{-3} K^{-1})$	2.175	2.470	2.604	2.450	1.988	1.988	2.226	2.226	1.839
Thermal conductivity ($J m^{-1} s^{-1} K^{-1}$)	3.13	2.28	6.00	3.286	1.491	2.100	3.460	3.460	3.055
Density of rock $10^3 (kg m^{-3})$	2.605	2.940	2.830	2.800	2.800	2.800	2.800	2.800	2.745
Albedo for rocky ground	0.30	0.30	0.30	0.30	0.30	0.30	0.30	0.30	0.30
Emissivity of rocky ground	0.95	0.95	0.95	0.95	0.95	0.95	0.95	0.95	0.95

(a)



(b)

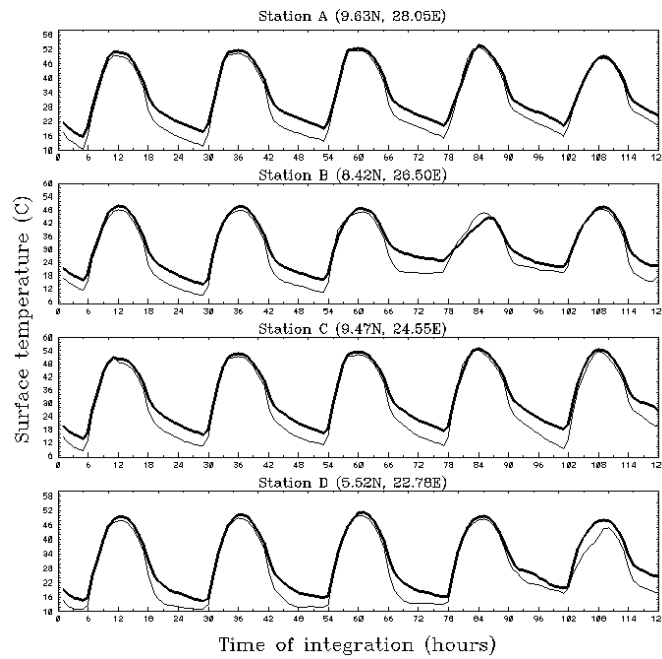


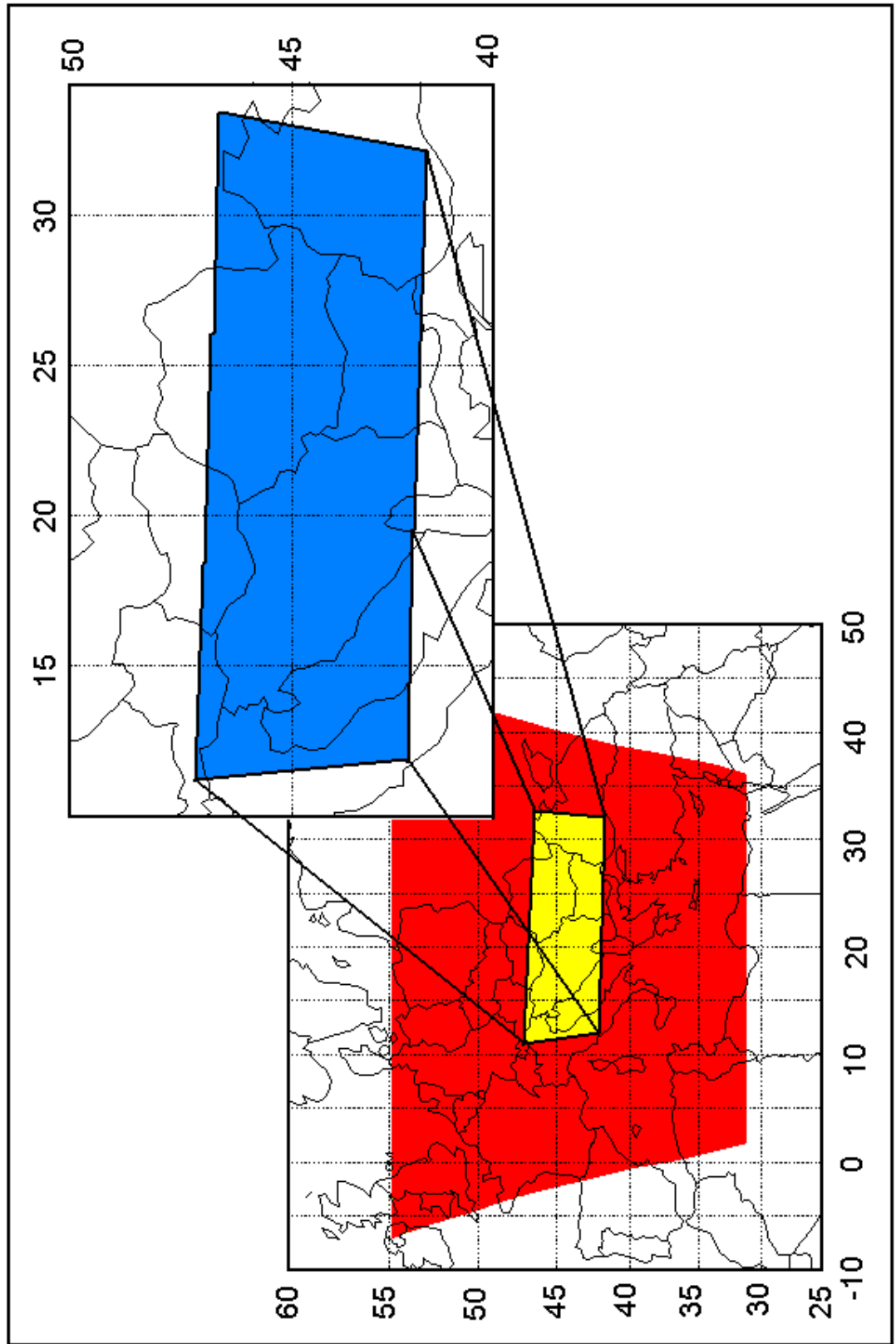
Figure 4. The diurnal cycle of the simulated air temperature at 2 m (a) and surface temperature (b) during the 5-day integrations, for the four stations. The solid and thin lines indicate the ROCK and SAND case, respectively, while the observations assigned by the empty circles.

NUMERICAL SIMULATIONS AND MODEL SET UP

We have performed a numerical case study. In this case study, we performed a numerical simulation for a period of 24 hours using the nonhydrostatic version of the NCEP Eta Mesoscale Model with the LAPS land surface scheme implemented in it. The σ terrain following coordinate is used with 38 levels in vertical. For the initial and the boundary meteorological conditions, the NCEP objective global analysis, gridded data in a 1° horizontal increment, for 23 pressure levels (up to 50 hPa) was used. The above data set is downloaded from the NCEP. The lateral boundaries of the model domain from the NCEP data were available every 6 hours. The starting time of the simulation was 0000 GMT 05 June 2002. The simulation period was 24 hours. The model has a horizontal increment of $0.222^\circ \times 0.205^\circ$, and time step of 100 s. The model domain shown in Figure 5 is shadowed by the red color. In the same figure the domain with meteorological stations having the SYNOP data sets is indicated by the blue color. These data sets were used to compare the modeled air temperatures at 2 m for the model cycle (0600 GMT, 1200 GMT, 1800 GMT and 2400 GMT) and extreme temperatures, against the observations.

In the preparation phase, surface parameters, observed or pre-defined (topography, sea surface temperature (SST), soil and vegetation types, soil temperatures and wetness, slopes and azimuths of the sloping surfaces) are interpolated to the model grid. The topographic data set used is the one provided by the US Geological Survey (USGS) with 10 x 10 arc min resolution. The vegetation data set is also available from USGS with 30 arc s x 30 arc s resolution, following the classification by Dickinson et al. (1986). For soil textural classes, the UNEP/FAO data set is used, after its conversion from soil type to soil textural ZOBLER classes. Figs. 6 and 7 depict the distribution of vegetation and soil textures from the blue domain from Figure 5, used in comparison between the modeled and the observed values. Albedo and surface roughness variations were computed, in the preprocessing stage, depending on vegetation.

Figure 5. Model domain (red color). The blue color indicates the domain including the SYNOP data of 05 June 2002 taken for comparison with outputs obtained by the Eta-LAPS



RESULTS AND COMMENTS

To examine how much the differences in the vegetation height over a large domain represent the influence of underlying surface on above air layer, in three dimensional simulations, we have performed a numerical experiment. The domain under consideration was an area that is in Figure 5 shadowed by the blue color, having 651 grid points, with the distribution of cover types [water (22.7%); crop (44.2%); short grass (3.2%); evergreen needle leaf (2.6%); deciduous broadleaf (4.3%) and mixed woodland (23.0%)], and soil textural classes [water (22.7%); loamy sand (4.5%); sandy loam 11.5%); silt clay loam (36.6%); clay loam (19.7%); sandy clay (2.5%) and silty clay (2.5%)] shown in Figs. 6 and 7, respectively. The control run (referred as Control) has been performed with this distribution of the cover types. The next three runs were made using the three different vegetation types and assuming that they completely cover the domain, instead of cover types used in the Control run. For that purpose the three vegetation types, representing broad interval of vegetation heights, were chosen (i.e., crop, tall grass and mixed woodland).

The parameterization of the sensible heat flux in a land surface scheme is one of the crucial points in its linking to an atmospheric model. Figure 8 shows temporal variation of sensible heat fluxes for the three different cover types also including the Control run calculated according to Eq. (16). From this figure, it is seen that there are not significant differences between the sensible heat fluxes up to 0500 GMT and mostly after 1800 GMT. However, they are more emphasized around noon time reaching the maximum value of 100 W m^{-2} between the crop (150 W m^{-2}) and mixed woodland (50 W m^{-2}). Let us note that the values of the sensible heat obtained by the Control run are closer to those obtained over the crop cover, because of it prevails in the cover mosaic in the Control run (44.2%).

In diagnostic calculating the near surface values of shelter temperature, wind speed and specific humidity, the key parameters are turbulent mixing coefficients in the layer between the canopy source height and the lowest model level. In linking the LAPS to the NCEP Eta Mesoscale Model, the heat turbulent coefficient is calculated from Eq. (16). The lower panel in Figure 9 depicts temporal variation of the heat turbulent coefficient and its sensitivity to cover type. The highest values are obtained for the crop while the lower ones are obtained for the Control run and tall grass. The lowest values of the heat turbulent coefficient calculated by the model are obtained for the mixed woodland. These values begin to differ when heating of the underlying surface intensively starts to grow up (after 0700 GMT). Up to the time indicated the values of the heat turbulent coefficient are quite close for all covers due to the initialization procedure in which all model variables, representative for the canopy layer and ground surface, are set to be equal. Accordingly, this remark is relevant for all surfaces and near surface variables so it will not be emphasized again in further text.

In land surface modelling the friction velocity is a key variable controlling the momentum exchange between the underlying surface and lower part of the atmosphere. It is very sensitive to the cover type, highly affecting the calculation of the momentum turbulent coefficient in the layer between the canopy source height and the lowest model level. The upper panel in Figure 9 shows the sensitivity of the momentum transfer coefficient to the cover type. Looking at this panel it is seen that the highest values of the momentum turbulent coefficient are obtained for the crop. They are higher than those calculated by the Control run. These differences are more emphasized

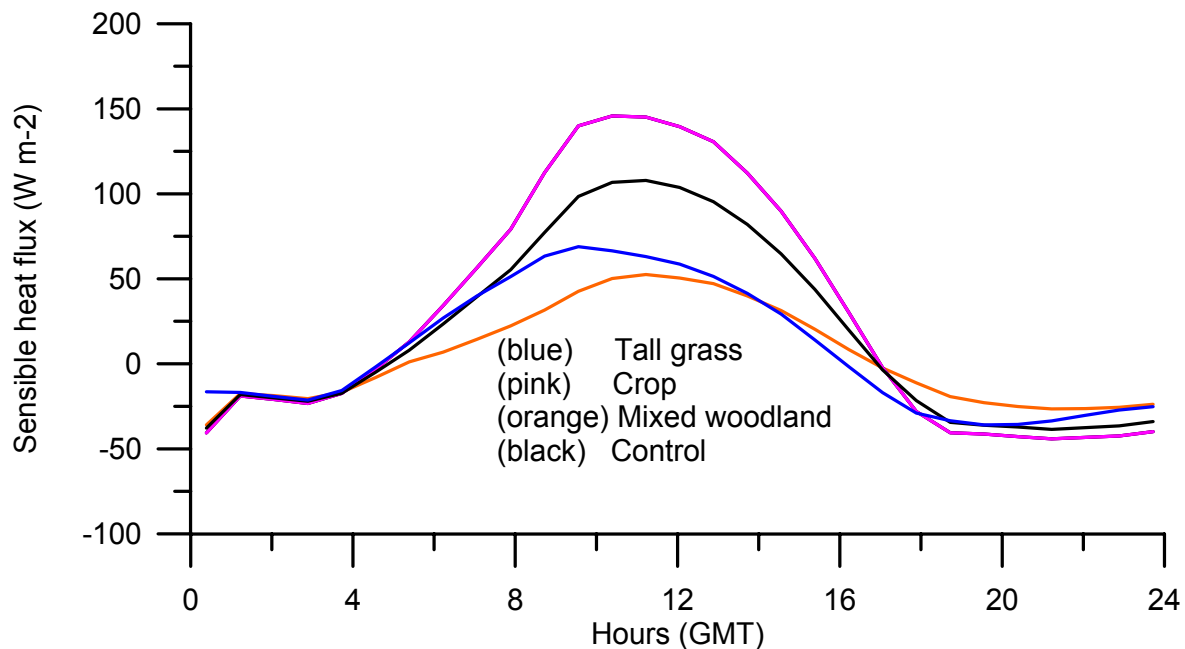


Figure 8. Sensitivity of the mean sensible heat flux to the cover type. The hourly means were made using all grid points in the blue domain in Figure 5

comparing to the values obtained for the tall grass and mixed woodland. The runs over the grass having different heights give the values which are very close up to the 0800 GMT. After that time they start to differ, approaching to each other after 2000 GMT

In the LAPS the temperature representing the thermal state of underlying surface is calculated diagnostically according to Eqs. (10), (12) and (16). Temporal variation of the hourly values of area averaged surface temperature, for different cover types, obtained from all grid points in blue domain in Figure 5, is shown on the lower panel in Figure 10. From this figure is seen that no differences occur between different cover types during the period between midnight and 0600 GMT. The minimum of the mean surface temperature, for all cover types, occurs approximately at the same time, i.e., around 0400 GMT. Also, there are not big differences in their values (11.5 °C – crop; 11.8 °C – control; 12.0 °C – mixed woodland; 12.1 °C – tall grass). This behavior comes from the fact that the night ground radiation is smaller over a vegetative cover than over a bare soil. Thus, the differences in the minimum of the surface temperatures over different covers are smaller than those between the covered surface and a bare soil. When the surface starts to absorb the shortwave radiation then differences in surface temperature become more evident. After the time indicated the increase of surface temperature is slower over the mixed woodland than over the other cover types. It could be expected because of a huge difference in thermal characteristics between forest and grass vegetation, so the forest surface takes more time to be heated. However, after 0700 GMT the mean surface temperature over the crop cover starts to grow up faster than over the tall grass and

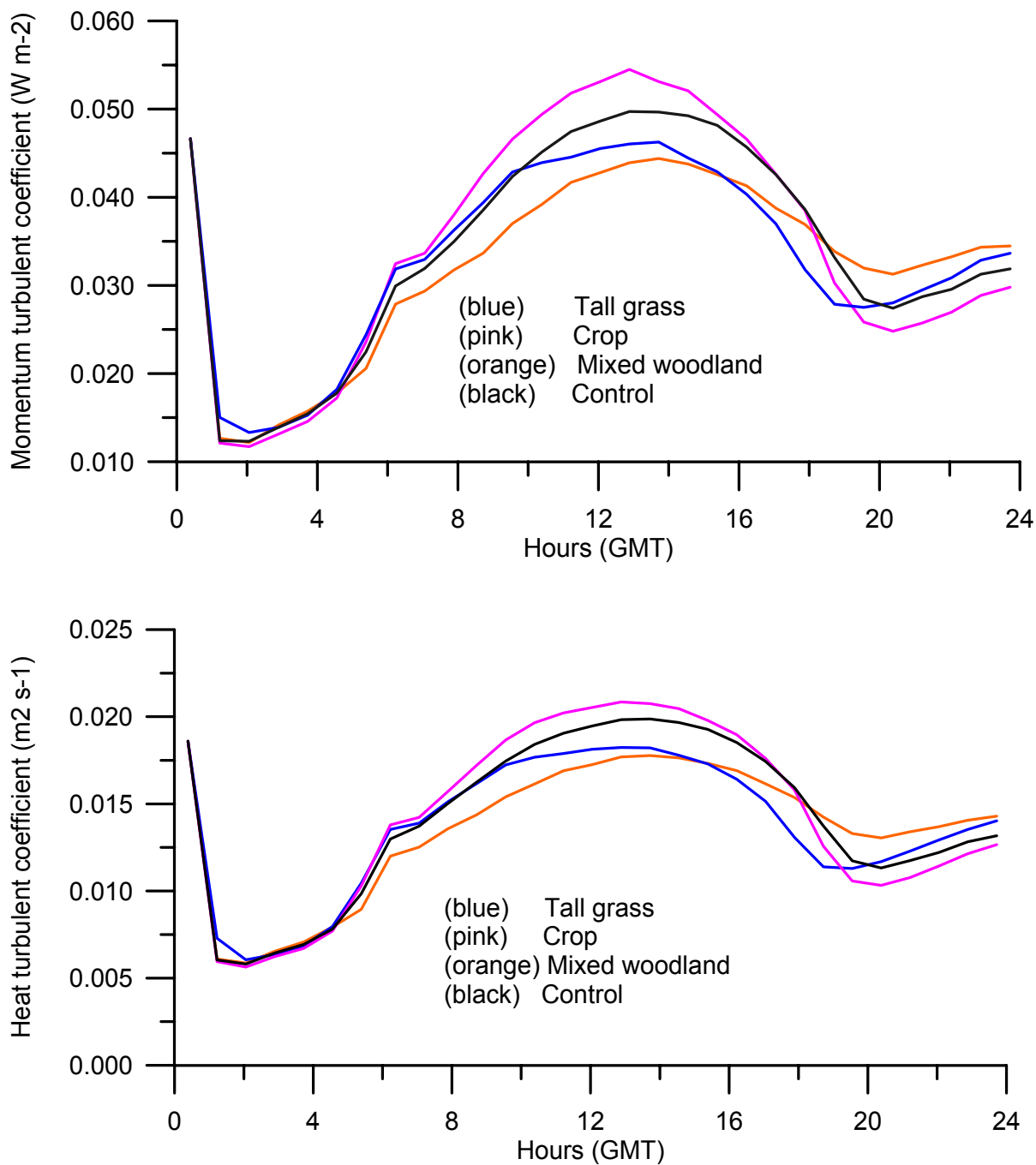


Figure 9. Sensitivity of the mean momentum turbulent coefficient and the mean heat turbulent coefficient, in the layer between the canopy source height Mihailovic and Rajkovic, 1993; Sellers et al., 1986) and the lowest model level, to the cover type. The hourly means were made using all grid points in the blue domain in Figure 5.

Control surface. Finally, the temperatures of the tall grass and Control surface begin to differ after 0900 GMT. The maximum of the surface temperature is firstly reached over the crop surface and then over the Control surface. Small time difference, in reaching the maximum of surface temperature, between these two surfaces can be explained by the fact that

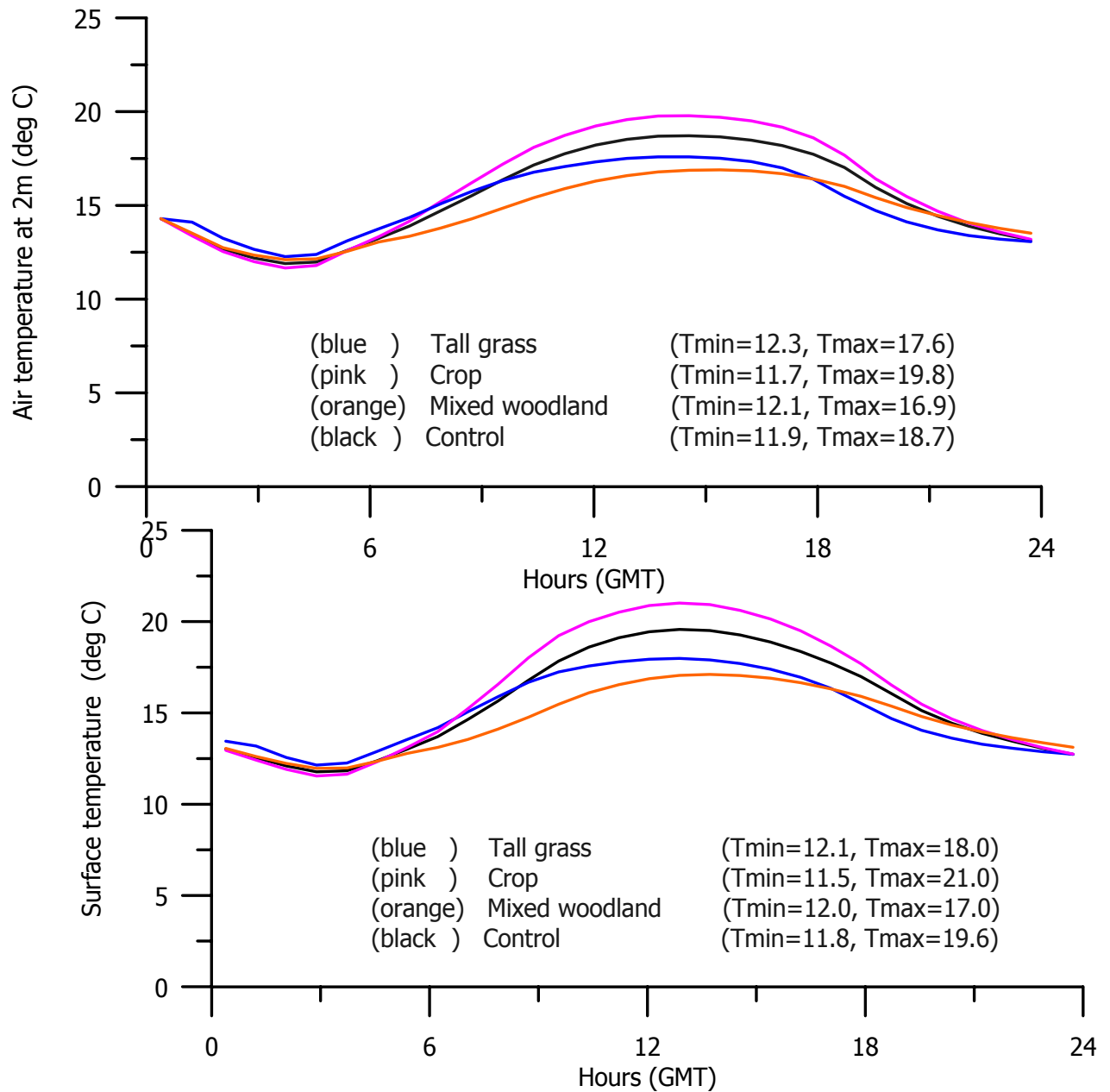


Figure 10. Sensitivity of the mean surface temperature (below) and air temperature at 2 m (above) to cover type. The hourly means were made using all grid points in the blue domain in Figure 5

the dominant cover type in the Control surface is the crop (45.6%) determining its thermal characteristics. The tall grass and mixed woodland maximum temperatures come later with a time shifting of 1 hour in their occurrence about. The differences in maximum values of the surface temperatures, over different cover types, are more pronounced than in the case of their minimum (17.0 °C – mixed woodland; 18(11.5 °C – crop; 11.8 °C – control; 12.0 °C – mixed woodland; 12.1 °C – tall grass)– Tall grass; 19.6 °C –Control; 21.0 °C – crop). The crop surface temperature is the highest among other surfaces. The difference of 4 °C, occurring between mean values of surface temperatures for different covers, is a

clear indication how a huge impact on the on the model physics can arise, when the cover in the part of integration domain is changed. Further, it points out that the parameterization of vegetation in numerical models, regardless of the scale of domain used, would be taken into account with high level of attention. The differences between temperatures are less going towards the evening hours. Thus, after 2000 GMT, practically they become negligible.

The air temperature at 2 m (shelter temperature) is a reliable indicator of the thermal state of the underlying surface. i.e., of the quality of the surface parameterization since the surface temperature strongly affects the air temperature at 2 m. This quantity is determined diagnostically. The upper panel of Figure 10 depicts the temporal variation of the mean surface air temperature at 2m depending on the different cover types in the blue domain in Figure 5. Physical behavior of all curves in this panel, is close to behavior of surface temperature curves in sense of their diurnal course. However, their daily amplitudes are smaller than those for the surface temperatures. Also, the time of reaching the maximum is shifted towards the later noon hours

If we intend to check the performance of the LAPS-NCEP to the Eta Mesoscale Model it is very useful to compare temporal variation of the modeled air temperature at 2m against the observed values. For this comparison, we used 11 differently covered grid points nearest to the stations available from the meteorological network located at different altitudes. All stations taken for comparison are from the blue domain in Figure 5. The indicator for the grid point, its latitude and longitude, coordinates of the nearest meteorological station and corresponding altitude are shown in Figs. 11-15. For comparison we used the following observed values: extreme temperatures and air temperatures at 2 m available every 6 hours in the model cycle (0600 GMT, 1200 GMT, 1800 GMT and 2400 GMT). These data are taken from the SYNOP of 05 June 2002. The measured as well as the modeled values of the extreme temperatures are also displayed in figures.

Figure 11 depicts temporal variation of air temperature at 2 m at stations Sremska Mitrovica (above) and Lom (below). From this figure is seen that the daily courses of temperature are correctly modeled in both cases. For Sremska Mitrovica the modeled values are in good agreement with the observations, particularly for 1200 and 2400 GMT. Also, the maximum of the modeled temperature is very close to measured value (25.1 °C – model; 26.0 °C - observed). However, the Eta-LAPS underestimates the observations for Lom that is also visible comparing the extreme temperatures (2.1 °C for the maximum and 2.7 °C for the minimum). Figure 12 and 13 show the temporal variations of 2m temperatures for stations having approximately the same altitudes. These variations show a similar behaviour resulting in: (a) more or less agreement with the observations for 1200, 1800 and 2400 GMT and (b) a good agreement between the modelled and observed values in maximum of temperatures (0.5 °C for Kikinda; 0.5 °C for Belgrade/Surcin Airport and 0.6 °C for Beograd/Karadjordje Park). However, in all cases the Eta-LAPS systematically underestimates the air temperature up to 0600 GMT. It seems that its radiation module simulates higher ground radiation, during the midnight-very early morning interval, resulting in a lower surface temperature than it is in the reality. Consequently, around 0600 GMT the Eta-LAPS cannot heat the lowest part of the atmosphere so quickly as it is done by the shortwave radiation from the Sun. Figure 14 is an illustrative example of the model output when the Eta-LAPS catches the low amplitude diurnal variation of temperature closely coinciding with the observations. The extreme values are also in a good agreement with the observed ones. Figures 15 and 16 show temporal variation of temperatures for the grid points nearest to stations located at higher altitudes. The lower panel of Figure 15 shows a good agreement of modeled values and the observations for station Valjevo (177m). Although, the maximum is correctly predicted (24.5 °C - modeled vs. 24.9 °C - observed), the Eta LAPS

still overestimates the observed minimum (13.5 °C - modeled vs. 11.0 °C – observed). The grid point nearest to the station Taszar, exhibits the temporal variation of the air temperature at 2 m, that follows the observations quite well except the minimum. However, at 0600 GMT the modeled value is higher than the value observed at the same time. Finally, the grid point courses of the air temperatures at 2m in Figure 16, plotted against the SYNOP data for stations Sibiu/Timisoar (444) and Niksic (47), are comparable with the observations, except the value modeled in the grid point (38,55) significantly differing from the value observed at 2400 GMT (Sibiu/Timisoar).

The result of comparison between the modeled and observed values of air temperature at 2m may be clearer if they are visualized as in Figure 17. This figure shows the values of the air temperature at 2 m obtained by the Eta-LAPS model plotted against the observed values, taken from the SYNOP data of 05 June 2002 for all 11 stations used in the previous analysis. The upper panel depicts the comparison for 0600, 1200, 1800 and 2400 GMT, while the lower panel indicates the comparison for extreme temperatures. It is seen that the Eta-LAPS overestimates air shelter temperature in the early morning hours comparing with the SYNOP data, while the shelter air temperatures simulated for the around noon and early night periods are in a good agreement with the observations. The simulated values obtained for daily extreme temperatures show better agreement with the observations in the case of maximum value rather than for the minimum.

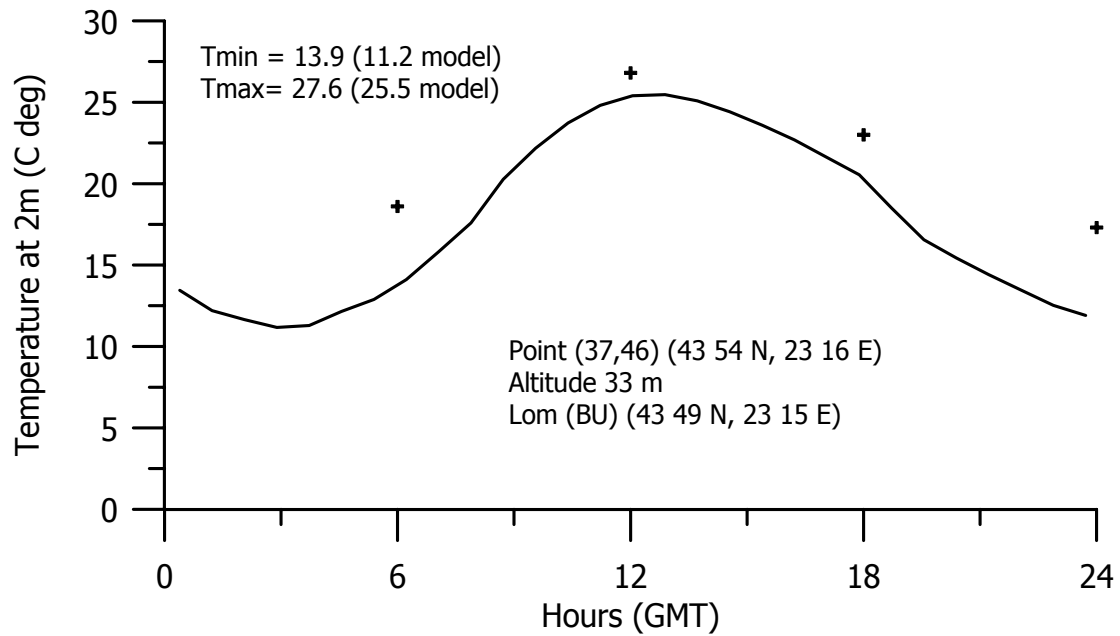
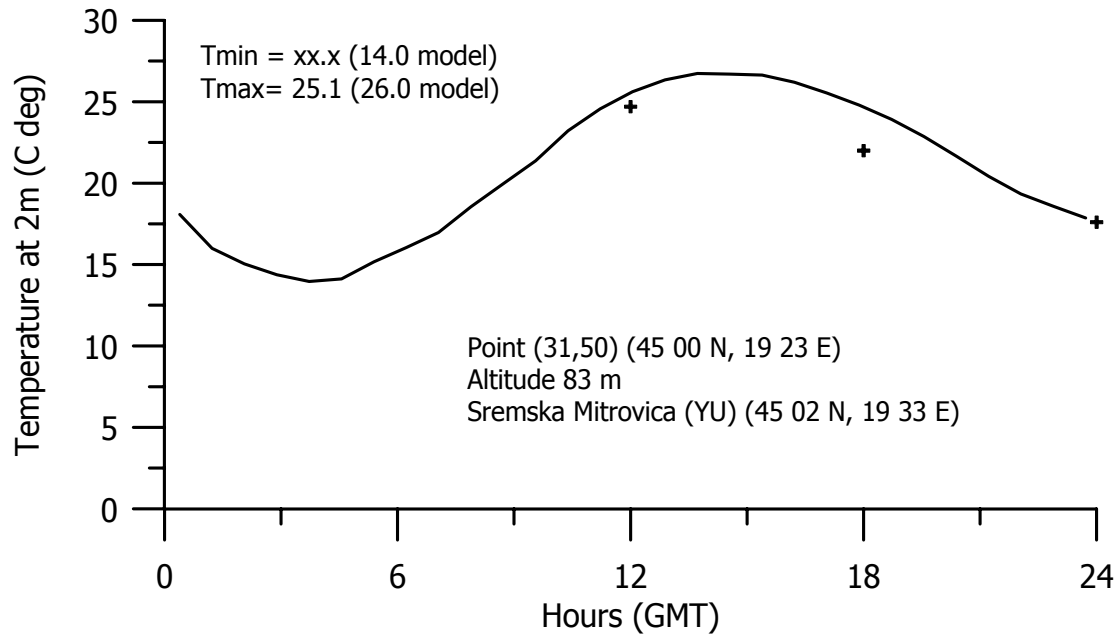


Figure 11. The diurnal cycle of the simulated air temperature at 2 m in the grid point obtained by the Eta-LAPS (solid line). Crosses indicate the values, taken from the SYNOP of 05 June 2002, observed at the station nearest to the grid point

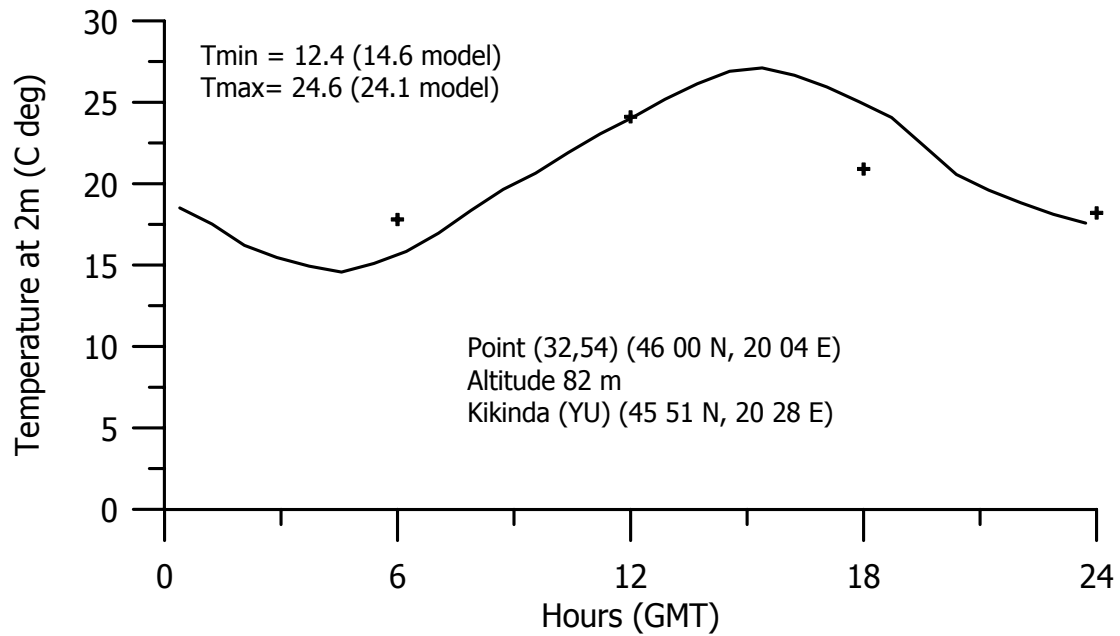
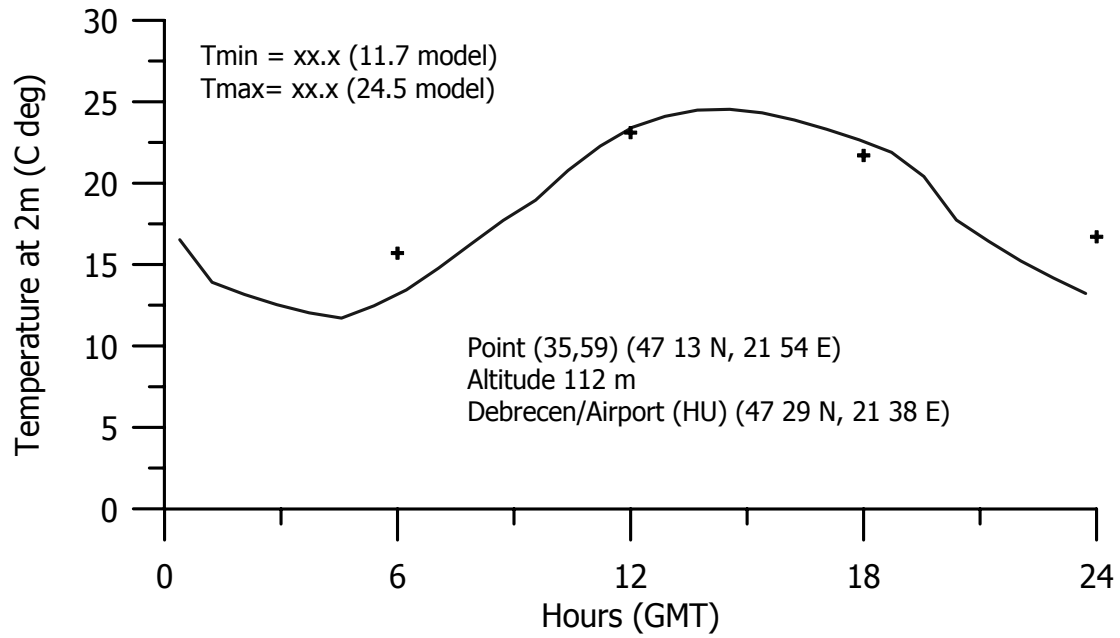


Figure 12. As in Figure 11

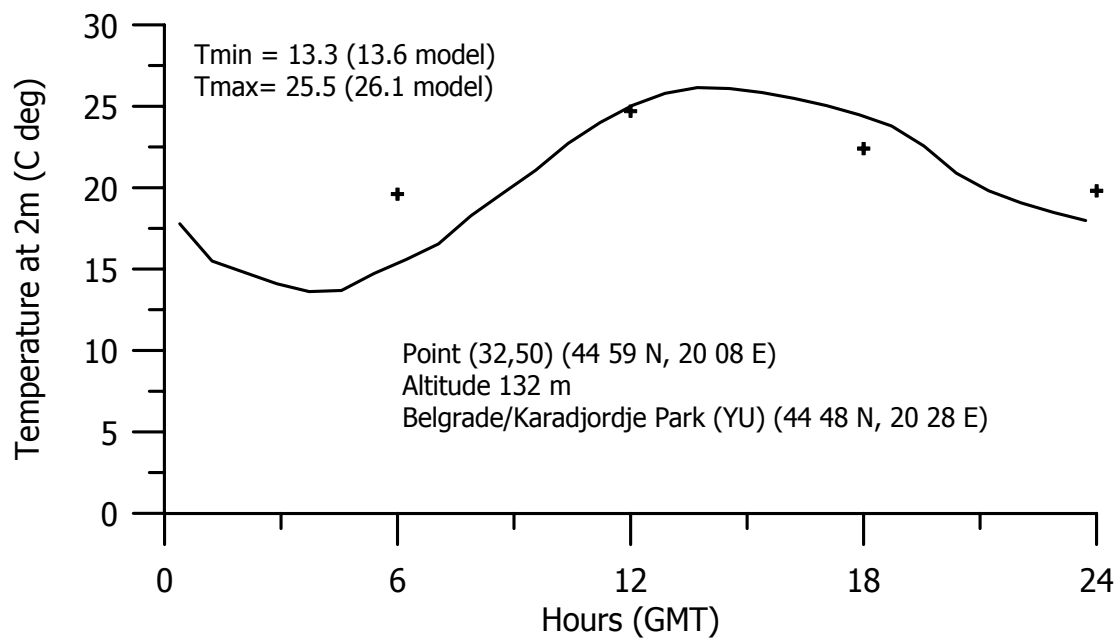
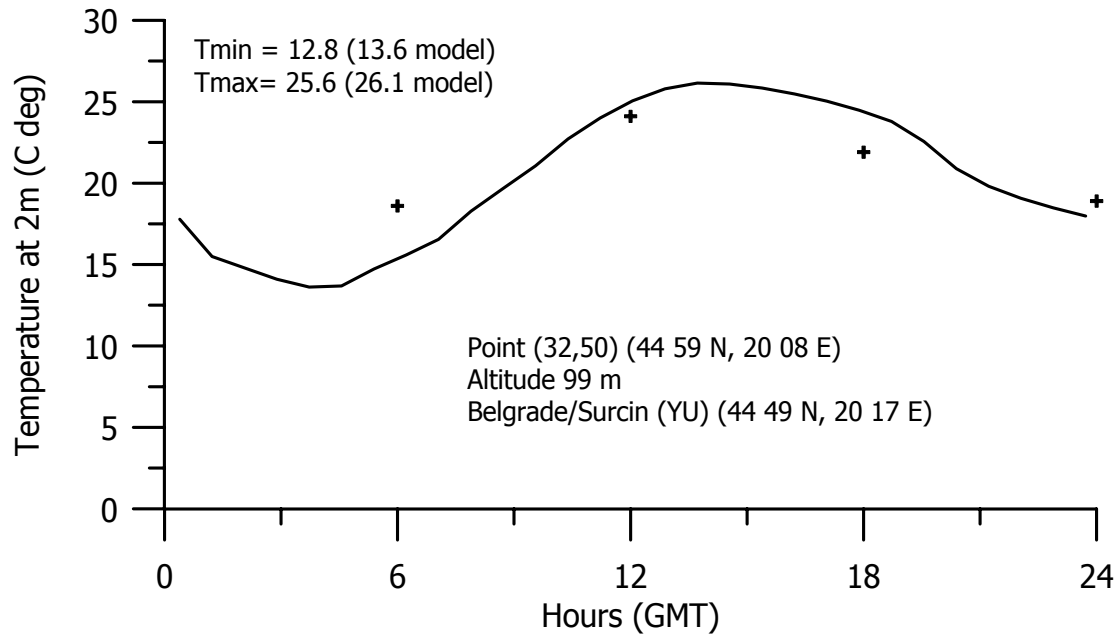


Figure 13. As in Figure 11

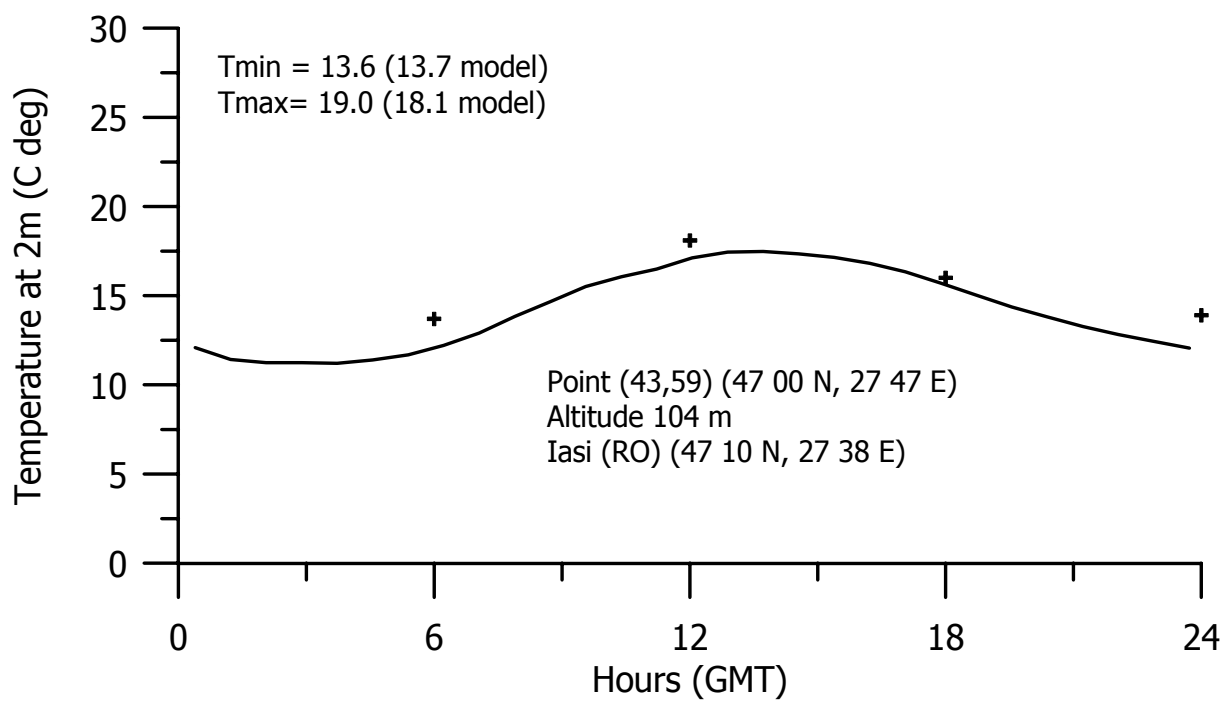


Figure 14. As in Figure 11

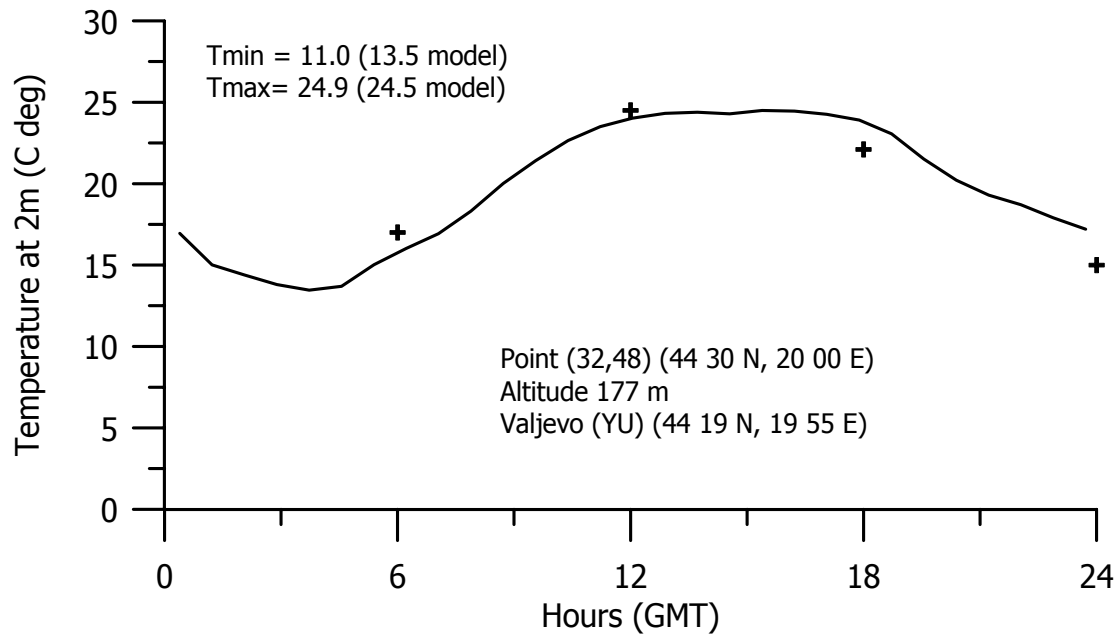
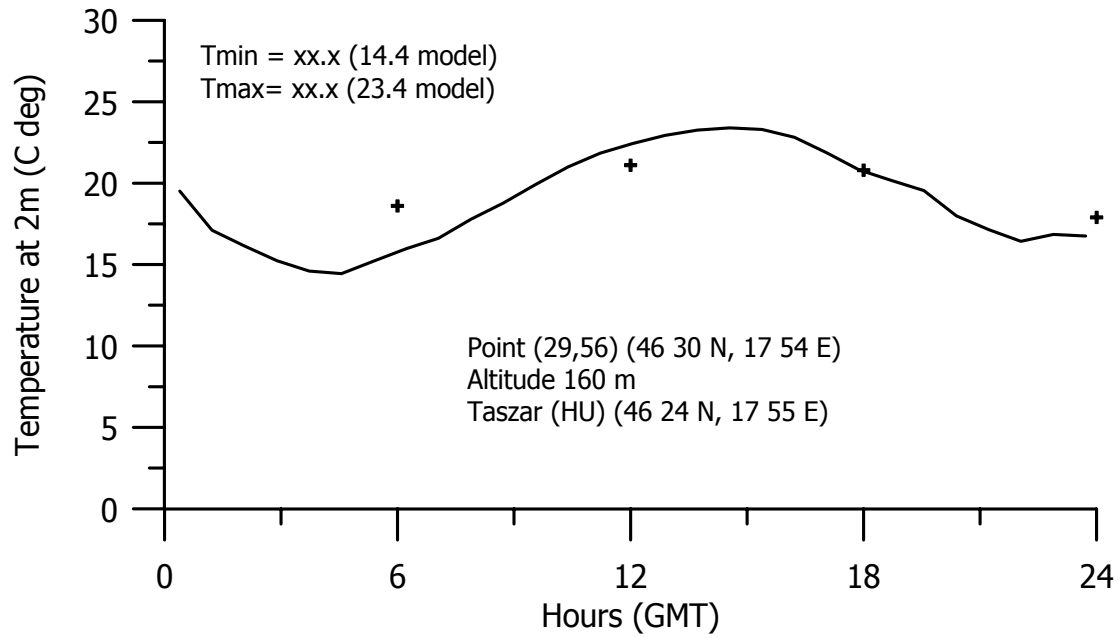


Figure 15. As in Figure 11

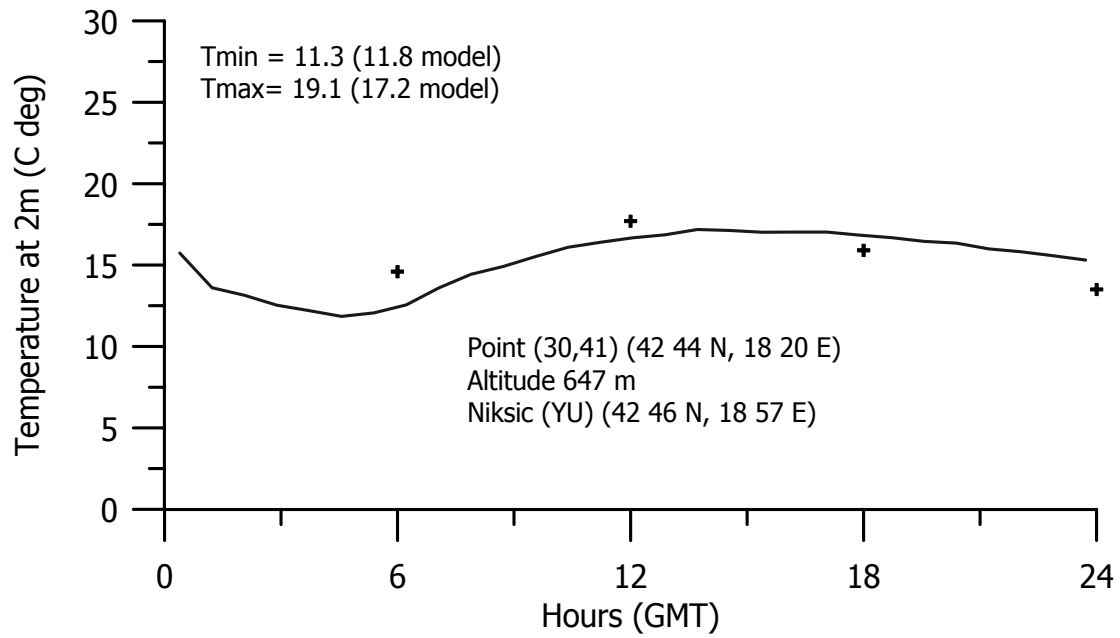
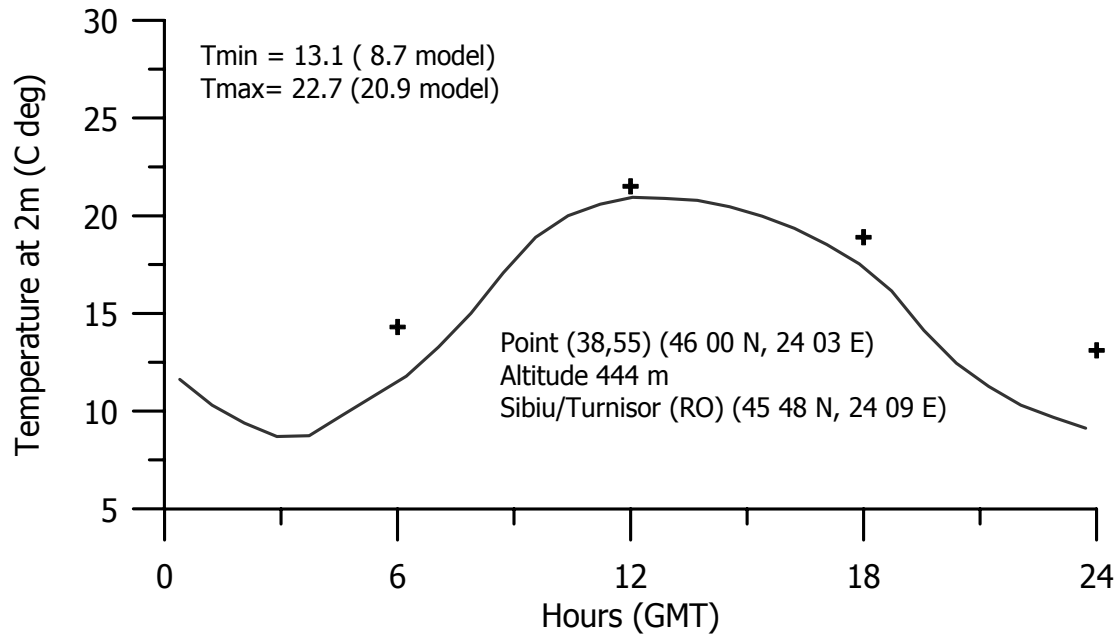


Figure 16. As in Figure 11

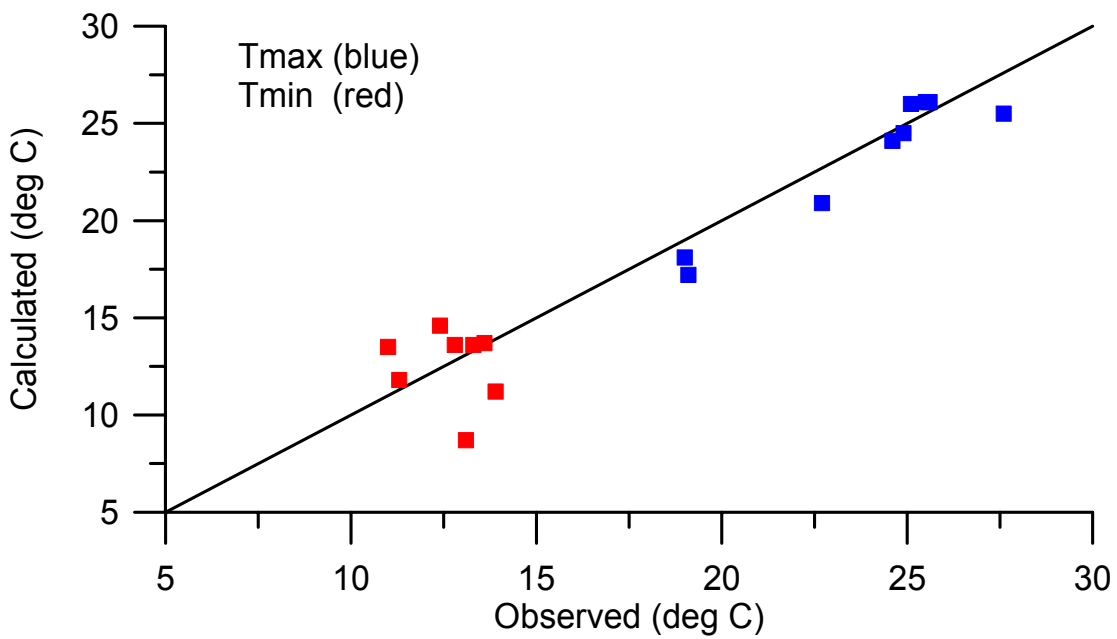
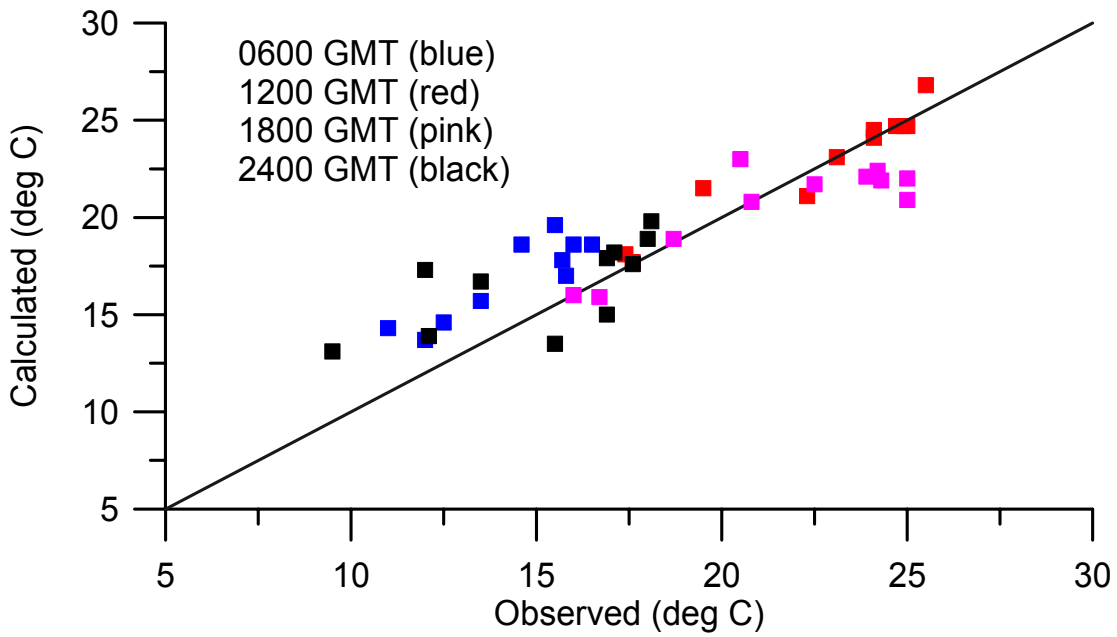


Figure 17. The values of the air temperature at 2 m obtained by the Eta-LAPS plotted against the observed values taken from the SYNOP of 05 June 2002. The upper panel depicts the comparison for 0600, 1200, 1800 and 24000 GMT while the lower panel indicates the comparison for the extreme temperatures.

ACKNOWLEDGMENTS

The research work described in this document has been funded by the NYSERDA under a contractual agreement No. 4914-ERTER-ES-99. The Investigator would like to thank Dr. Bora Rajkovic (Belgrade University), Prof. George Kallos, Dr. Anastasios Papadopoulos, Petros Katsafados and Antigoni Voudouri (University of Athens) for their help during the project.

REFERENCES

- Abramopoulos, F., Rosenzweig, C. and Choudhury, B., 1988: Improved ground hydrology calculations for global climate models (GCMs): Soil water movement and evapotranspiration. *J. Climate*, 1, 921-941.
- Arakawa, A., 1966: Computational design for long-term numerical integration of the equations of fluid motion: Two dimensional incompressible flow. Part I. *J. Comp. Phys.* 1, 119-143.
- Arsenic, I.D., D.T. Mihailovic, D.V. Kapor, G. Kallos, B. Lalic, and A. Papadopoulos, 2000: Calculating the surface temperature of the solid underlying surface by modified "Force Restore" method. *Theor. and App. Climatol.*, 67,1/2, 109-113.
- Arsenic, I., Mihailovic, D.T, Kallos, G., and Lalic, B, 1997: Calculation of rocky surface temperature in LAPS land surface scheme: methodology and corresponding mapping of rocky soils. *Proceedings of the Symposium on Regional Weather Prediction on Parallel Computer Environments*, 99-105.
- Betts, A. K., 1986: A new convective adjustment scheme. Part I: Observational and theoretical basis. *Quart. J. Roy. Meteor. Soc.*, 112, 677-691.
- Betts, A. K., and Miller, M.J., 1986: A new convective adjustment scheme. Part II: Single column tests using GATE wave, BOMEX, ATEX and Arctic air-mass data sets. *Quart. J. Roy. Meteor. Soc.*, 112, 693-709.
- Businger, J.A., Wyngaard, J.C., Izumi, Y.I. and Bradley, E.F., 1971: Flux-profile relationship in the atmospheric surface layer. *J. Atmos. Sci.*, 28, 181-189.
- Clapp, R.B. and Hornberger, G.M., 1978: Empirical equations for some soil hydraulic properties. *Water Resour. Res.*, 14(4): 601-604.
- Cosby, B.J., Hornberger, G.M., Clapp, B., and Ginn, T.R., 1984: A statistical exploration of the relationship of soil moisture characteristics to the physical properties of soils. *Water Resour. Res.*, 20, 682-690.
- Deardorff, J.W., 1978: Efficient prediction of ground surface temperature and moisture with inclusion of a layer vegetation. *J. Geophys. Res.*, 83, 1889-1903.
- Dekic, Lj., D.T. Mihailovic and B. Rajkovic, 1995: A study of the sensitivity of bare soil evaporation schemes to soil surface wetness, using the coupled soil moisture and surface temperature prediction model, BARESOIL. *Meteorol. Atmos. Phys.*, 55, 101-112.
- Dickinson, R.E., 1984. Modeling evapotranspiration for threedimensional global climate models. In: J.E.

- Hansen and T. Takahashi (Editors), *Climate Processes and Climate Sensitivity*. Am. Geophys. Union, Washington, DC, pp. 58-72.
- Dickinson, R.E., Henderson-Sellers, A., Kennedy, P. and Wilson, M., 1986: Biosphere/Atmosphere Transfer Scheme for NCAR Community Climate Model. NCAR Tech. Note TN 30.
- Ek, M. and L. Mahrt, 1991: OSU 1-D model. User Guide (version 1.0.4): A one-dimensional planetary boundary layer model with interactive soil layers and plant canopy. *College of Oceanic and Atmospheric Sciences*, Oregon state University, Corvallis, Oregon 97331-2209, 54 pp.
- Federer, C.A., 1979: A soil-plant-atmosphere for transpiration and availability of soil water. *Water Resour. Res.*, 15(3), 555-562.
- Fels, S.B, and Schwarzkopf, 1975: The simplified exchange approximation: A new method for radiative transfer calculations. *J. Atmos. Sci.*, 32, 1475-1488.
- Goudriaan, J., 1977: Crop Micrometeorology. A Simulation Study. Wageningen Center for Agric. Publ. Doc., 249 pp.
- Idso, S., Jackson, R., Kimball, B. and Nakagama, F., 1975: The dependence of bare soil albedo on soil water content. *J. Appl. Meteorol.*, 14, 109-113.
- Janjic, Z.I., 1977: Pressure gradient force and advection scheme used for forecasting with steep and small scale topography. *Contrib. Atmos. Phys.*, 50, 186-199.
- Janjic, Z.I., 1980: Numerical problems related to steep mountains in sigma coordinates. *Mountains and Numerical Weather Prediction*. Workshop, ECMWF, 1979, Reading, U.K..Shinfield Park, Reading, Berkshire RG2 9AX, U.K. , 48-89.
- Janjic, Z.I., 1984: Non-linear advection schemes and energy cascade on semi-staggered grids. *Mon. Wea. Rev.*, 112, 1234-1245.
- Janjic, Z.I., 1990: The step-mountain coordinate: physical package. *Mon. Wea. Rev.*, 118, 1429-1443.
- Janjic, Z.I., 1994: The step-mountain eta coordinate model: Further developments of the convection, viscous sublayer and turbulence closure schemes. *Mon. Wea. Rev.*, 122, 927-945.
- Janjic Z.I., 1996: The Mellor-Yamada Level 2.5 turbulence closure scheme in the NCEP Eta Model. *Research Activities in Atmospheric and Oceanic Modelling*, WMO, Geneva, CAS/WGNE, 4.14-4.15.
- Janjic, Z.I., 2002: A nonhydrostatic model based on a new approach. *Meteorol. Atmos. Phys.* (In press).
- Jarvis, P.G., 1976: The interpretation on the variations in leaf water potential and stomatal conductance found in canopies in the field. *Philos. Trans. R. Soc.*, B273, 593-610.
- Jones, W.P., Watkins, J.R., and Calvert, T.A., 1975: Temperatures and thermophysical properties of the lunar outermost layer. *The Moon*, 13, 475-495.
- Kallos, G., Nickovic, S. Papadopoulos, A. Jovic, D., Kakaliagou, O., Misirlis, N., Boukas, L., Mimikou, N., Sakellaridis, G., Papageorgiou, J., Anadranistakis, E., and Manousakis, M., 1997: The regional weather forecasting system SKIRON: An overview. *Proceedings of the Symposium on Regional Weather Prediction on Parallel Computer Environments*, 15-17 October 1997, Athens, Greece, 109-122.

- Lalic, B., and Mihailovic, D.T., 1998: Derivation of aerodynamic characteristics using a new wind profile in the transition layer above the vegetation. *Research Activ. in Atmos. and Oceanic Modelling Rept.*, 27, 4.25-4.26.
- Mesinger, F., Janjic, Z.I., Nickovic, S., Gavrilov, D. and Deaven, D.G., 1988: The step-mountain coordinate: model description and performance for cases of Alpine lee cyclogenesis and for a case of an Appalachian redevelopment. *Mon. Wea. Rev.*, 116, 1493-1518.
- Mihailovic, D.T., 1990: Testing the Biosphere-Atmosphere Transfer Scheme (BATS) using Penman and Long (1960) data: Preliminary results. Int. Rep. Dep. Meteorol. Wageningen Agric. Univ., 40 pp.
- Mihailovic, D.T., 1991: A model for prediction of the soil temperature and the soil moisture content in three layers. *Z. Meteorol.*, 41, 29-33.
- Mihailovic, D.T., 1996: Description of a land-air parameterization scheme (LAPS). *Special Issue of Global & Planetary Change on Soil Moisture Simulation*, 13, 207-215.
- Mihailovic, D.T. and Jeftic, M., 1994: An efficient but simple biophysical scheme UNICOS for use in different scale modeling. *Environ. Soft.*, 9, 47-60.
- Mihailovic, D.T. and Rajkovic, B., 1993: Surface vegetation parameterization in atmospheric models: A numerical study. *Z. Meteorol.*, 2, 239-243.
- Mihailovic, D.T. and Ruml, M., 1996. Design of land-air parameterization scheme (LAPS) for modeling boundary layer surface processes. *Meteorol. Atmos. Phys.*, 58, 65-81.
- Mihailovic, D.T. and Kallos, G., 1997: A sensitivity study of a coupled soil-vegetation boundary-layer scheme for use in atmospheric modeling. *Boundary-Layer Meteorol.*, 82, 283-315.
- Mihailovic, D.T., Rajkovic, B., Lalic, B. and Dekic, L., 1995a: Schemes for parameterizing evaporation from a non-plant-covered surface and their impact in on partitioning the surface energy in land-air exchange parameterization. *J. Appl. Meteor.*, 34, 2462-2475.
- Mihailovic, D.T., Arsenic, I.D., and Lalic, B., 1996: Calculating the rocky surface temperature and its sensitivity to the thermal properties, slope and orientation of rocks. *Novi Sad Journal of Physics (former: Review of Research Faculty of Science, Physics series)*, 26, 80-86.
- Mihailovic, D.T., de Bruin, H.A.R, Jeftic, M. and van Dijken, 1992: A study of land-surface parameterization to inclusion of different fractional covers and soil textures *J. Appl. Meteorol.*, 31, 1477-1487.
- Mihailovic, D.T., Pielke, R.A, Rajkovic, B., Lee, T.J. and Jeftic, M., 1993: A resistance representation of schemes for evaporation from bare and partly plant-covered surface for use in atmospheric models. *J. Appl. Meteorol.*, 32, 1038-1054.
- Mihailovic, D.T., Rajkovic, B., Dekic, Lj, Pielke R.A., Lee, T.J. and Ye, Z., 1995b: The validation of various schemes for parameterizing evaporation from bare soil for use in meteorological models: A numerical study using in situ data. *Boundary-Layer Meteorol.*, 76, 259-289.
- Mihailovic, D.T., Rajkovic, B., Lalic, B., Jovic, D. and Arsenic, I., 1997: The main features of the hydrological module in the land air parameterization scheme (LAPS). *Phys. Chem. Earth*, 21, 201-204.
- Mihailovic, D.T, B. Rajkovic, B. Lalic, D. Jovic, Lj. Dekic, 1998: Partitioning the land surface water simulated

- by a land-air surface scheme. *J. Hydrology*, 211, 17-33.
- Mihailovic, D.T., Lee, T.J., Pielke, R.A., Lalic, B., Arsenic, I., Rajkovic, B., Vidale, P.L., 2000: Comparison of different boundary layer schemes using single point micrometeorological field data. *Theor. and App. Climatol.*, Vol. 67, Issue 3/4, 135-151.
- Papadopoulos, A., Kallos G., Mihailovic, D., Katsafados, P., Arsenic, I. and Lalic, B., 1999: Influence of rocky ground parameterization on surface temperature. *Geoph. Res. Lett.* (submitted).
- Sellers, P.J., Mintz Y., and Dacher X., 1986: A simple biosphere model (SiB) for use within general circulation model. *J. Atmos, Sci.*, 43, 506-531.
- Sellers, P.J., Shuttleworth, W.J., Dorman, J.L., Dalcher, A. and Roberts, J.M., 1989: Calibrating the simple biosphere model for Amazonian forest field and remote sensing date. Part I: Average calibration with field data. *J. Appl. Meteorol.*, 28, 727-759.
- Simmons, A.J., and Burridge, D.M, 1981: An energy and angular-momentum conserving vertical finite-difference scheme and hybrid vertical coordinates. *Mon. Wea. Rev.*, 109, 758-766.
- Simpson , L.D., and J.W. Lucas, 1972: Lunar aspects from surveyor data. *In: Thermal characteristics of the Moon*. Edited by J.W. Luckas, Cambridge Massachusetts, and London, England, The MIT Press, Vol. 28, 121-149.
- Sun, S.F., 1982: Moisture and heat transport in a soil layer forced by atmospheric conditions. M.S. Thesis. Dep. Civ. Eng. Univ. Conn., 72 pp.
- Van der Honert, X., 1948: Water transport as a catenary process. *Disc. Faraday Soc.*, 3, 146-153.
- Zhang, D. and Anthes, R.A., 1982: A high-resolution model of the planetary boundary layer-sensitivity tests and comparisons with SESAME-79 data. *J. Appl. Meteorol.*, 21, 1594-1609.

For information on other
NYSERDA reports, contact:

New York State Energy Research
and Development Authority
17 Columbia Circle
Albany, New York 12203-6399

toll free: 1 (866) NYSERDA
local: (518) 862-1090
fax: (518) 862-1091

info@nysERDA.org
www.nysERDA.org

**ANALYSIS OF OZONE AND FINE PARTICULATE MATTER
IN THE NORTHEASTERN UNITED STATES**

FINAL REPORT 03-04

**STATE OF NEW YORK
GEORGE E. PATAKI, GOVERNOR**

**NEW YORK STATE ENERGY RESEARCH AND DEVELOPMENT AUTHORITY
VINCENT A. DEIORIO, ESQ., CHAIRMAN
PETER R. SMITH, PRESIDENT**

